Universidade Federal de Minas Gerais
Programa de Pós Graduação em Engenharia Elétrica

Aquisição simultânea de eletroencefalografia e ressonância magnética funcional para investigação da plasticidade neural

Ana Cláudia Silva de Souza

Tese submetida ao Programa de Pós Graduação em Engenharia Elétrica da Universidade Federal de Minas Gerais como requisito parcial para obtenção do grau de Doutor em Engenharia Elétrica.

Belo Horizonte
Agosto, 2010

Universidade Federal de Minas Gerais
Graduate Program in Electrical Engineering

Simultaneous acquisition of electroencephalography and functional magnetic resonance for the investigation of neural plasticity

Ana Cláudia Silva de Souza

A dissertation submitted to the Graduate Program in Electrical Engineering of the Universidade Federal de Minas Gerais in partial fulfillment of the requirements for the degree of Doctor of Electrical Engineering.

Belo Horizonte
August, 2010

Resumo

Este trabalho apresenta um estudo sobre plasticidade neural baseado em registros simultâneos de eletroencefalografia (EEG) e ressonância magnética funcional (fMRI). Diversas evidências indicam que a especificidade neural à estimulação sensorial básica é mutável e dependente da experiência do indivíduo. Uma maneira de se verificar essa plasticidade é por meio da aprendizagem perceptiva, a qual consiste em uma melhoria na discriminação sensorial após um período de treinamento. Para este fim, foi implementada uma tarefa de discriminação de frequências, com tons padrão e desviantes apresentados a voluntários. A hipótese investigada é se o direcionamento da atenção do indivíduo à tarefa sendo executada melhora a habilidade em distinguir os tons desviantes em um treinamento de curta duração.

Uma primeira contribuição deste estudo está no fato de a atividade cerebral ser explorada *durante* o processo de aprendizagem, enquanto a maioria dos trabalhos na área investiga esta atividade *antes* e *após* a aprendizagem perceptiva. Os resultados obtidos mostram que este tipo de aprendizagem pode ser medida por meio de uma melhoria no desempenho da tarefa ao longo de um intervalo de curta duração.

Além disso, o registro simultâneo do EEG e da fMRI fornece uma melhor localização espacial e temporal das fontes de ativação da atividade neural. Isto é importante no problema de localização das fontes neurais que geram um determinado grupo de sinais registrados no escalpo (problema inverso). A partir dos dados coletados nas duas modalidades, implementa-se um método hierárquico Bayesiano variacional onde as soluções inversas do EEG estão restritas às regiões de ativação elevada vistas nas imagens de ressonância magnética funcional.

Finalmente, a principal contribuição deste trabalho é revelar que mesmo alterações provocadas por um aprendizado de rápida duração não estão restritas ao córtex sensorial, e compõem um substrato neural para modulações de atenção seletiva que iniciam o processo de aprendizagem perceptiva auditiva.

Abstract

This thesis presents a study on neuronal plasticity based on simultaneous recording of electroencephalography (EEG) and functional magnetic resonance (fMRI). There is an accumulating body of evidence indicating that neuronal functional specificity to basic sensory stimulation is mutable and subject to experience. One way to look at this plasticity is by means of perceptual learning, which is an improvement in sensory discrimination after a period of training. For that purpose, a frequency discrimination task was performed with standard and deviant tones presented to subjects. The hypothesis investigated is whether focused attention enhanced the discrimination of the deviant tones.

The first original contribution of this study is that brain activity is explored *during* the process of learning whereas most works have investigated brain activity *after* relative to *before* perceptual learning. The results obtained show that perceptual learning can be assessed in rapid early performance having the improvement in behavioral performance as reference.

Moreover, recording EEG and fMRI simultaneously provides better spatial and temporal localization of activated sources. This is important in the problem of localizing the activated sources that generated the signals measured at the scalp (inverse problem). Based on data from both modalities, this thesis employs a method in which the EEG inverse solutions are constrained to regions where fMRI indicates large hemodynamic activation. The variational hierarchical Bayesian method used overcomes problems such as false positive, incorporating fMRI information as a hierarchical prior on the variance distribution.

Finally, the main contribution of this work is to show that even fast learning changes are not confined to sensory cortex, providing a potential neural substrate for top-down modulation of auditory selective attention that gives rise to auditory perceptual learning.

À minha mãe, meu pai e irmãos, pelo carinho. À Deus por tudo.

To mom, dad and my brothers, for their affection.
To God for everything.

Agradecimentos

Durante a realização deste trabalho, contei com a colaboração de muitas pessoas, as quais não poderia deixar de agradecer:

Ao Prof. Hani Camille Yehia, meu orientador, pelo seu apoio e incentivo. Por acreditar no meu trabalho e me fazer acreditar que seria possível. Ao longo destes anos o Prof. Hani tornou-se mais do que um professor, mas um amigo que sempre depositou grande confiança em mim. Foi ele também que me incentivou e criou a oportunidade de eu desenvolver parte deste trabalho na ATR (*Advanced Telecommunications Research Institute International*), em Kyoto, Japão. Lá, tive a oportunidade de trabalhar com grandes cientistas, aumentando ainda mais meu interesse pela pesquisa científica.

Ao Dr. Daniel Callan, meu co-orientador na ATR, por todo o apoio que recebi durante minha estadia em Kyoto. Meus agradecimentos vão muito além de seus valiosos ensinamentos na condução deste trabalho, discussões que me auxiliaram nos caminhos da ressonância magnética, mas, agradeço também, imensamente, pela companhia de sua família, as sexta-feiras no Kiichi e tudo que ele fez para que minha estadia fosse a mais proveitosa e agradável possível.

Ao Prof. Márcio Morais por suas ricas sugestões e incentivo desde o início deste projeto de doutorado.

Agradeço à ATR, e principalmente aos laboratórios CNS (*Computational Neuroscience Laboratories*) que me receberam tão amigavelmente. Lá, tive toda a infra-estrutura necessária para a condução de meus experimentos, e todo o apoio para minha adaptação, incluindo o esforço de todo o grupo para melhorarmos nossa comunicação. Apesar do apoio de todos, gostaria de ressaltar os colegas Ryosuke Hayashi, Taku Yoshioka e Yuka Furukawa. Não poderia deixar de lembrar de dois grandes amigos que tanto me ajudaram nas mais diversas situações: Eiji Nawa e Ranniery Maia. Por fim, agradeço meus amigos brasileiros de Kyoto que participaram como voluntários no meu experimento.

Aos meus amigos que de forma direta ou indireta contribuíram com este trabalho, em especial os amigos do PPGEE e do CEFALA sempre dispostos a ajudar. Em especial, ao Leo Carneiro, João Pedro, Damares e Leonardo Almeida o meu muito obrigada.

Deixo aqui meu agradecimento à Capes, por financiar minha pesquisa durante estes anos, e o CNPq, cujo financiamento me possibilitou a rica experiência no Japão.

Por fim, um agradecimento mais que especial às pessoas que estão sempre me apoiando e caminhando ao meu lado. Aos meus pais, cujo amor infindável faz compreender minha ausência, e cujos esforços me proporcionaram uma educação de qualidade e me fizeram chegar até aqui. Aos meus irmãos Cláudio e Rodrigo e à Erlaine cujas presenças, mesmo que virtuais, foram fundamentais nos meus momentos mais solitários no Japão. Enfim, agradeço ao Pai, por me trazer até aqui, colocando todas essas pessoas na minha vida.

Acknowledgements

During this work, I had the collaboration of many people who I cannot forget to thank:

To Professor Hani Camille Yehia, my advisor, for his support and encouragement. For believing in my work and making me believe it would be possible. During all these years, Professor Hani became more than an advisor, but a friend who always trusted me. He encouraged me and gave me the opportunity to develop part of this work at ATR (*Advanced Telecommunications Research Institute International*), in Kyoto, Japan. I could in this place work with great cientists and this environment made me even more fascinated with the field of scientific research.

I am grateful to Dr. Daniel Callan, my co-advisor at ATR, for all the support given during my stay in Kyoto. My acknowledgements go far beyond his valuable lessons in conducting this work, discussions that helped me in the field of magnetic resonance imaging, but I also thank him immensely for the company of his family, Fridays at Kiichi and everything he did to make my stay as enjoyable as possible.

To Professor Márcio Morais for the rich suggestions and incentive since the beginning of this research.

I would like to thank ATR and especially CNS labs (*Computational Neuroscience Laboratories*) where I was very welcomed. At ATR I had all the infrastructure necessary to conduct my experiments and the support for my adaptation, including the effort of the whole group to improve our communication. Among the many people who helped me, I would like to thank in particular Ryosuke Hayashi, Taku Yoshioka e Yuka Furukawa. I cannot forget to thank two good friends who helped in many situations: Eiji Nawa and Ranniery Maia. At last, my Brazilian friends in Kyoto who were subjects in my experiments.

To all my friends who have contributed directly or indirectly to this work, in particular my colleagues from the Graduate Program in Electrical Engineering (PPGEE) and my friends from CEFALA (Center for Research on Speech, Acoustics Language and Music). Thanks to João Pedro, Damares, Leonardo Carneiro, and Leonardo Almeida for the

friendship.

I am grateful to Capes for the finantial support received during all my graduate program, and CNPq for the scholarship for staying one year abroad.

At last, a very especial thanks to the ones who are always by my side suppporting me in everything. To my parents, whose unconditional love made them understand my absense in many moments. They have done more than they could to give me a high quality education. To Cláudio, Rodrigo and Erlaine whose presence (even virtually) were essential during the lonely momments in Japan. Thank God for bringing me up here and putting all these people in my life.

Resumo Estendido

Introdução

O cérebro é capaz de se reorganizar. Embora esta afirmação pareça óbvia nos dias atuais, ela era impensável há 20 anos. À medida que novas habilidades são aprendidas e novas experiências adquiridas, as células nervosas alteram sua forma de responder ao ambiente e, com isso, refletir as circunstâncias de sua alteração. A isto chama-se plasticidade. Uma maneira de se investigar a plasticidade é por meio da aprendizagem perceptiva definida como uma melhoria na discriminação sensorial após um período de prática, que normalmente varia de dias a semanas (Polley, Steinberg, and Merzenich, 2006; Moore, Amitay, and Hawkey, 2003; Demany, 1985; Watson, 1980). Os estudos mostram que os efeitos da aprendizagem perceptiva podem ser bastante específicos às características do estímulo sendo treinado, desta forma a falta de generalização pode ser uma evidência que o aprendizado é mediado por células em áreas sensoriais (Polley, Steinberg, and Merzenich, 2005). Embora seja aceito que a plasticidade neural ocorre após um treinamento extensivo, ainda há muito o que investigar sobre os substratos neurais envolvidos quando indivíduos apresentam melhorias rápidas no desempenho de tarefas ocorridas na primeira hora de treinamento (Alain, Snyder, He, and Reinke, 2007). Neste contexto, a atenção pode exercer papel importante na supressão de estímulos distratores. Vários trabalhos mostram evidências deste papel na aprendizagem perceptiva (Yotsumoto and Watanabe, 2008; Paffen, Verstraten, and Vidnyánszky, 2008; van Wassenhove and Nagarajan, 2007), enquanto outros apresentam evidências de aprendizagem passiva (Seitz and Watanabe, 2003; Watanabe, Nanez, and Sasaki, 2001). Em especial, durante tarefas auditivas de discriminação de frequências, a atenção parece desenvolver um papel especial em tarefas complexas como compreensão e cognição (Petkov, Kang, Alho, Bertrand, Yund, and Loods, 2004; Kiehl, Laurens, Duty, Foster, and Liddle, 2001b). Desta forma, é de grande importância um melhor entendimento das demandas de atenção e um dos caminhos que podem ser abordados é por meio da atenção seletiva.

Para o estudo da aprendizagem e atenção, esta tese empregou o registro simultâneo

da ressonância magnética funcional (RMf) e da eletroencefalografia (EEG), permitindo um ambiente mais realista que combine alta resolução espacial e temporal em experimentos cognitivos. Este protocolo garante não somente a mesma estimulação sensorial, percepção e comportamento, mas também permite o estudo das interações entre estados cerebrais intrínsecos e processamento relacionado a eventos em um mesmo estado cognitivo (Debener, Ullsperger, Siegel, and Engel, 2006). A principal desvantagem ao se trabalhar com a aquisição simultânea é a complexidade do experimento e os artefatos que surgem em ambas modalidades (Yan, Mullinger, Brookes, and Bowtell, 2009; Debener, Mullinger, Niazy, and Bowtell, 2008).

A partir dos dados de ambas as modalidades nós trabalhamos com o problema inverso para localização das fontes neurais que geraram os potenciais registrados no EEG. As soluções inversas da eletroencefalografia foram restritas às regiões onde o córtex indicou uma maior ativação dinâmica. Para isto, foi usado o método hierárquico Bayesiano (VBMEG) proposto por Sato, Yoshioka, Kajiwara, Toyama, Goda, Doya, and Kawato (2004).

Questionamento científico

Este trabalho tem por objetivo investigar os mecanismos que iniciam a aprendizagem perceptiva no sistema auditivo, baseado em duas hipóteses: (i) o aperfeiçoamento em tarefas de discriminação perceptiva resulta em um aumento da atividade cerebral no córtex sensorial específico e (i) regiões frontais estão envolvidas com a predição e modulação de cima para baixo da atenção seletiva que inicia a aprendizagem auditiva perceptiva. A maior contribuição deste trabalho consiste no uso de diferentes técnicas de imageamento para mostrar a importância da atenção na supressão de estímulos irrelevantes durante a aprendizagem perceptiva.

Organização do texto

Esta tese está organizada em sete capítulos. O Capítulo 1 contém a introdução e o propósito da tese. No Capítulo 2 a teoria básica e as técnicas implementadas são apresentadas, assim como uma breve descrição dos processos cognitivos investigados. O Capítulo 3 descreve como a eletroencefalografia é usada para investigar a comunicação neural, além das técnicas usadas no processamento dos dados. No Capítulo 4 são apresentadas as etapas do pré-processamento dos dados da ressonância magnética funcional e o método estatístico paramétrico adotado para testar a ativação de áreas corticais específicas. O Capítulo 5 mostra a metodologia usada nos experimentos, descrevendo o delineamento experimental dos estudos de RMf e como é feita a combinação com os registros de EEG.

O Capítulo 6 apresenta e interpreta os resultados obtidos. Por fim, o Capítulo 7 traz as conclusões deste trabalho apontando os principais resultados e fornecendo sugestões para questões que ainda precisam ser investigadas. O Apêndice A descreve o método hierárquico Bayesiano usado no procedimento de estimação de fontes.

Metodologia

Participantes

Foram coletados dados de EEG/RMf de 11 participantes (10 do sexo masculino), com idade entre 22 e 40 anos, sem registros de deficiência auditiva ou visual. Todos os participantes assinaram um termo de consentimento antes de se iniciar o experimento, de acordo com o comitê de ética da ATR (*Human Subject Review Commitee*).

Estímulo auditivo

Cada estímulo auditivo era composto por cinco tons de frequências diferentes (400Hz, 600Hz, 700Hz, 800Hz e 1000Hz) com duração total de 150 ms (10 ms de tempo de descida e tempo de subida). Um estímulo desviante é caracterizado por uma alteração na frequência do quarto tom. Os desvios variaram de 1 Hz a 40 Hz com passos de 1 Hz. Os estímulos eram entregues em sequências de cinco sons com intervalos variando de 450 a 500 ms entre eles. Cada sequência possuía no máximo um estímulo desviante nas posições 2, 3, 4 ou 5. Os demais foram denominados estímulos padrão. A estímulação foi feita de forma binaural por meio de um tubo de plástico cujas extremidades eram compostas por protetores auriculares de espuma, em um sistema compatível de EEG e RM. O tubo introduziu um atraso constante de 64 ms entre o envio do som e a chegada aos ouvidos.

Estímulo visual

O estímulo visual seguiu o mesmo modelo. O estímulo padrão consistiu de barras brancas retangulares, horizontalmente dispostas e posicionadas no centro da tela (40 cm dos olhos, vistos por um espelho). As barras desviantes também eram posicionadas no centro, porém rotacionadas em passos que variaram de 0,2 a 12 graus, em sentido horário. Os estímulos eram enviados em sequências de cinco barras separadas, temporalmente, de 450 a 500 ms. Assim como na apresentação dos estímulos auditivos, em cada sequência de cinco estímulos apenas uma barra desviante poderia estar presente e esta nunca aparecia na primeira posição.

Teste comportamental

Em cada participante foram testados os limiares de discriminação em frequência e posição nos testes auditivos e visuais, separadamente, em uma câmara acústica com isolamento de 40 dBA. A diferença em frequência entre os tons desviantes em cada tentativa era alterada de acordo com um procedimento em escada (*staircase*) convergindo para 71% de respostas corretas (Levitt, 1971). No teste visual, foi testada a habilidade do participante em determinar pequenas variações na rotação de barras retangulares a partir de sua posição horizontal inicial. O nível de discriminação obtido no teste comportamental foi usado como um ponto inicial para a escada no experimento com o escaner.

Escaneamento 3D

Após o teste comportamental, foi colocado um capacete com 64 eletrodos em cada participante (BrainCap-MR 64 BrainProducts, Munique, Alemanha). Um digitalizador tridimensional (*FastScan hand-held laser scanner*) foi usado para registrar o formato da cabeça e a posição de cada eletrodo. Posteriormente, estas informações foram usadas na construção dos modelos da cabeça para o procedimento de localização de fontes.

Modelo da superfície cortical

Foi construído um modelo poligonal do córtex cerebral usando a imagem estrutural T_1 de cada participante. O modelo cortical assume um dipolo de corrente em cada vértex no qual a atividade de RMf eliciada pelo estímulo ultrapassa um limiar. As direções deste dipolo são consideradas perpendiculares à superfície cortical (Yoshioka, Toyama, Kawato, Yamashita, and Nishina, 2008). Além disso, as imagens com o formato da cabeça de cada participante adquiridas com o escaner 3D foram ajustadas às imagens estruturais T_1 usando um método de mínimos quadrados. A cabeça foi segmentada em três compartimentos: pele, crânio e fluido cerebroespinal. Tal segmentação foi feita usando o método de elementos de contorno (*Boundary Element Method - BEM*) disponível no software Curry (Neuroscan, EUA).

Delineamento Experimental

No experimento principal, o EEG e a RMf foram registrados simultaneamente. Os estímulos foram enviados baseados no mesmo método das escadas usado no teste comportamental. Para a aquisição das imagens foi usada a técnica esparsa para se evitar contaminação da resposta BOLD pelo ruído acústico vindo do escaner. Outra vantagem do escaneamento esparso é limitar os trechos do EEG contaminados pelo chaveamento

dos gradientes magnéticos durante a aquisição das imagens. Os dados da ressonância magnética funcional foram coletados usando-se um escaner Shimadzu Marconi's Magnex Eclipse 1.5T PD250. Para registro das imagens funcionais foi usada uma sequência eco-planar (EPI) ponderada em T_2 com tempo de excitação (TE) de 48 ms e ângulo de rotação (*flip angle*) de 90°. Foram produzidos, continuamente, 165 volumes em 16,5min, sendo cada volume composto por 20 fatias axiais com voxels de dimensões 4x4x5mm e um espaçamento (gap) de 1mm entre fatias. O tempo de repetição (TR) era de 6 segundos e o tempo de aquisição 2 segundos. A apresentação dos estímulos deu-se nos períodos de 4 segundos de "silêncio". As imagens dos dois primeiros volumes de cada sessão foram descartadas para se evitar efeitos de saturação magnética. Ao final do experimento foram coletadas imagens estruturais ponderadas em T_1 que seriam, posteriormente, usadas como referência no alinhamento das imagens funcionais coletadas em múltiplas sessões.

O experimento era composto por duas condições: auditiva e visual. Trechos referentes à mesma condição experimental foram agrupados em blocos compostos por 18 sequências de 10 estímulos (cinco estímulos auditivos e cinco estímulos visuais) com duração total de 120 segundos. Os estímulos auditivos e visuais eram intercalados na sequência, separados por intervalos pseudo-aleatórios variando de 150 a 175 ms. Cada bloco era iniciado com uma instrução posicionada no centro da tela, a uma distância de 40 cm dos olhos do participante. Dependendo do que era mostrado (imagem de uma orelha para a condição auditiva ou um olho para a condição visual), o participante deveria prestar atenção no estímulo auditivo ou visual. Cada instrução durava quatro segundos na tela. A ordem das tarefas era intercalada entre sessões e também entre participantes. Os estímulos eram apresentados durante os quatro segundos de silêncio entre períodos de escaneamento. Anterior à sequência de 10 estímulos (cinco auditivos e cinco visuais) havia um período basal (*baseline period*) de 650 ms a 800 ms. Após cada sequência, aparecia uma cruz verde na tela e o participante deveria indicar se havia ou não um sinal desviante inserido na sequência. Caso a resposta estivesse correta, aparecia uma imagem de uma face feliz e se a resposta estivesse incorreta, aparecia uma face triste. Havia também um período de repouso após o aparecimento da instrução assim como ao final de cada bloco. A Figura 1 apresenta um esquemático do experimento. O registro total consistiu de quatro sessões de oito blocos cada (quatro blocos onde a atenção era direcionada ao estímulo auditivo e quatro blocos onde a atenção era direcionada ao estímulo visual) totalizando 144 trechos por condição para cada sessão, com intervalos curtos de repouso entre sessões. Neste experimento, a condição de não-atenção ao estímulo (auditivo ou visual) foi atingida direcionando-se a atenção do participante à outra modalidade também sendo apresentada.

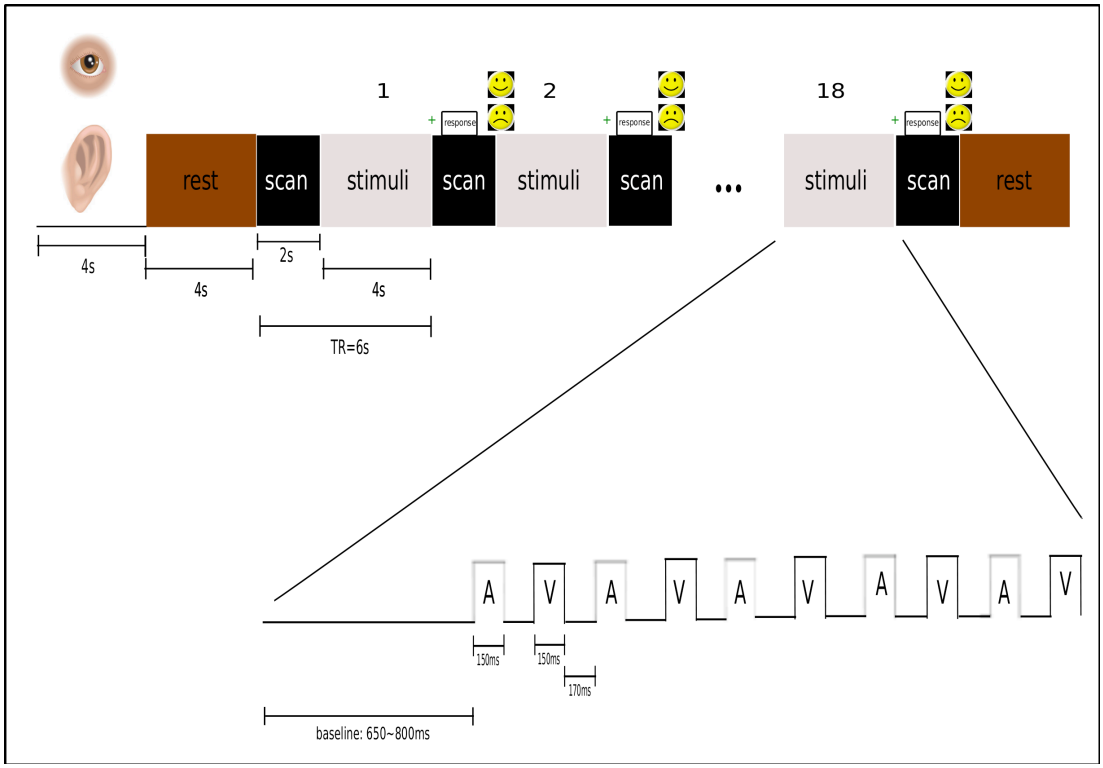

Figura 1: Esquemático do experimento.

Registro do EEG

O EEG foi registrado simultaneamente ao experimento, de modo contínuo, usando um sistema de registro compatível com ressonância magnética (*Brain Amp MR+fMRI-compatible*) e um capacete com 64 eletrodos. Os potenciais registrados tinham como referência o centro do escalpo (Cz). A atividade ocular foi monitorada com um eletrodo posicionado abaixo do olho esquerdo. Foi feito também o registro simultâneo do eletrocardiograma. A resistência de cada eletrodo foi mantida inferior a 5kΩ e os dados foram digitalizados a 5kHz por canal.

Análise das imagens funcionais

A análise foi realizada usando o SPM2 (Wellcome Trust Centre for Neuroimaging, UK). O pré-processamento foi feito nas imagens funcionais e anatômicas usando-se o seguinte procedimento: correção do tempo de aquisição (*slice timing*), correção do movimento, normalização e suavização. As imagens funcionais de cada participante foram coregistradas às imagens estruturais T_1 dos mesmos. As imagens foram normalizadas espacialmente em relação a um padrão anatômico definido por uma imagem ponderada em T_2 do MNI (Montreal Neurological Institute). A reamostragem foi feita a cada 3 mm usando interpolação *sinc*. Finalmente, as imagens funcionais foram suavizadas com um

kernel gaussiano com FWHM (full-width half maximum) igual a 8 mm. A ativação cerebral durante as condições experimentais eram estimadas usando-se a RMf relacionada a eventos, utilizando o início de cada evento (*onset time*) no modelo linear (*general linear model*). Os mapas paramétricos estatísticos foram gerados para cada participante em cada condição experimental: resposta auditiva na tarefa auditiva (atenção ao estímulo), resposta auditiva na tarefa visual (não atenção ao estímulo) e repouso. A ativação significativa de um voxel foi determinada usando-se a estatística-t com limiar de audição $p<0{,}005$, não corrigido. A fim de localizar as regiões cerebrais envolvidas em demandas de atenção, a ativação nas condições de atenção e não atenção foram constrastadas diretamente. Em seguida, foi usada uma medida da alteração do desempenho do participante como um indicador de aprendizagem, usando-se a diferença entre os limiares de percepção no início e ao final de cada sessão como regressores no modelo linear. Para se levar em consideração a variabilidade entre participantes, a matriz de projetos foi ponderada, durante a análise de segundo nível, com o ganho total de cada participante.

Processamento dos dados do EEG

Neste trabalho o método de subtração de artefatos proposto por Allen, Josephs, and Turner (2000) foi usado para remover os ruídos dos gradientes provocados pelo chaveamento dos gradientes magnéticos. Esta abordagem assume que o formato do artefato é constante ao longo do tempo e aditivo ao sinal fisiológico. Em sequência, a análise em componentes independentes (ICA) foi usada nos trechos do EEG após remoção do período basal (650 ms antes e 3075 ms após o início do estímulo) para remoção dos artefatos balistocardiográfico, ocular e relativos ao movimento (Jung, Makeig, Humphries, Lee, and Mckeown, 2000; Callan, Callan, Kroos, and Vatikiotis-Bateson, 2001). As componentes independentes (IC) que correspondiam a fontes de artefatos foram identificadas verificando-se a correlação cruzada entre cada componente, o canal de eletrooculograma (EOG) e o canal de eletrocardiograma (ECG), registrados simultaneamente com os canais neuronais. O limiar necessário para se considerar correlação era $r>0{,}3$. Tendências anormais (*drifts* lineares) foram removidas usando-se um polinômio de primeira ordem calculado por meio de uma regressão linear ajustada à cada sessão do EEG. Os dados (no domínio das componentes) foram ajustados a uma linha reta cuja inclinação máxima aceitável era de 0,5. Os trechos rejeitados apresentavam $R^2 > 0{,}2$.

O método variacional Bayesiano foi usado para restringir as soluções inversas do EEG a regiões onde a ressonância funcional indicava intensa ativação hemodinâmica.. Para a estimação, os dados do EEG foram divididos em janelas de 600 ms com sobreposição de 85%. A informação a priori de cada janela temporal foi dada pela atividade de RMf correspondendo ao estímulo apresentado durante aquele intervalo de tempo. Os hiper-

parâmetros foram ajustados em m_0=100 e γ_0=100. A estimação da variância da corrente foi feita usando-se as sequências temporais de todos os trechos. As atividades de RMf individuais de cada participante para todas as condições experimentais (atenção e não-atenção ao estímulo auditivo) foram usadas como restrição à posição das fontes de correntes. Para a estimação da fonte de corrente, foi usado um filtro Bayesiano inverso em três áreas de interesse que foram determinadas usando-se uma máscara com o contraste de aprendizagem.

Resultados e discussões

Dados comportamentais

Os dados comportamentais coletados durante o experimento apresentaram uma tendência decrescente exponencial, quasi-linear nos limiares de percepção de frequência (r=0,99, p=0,0041). A Figura 6.3(a) apresenta a média geral e o erro padrão de 11 participantes enquanto a Figura 6.3(b) mostra o ganho entre as sessões

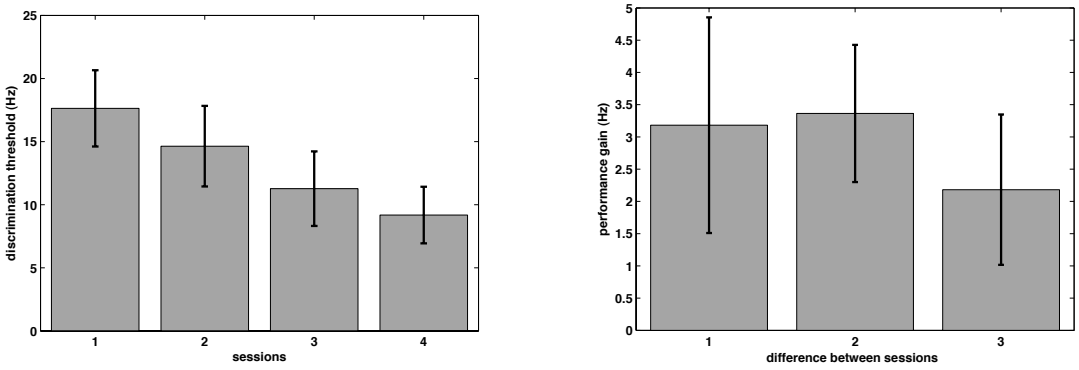

(a) (b)

Figura 2: Dados comportamentais registrados durante o experimento. (a) Média geral e erro padrão de 11 participantes para o limiar de percepção ao final de cada sessão. (b) Média do ganho de desempenho (em Hz) entre as sessões de 11 participantes ($1^a - 2^a, 2^a - 3^a, 3^a - 4^a$).

RMf

Os resultados da ressonância magnética para o contraste atenção ao estímulo auditivo versus a condição de repouso mostra ativação nos córtices temporal, frontal e parietal. Este componente frontal não é visto quando o participante não está atento ao estímulo auditivo, mas sim ao estímulo visual. Neste caso, as ativações ocorreram nos córtices parietal, occipital e temporal conforme resumo na Tabela 6.2. É possível observar que os

cortices temporais esquerdo e direito estavam sempre ativados como resultado da constate estimulação auditiva. Observa-se também que a resposta occipital é mais forte quando o participante presta atenção ao estímulo visual. Os mapas paramétricos estatísticos para estas condições estão apresentados na Figura 6.5 (p<0,05 FDR corrected). Verifica-se uma ativação constante dos córtices parietais em ambas as condições, devido ao fato do participante estar constantemente pressionando um botão.

Tabela 1: Áreas ativadas durante tarefas de atenção auditiva e visual.

	Parietal	Temporal	Frontal	Occipital
Contraste auditivo vs. repouso	X	X	X	
Contraste visual vs. repouso	X	X		X

Além disso, pretendíamos avaliar a influência da atenção na tarefa sendo executada e para isso foi feito um constraste direto entre as condições de atenção e não atenção. Quando se está interessado em áreas específicas de ativação, pode-se restringir a correção para comparações múltiplas a estes pequenos volumes de interesse. A Figura 6.7 mostra o efeito da atenção, com atividade considerável no giro frontal esquerdo (-45,24,24; p<0,05 correção SVC), giro temporal superior esquerdo (-57,-51,6; p<0,05 correção SVC) e giro temporal superior direito (57,-33,3; p<0,05 correção SVC). A análise SVC foi baseada em coordenadas dadas por trabalhos encontrados na literatura sobre demandas de atenção (Zhang, Feng, Fox, Gao, and Tan, 2004; Kiehl, Laurens, Duty, Foster, and Liddle, 2001a; Zatorre, Mondor, and Evans, 1999).

O efeito da aprendizagem foi estudado para cada participante usando-se o ganho no desempenho individual em cada sessão na matriz de projeto. A diferença entre os limiares de percepção final e inicial foi usada na análise de primeiro nível, como contraste em cada coluna da matriz de projeto. Para a análise em segundo nível, as diferenças entre participantes foram levadas em consideração usando-se o ganho de desempenho total (ganho final após todas as sessões) como peso na matriz de projeto. Os resultados são apresentados na Figura 6.8. A correção em pequenos volumes foi feita em volumes de interesse (VOI) de 3x3x3mm. Foram observadas atividades na região frontal esquerda (-45,15,36; p<0,05; correção SVC), temporal esquerda (-57,-51,24; p<0,05; correção SVC) e temporal direita (60,-39,15; p<0,05; correção SVC). Os dados acima sugerem que a atenção pode estar envolvida e provavelmente contribui para um melhor desempenho das atividades neurais específicas em treinamentos de curta duração. Estudos anteriores sobre atenção auditiva seletiva (Neelon, Williams, and Garell, 2006; Kiehl, Laurens, Duty, Foster, and Liddle, 2001a) demonstraram melhorias relacionadas a diversas tarefas auditivas, com modulações ocorrendo a 20-50ms do início da estimulação. A fonte neural desta modulação está localizada na parte posterior do giro temporal superior. O achado deste tipo de resposta para

a condição de atenção sugere a existência de uma plasticidade cortical rápida. Verifica-se também que as ativações nas regiões frontal e temporal são consistentes com a hipótese de envolvimento da região frontal com a predição e modulação de cima para baixo (*top-down*) da atenção seletiva que dá origem à aprendizagem perceptiva auditiva. Embora alguns estudos apresentem efeitos da atenção nos córtices auditivo primário e secundário (Grady, van Meter, Maisog, Pietrini, Krasuski, and Rauschecker, 1997), Petkov, Kang, Alho, Bertrand, Yund, and Loods (2004) mostraram efeitos de atenção auditiva em áreas associativas de ordem superior quando uma modalidade é atendida e outra é ignorada. Estes resultados são consistentes com nossos achados no córtex temporal superior. Como a atenção é bastante dependente da tarefa sendo executada, o conhecimento exato das condições na quais os córtices direito ou esquerdo são ativados é contraditório e necessita de uma investigação mais profunda (Eichele, Specht, Moosmann, Jongsma, and Quiroga, 2005; Doeller, Opitz, Mecklinger, Krick, Reith, and Schröger, 2003).

EEG e RMf

Em cada região de interesse (frontal esquerda [IFG: -45,15,36], temporal esquerda [LSTG: -57,-51,24] e temporal direita [RSTG: 60,-39,15]) dipolos de corrente foram selecionados em um raio de 3 mm do pico de corrente estimado. Com o objetivo de investigar oscilações neuronais, foi empregada uma análise tempo-frequência em cada um dos dipolos de corrente, o que denominamos de análise referente à tarefa (blocos com desvios auditivos versus blocos com desvios visuais). Estudos mais recentes têm trabalhado com diferentes respostas de estruturas neurais, que são específicas em frequência, em termos de sincronismo e desincronismo (ERS/ERD). A quantificação dos ERS/ERD no tempo e no espaço tem sido investigada de forma intensiva, mostrando que estas respostas estão relacionadas funcionalmente ao processamento cognitivo (Basar, 2004; Basar and Schürmann, 2001; Pfurtscheller and Lopes da Silva, 1999).

As amplitudes dos picos de corrente foram promediadas não se importando com a fase. Este procedimento realçou alterações no EEG relacionadas ao estímulo em fase (i.e. potenciais relacionados a eventos) e fora de fase (i.e. sincronismo e desincronismo relacionado a eventos) com o início do estímulo. A análise tempo-frequência nas três áreas revelaram diferentes padrões de ativação para cada participante. A Figura 6.18 mostra a estatística-t de 11 participantes na condição "atenção x não atenção" nas regiões IFG, LSTG e RSTG, respectivamente. Nos testes estatísticos a hipótese nula era de média zero. As respostas na região LSTG são mais espalhadas que em RSTG, a qual concentra-se em 10 a 20Hz (bandas alfa e beta). A resposta em IFG tem um pico em torno de 200ms, ocorrendo mais tardiamente que nos cortices temporais, como era esperado. Neste trabalho também foi apresentado o método hierárquico Bayesiano proposto por Sato, Yoshioka,

Kajiwara, Toyama, Goda, Doya, and Kawato (2004) aplicado a eletroencefalografia em vez de magnetoencefalografia. Embora a eficiência deste método já tenha sido relatada em um experimento visual (Yoshioka, Toyama, Kawato, Yamashita, and Nishina, 2008) e percepção de fala (Callan, Callan, Gamez, Sato, and Kawato, 2010) usando-se MEG, esta foi a primeira implementação com EEG. Com este procedimento incorporamos os dados de EEG e RMf registrados simultaneamente para estimar os padrões espaço-temporais de ativações cerebrais de uma tarefa de discriminação de frequências. O papel da atenção pode ser observado nas respostas tardias das correntes na região IFG se comparadas ao STG (Figura 6.18). Embora nestes cortices as respostas ocorrem antes e com valores de amplitude mais elevados (o que pode ser visto como um processo de baixo para cima), a resposta frontal ocorre aproximadamente 200 ms na banda beta (14-28 Hz) durante a condição de atenção versus a condição de não atenção, o que evidencia o efeito de atenção. Neste caso, é provável que os participantes tenham aprendido a prestar mais atenção ao estímulo, como parte de sua experiência de aprendizagem na tarefa. Um dos resultados mais interessantes deste trabalho vem da análise de localização das fontes, mostrando que a plasticidade também manifesta-se como um aumento na energia das bandas beta (14-28 Hz) e gama (30-70 Hz).

Para se verificar a aprendizagem ocorrida, testamos o coeficiente de correlação entre os resultados da análise tempo-frequência ($p<0,01$) em cada imagem das respostas relativas à condição atenção e os limiares de percepção do teste comportamental para cada participante. Os resultados da análise de grupo são mostrados na Figura 6.19. A evidência da ocorrência de uma correlação foi posteriormente investigada. O sinal foi separado em cinco faixas de frequência: delta, teta, alfa, beta e gama (0.5-3.Hz, 4-7Hz, 8-13Hz, 14-28Hz, 30-70Hz) e a energia de cada banda foi calculada em cada trecho. Os coeficientes de correlação apresentados na Tabela 6.6 são suficientes para sugerir uma correlação, especialmente nas bandas gama e beta.

Tabela 2: Coeficientes de correlação entre a transformada de Fourier do sinal de EEG e os limiares de percepção do teste comportamental, para cada participante. A energia de cada banda foi calculada e a correlação testada com os dados comportamentais. Esta tabela apresenta os coeficientes de correlação para $p<0,05$. Valores inferiores foram zerados.

Subject	LIFG					LSTG					RSTG				
	delta	teta	alfa	beta	gama	delta	teta	alfa	beta	gama	delta	teta	alfa	beta	gama
1	0	0	0	0	-0.29	0	-0.24	0	0	0	0	0	0	-0.25	0
2	0	-0.35	-0.43	0	0.52	0	0	0	0.41	0.22	0	0	0	0.42	0.32
3	0	0.23	0	0.33	0	0	0	0.35	0.39	0	0	-0.22	0	0.35	0
4	0	0	0	0.23	0.30	0	0	0.21	0	0	0	0	-0.23	0	0
5	0	0	0	0.77	0.68	0	0	0.39	0.73	0.77	0	0	0	0.73	0.77
6	0.32	0.35	0.51	0.21	0.28	0.24	0.32	0	0	0	0.32	0.36	0.54	0.26	0.40
7	0	0	0.46	0	0.28	0	0.21	0.2	0	-0.2	0	0.21	-0.43	0	0.47
8	0	0	0	0.44	0.26	0	0	0	0	0	0	0	0	0.43	0.30
9	0	0.22	0	0.29	-0.77	0	-0.49	0	-0.65	-0.76	0	0.22	0	0.29	-0.77
10	0	0	0	0	0.25	0	0	0	0	0.22	0	0	0	0	0.26
11	0	0	-0.41	-0.38	0	0	0	-0.41	-0.38	0	-0.23	-0.30	-0.50	0	0.72

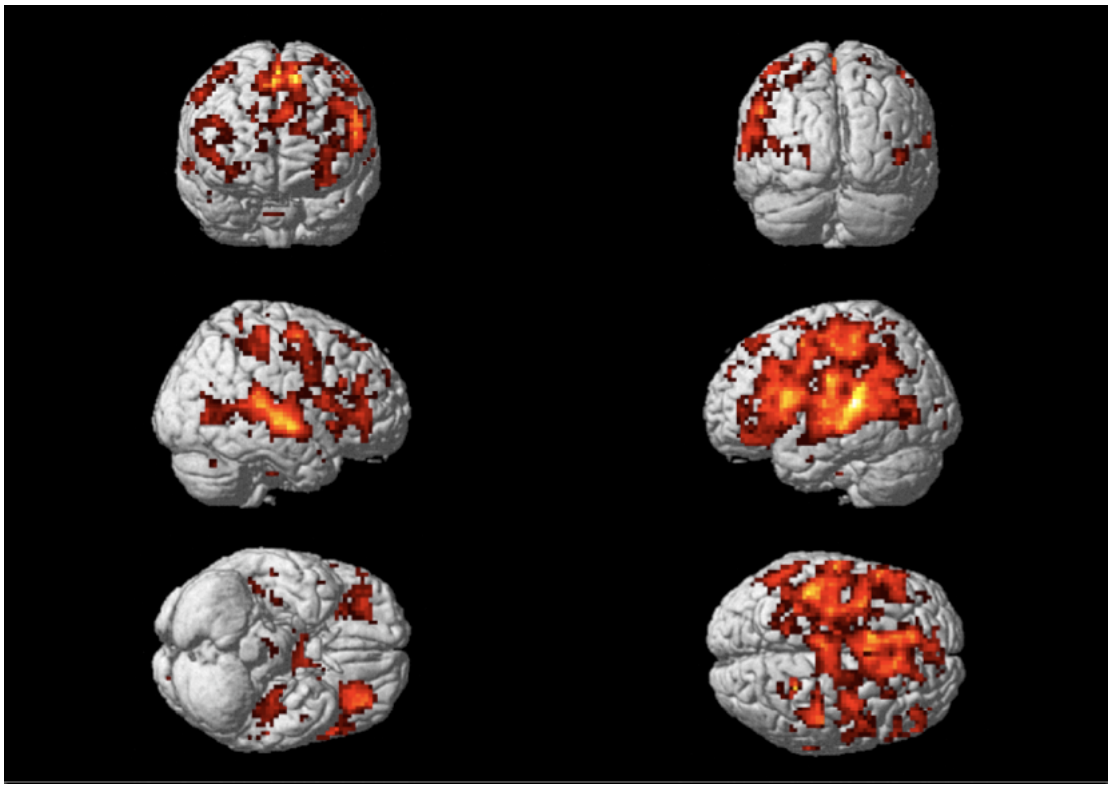

(a) Tarefa auditiva comparada a período de repouso.

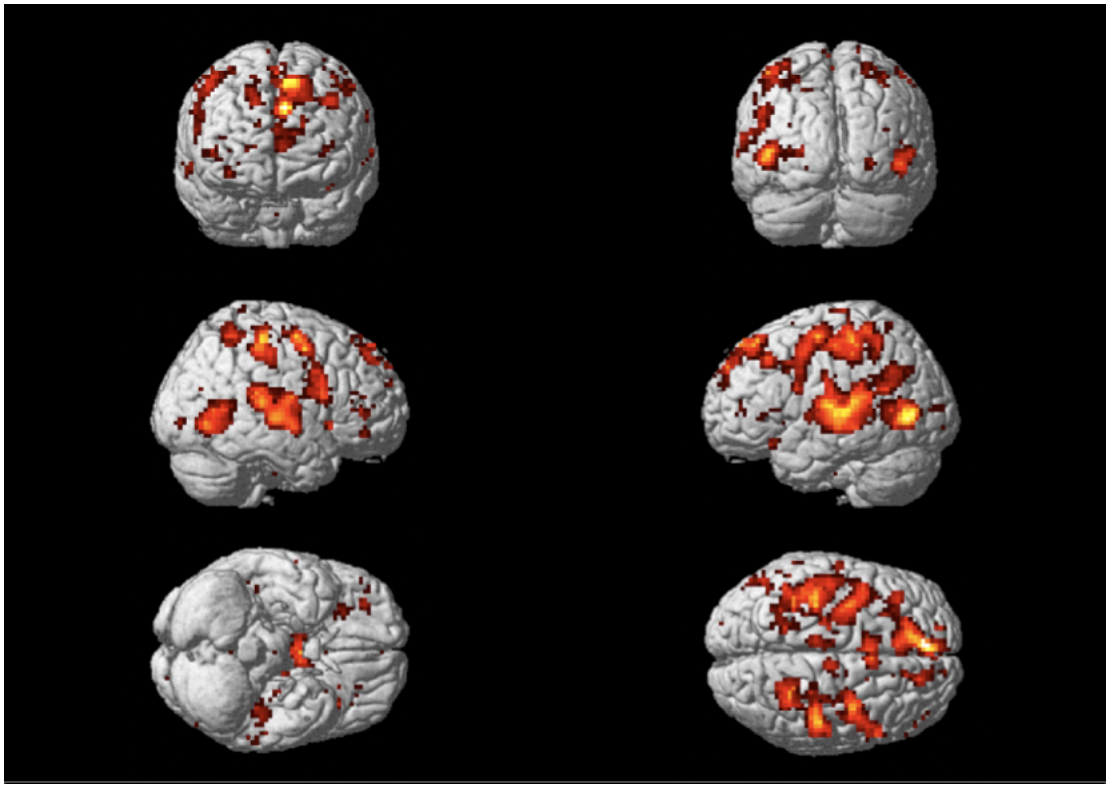

(b) Tarefa visual comparada a período de repouso.

Figura 3: Resultado da análise de efeitos aleatórios (*random effects*) (p_{FDR}<0,05).

Figura 4: Efeito da atenção (p<0,05, correção SVC). A correção SVC é feita em um pequeno volume.

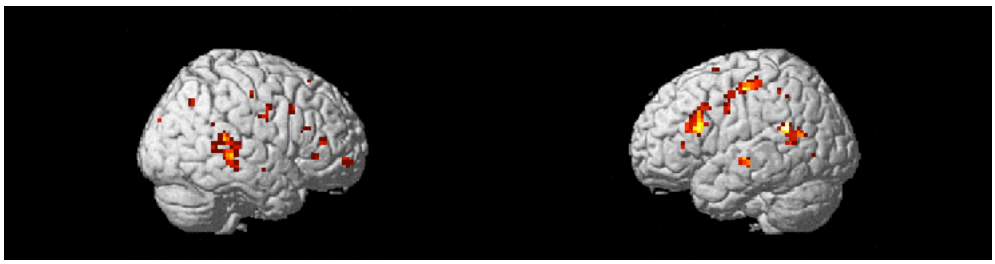

Figura 5: Contraste de aprendizagem. Ativações com p<0,005.

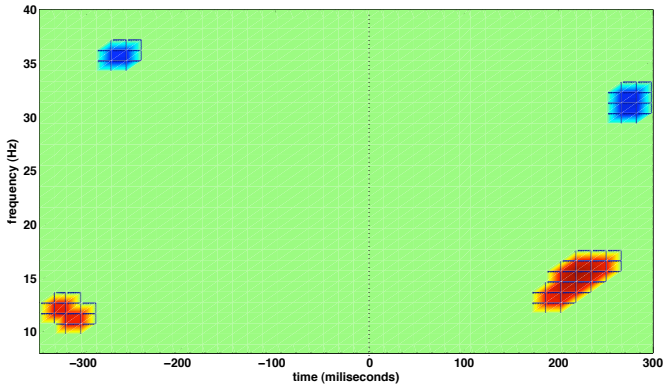

(a) IFG

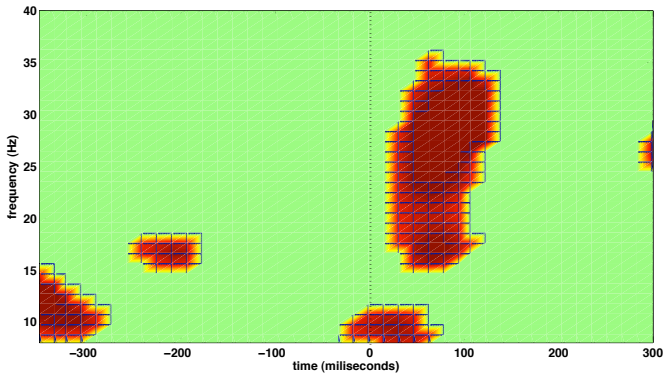

(b) LSTG

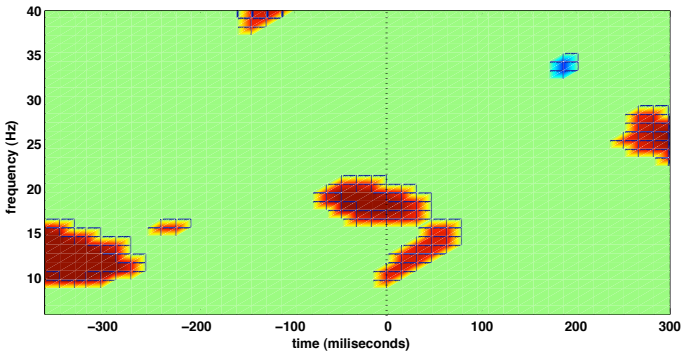

(c) RSTG

Figura 6: Testes estatísticos realizados na representação tempo-frequência dos picos de corrente nas três regiões analisadas. O teste-t (p<0,05) foi feito nas imagens dos 11 participantes (10 graus de liberdade). A análise tempo-frequência foi feita no pico de maior intensidade nas regiões a) IFG, b) LSTG e c) RSTG. Em vermelho: estatística superior à hipótese nula de média zero. Em azul: estatística inferior à hipótese nula de média zero. A figura mostra a condição "trechos com respostas auditivas versus visuais" (condição de atenção versus condição de não-atenção).

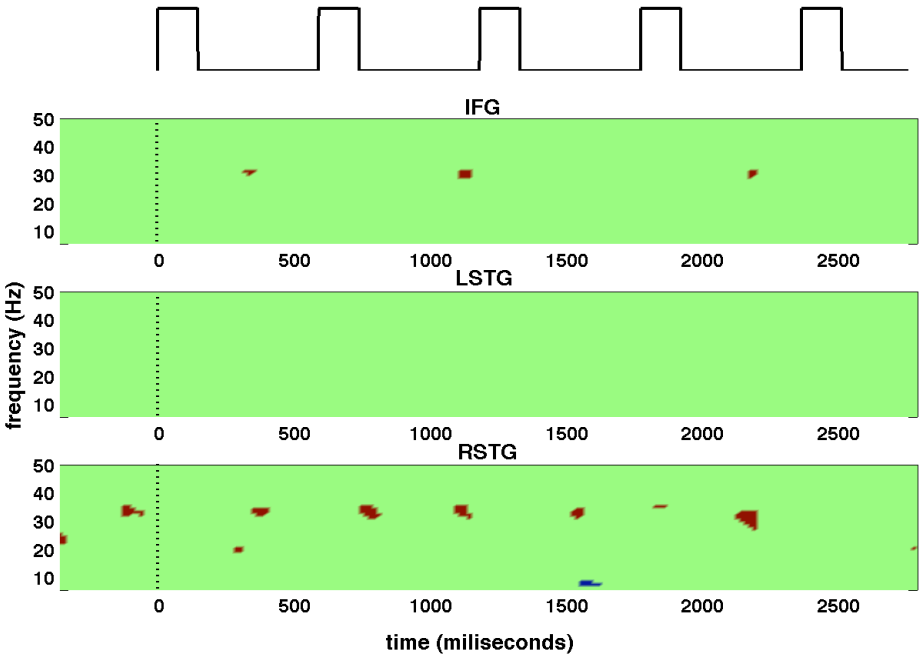

Figura 7: Correlação entre o resultado da análise tempo-frequência e os limiares de percepção do teste comportamental. Estatítica-t da tarefa auditiva dos 11 participantes. 11 amostras foram testadas contra a hipótese nula de média zero em cada faixa tempo-frequência. Os resultados são mostrados para o IFG, LSTG e RSTG. No topo, o instante inicial do estímulo auditivo.

Conclusão

Este trabalho explora a vantagem do registro simultâneo de eletroenfalografia e ressonância magnética funcional para investigar a atividade neural durante a aprendizagem perceptiva de curta duração. A ressonância magnética funcional tornou-se uma técnica padrão para o mapeamento da atividade funcional. Sua alta resolução temporal permite que áreas ativadas sejam localizadas com resolução milimétrica. Entretanto, a neurociência cognitiva vai além da localização anatômica de estruturas neurais e os potenciais relacionados a eventos podem ser bastante úteis na investigação de mecanismos cognitivos e seus substratos neurais. A técnica permite a detecção de alterações neurais na ordem de milisegundos. Portanto, diversos esforços têm sido feitos para integrar a informação proveniente da RMf e do EEG e prover uma técnica alternativa de imageamento que configure uma alta resolução espaço-temporal. Além disso, o registro simultâneo de EEG e RMf implementado nesta tese, forma um *setup* mais realístico para a investigação de fenômenos cognitivos. Estes dados foram combinados em um modelo Bayesiano variacional para localização das fontes que geraram os ERPs registrados.

A complexidade do experimento foi abordada nesta tese, sendo os artefatos tratados cautelosamente. O impacto do sistema de registro eletrofisiolgico nas imagens de ressonância foi visto especialmente na qualidade destas imagens, quando os participantes usavam o capacete de eletrodos dentro do escaner. Apesar disso, as imagens ainda eram adequadas para o procedimento de segmentação. Os registros de EEG também foram fortemente afetados pelo processo de aquisição da RM. Neste caso foram usados métodos de subtração para remoção dos artefatos de gradiente e ICA para remoção dos demais artefatos (cardíaco, musculares, etc.).

Esta tese teve como objetivo investigar se o treinamento rápido pode evocar respostas corticais e até que ponto isso pode acontecer. Os resultados obtidos sugerem que as pessoas podem melhorar rapidamente seu desempenho em identificar sons desviantes embutidos em sequências com sons padrão. Esta melhoria rápida no desenvolvimento da tarefa é acompanhada de alteraçes plásticas no córtex sensorial assim como em áreas superiores conforme as evidências encontradas pelas atividades realçadas das respostas sensoriais. Além disso, a correlação entre a resposta tempo-frequência do potencial relacionado a eventos e os resultados comportamentais dão suporte à nossa hipótese de ocorrência de aprendizagem durante treinamento de curta duração.

List of Symbols

ω	Larmor frequency
$\mathbf{B_0}$	magnetic field
γ	gyromagnetic constant
T_1	longitudinal relaxation
T_2	transversal relaxation
$\mathbf{M}$	transformation matrix
$\mathbf{R}$	rotation matrix
$\mathbf{T}$	translation matrix
ϕ, φ and ψ	rotation angles
I(**f**,**g**)	mutual information between images **f** e **g**
H(f,g)	entropy of the joint probability distribution
H(f)	marginal entropy of **f**
H(g)	marginal entropy of **g**
p(f,g)	joint distribution probability
θ	deformation parameters that map the image onto a template
$p(\theta\|y)$	posterior probability of parameter θ given the data y
$\hat{\beta}$	estimated parameters of the linear model
α	level of significance of the statistical hypothesis
P^{FWE}	probability that one or more values is greater than α
Z_t	Z score threshold
R	number of resels in a thresholded image
E[EC]	expected value of the Euler characteristic
$\mathbf{u}$	vector containing the time courses of activations of the ICA components
$\mathbf{x}$	vector containing the EEG signals recorded at different electrodes
$\mathbf{W}$	weight matrix of the ICA decomposition
X	design matrix

m_0	variance magnification
γ_0	confidence parameter
$\rho_{X,Y}$	correlation coefficient between X and Y
K_e	number of voxels in the cluster
T	height threshold in the statistical parametric map
R^2	R-squared measure of fitting
μ_0	permitivity of free space
$\mathbf{J}(\mathbf{r'})$	current flow at location r'
$\mathbf{J^P}(\mathbf{r'})$	primary current flow
$\mathbf{J^v}(\mathbf{r'})$	volume current flow
$\sigma(\mathbf{r'})$	conductivity of the head tissue
$\mathbf{V}(\mathbf{r'})$	electric potential
$\nabla\mathbf{V}(\mathbf{r'})$	gradient of the electric potential
V_0	potencial due to the primary current
δ	Dirac delta function
q	electric moment
$\mathbf{A}$	diagonal matrix of current inverse variance parameters
$\Gamma(\alpha \mid \bar{\alpha}, \gamma)$	gamma distribution with mean $\bar{\alpha}$ and γ degrees of freedom
$\gamma_{0n\alpha}, \bar{\alpha}_{0n}$	hyperparameters of the prior distribution
$\bar{\alpha}_{0n}^{-1}$	prior mean variance
$\sum_{\alpha}^{-1}$	current covariance matrix

List of Abbreviations

2D	Two Dimensional
AEP	Auditory Evoked Potential
ANC	Adaptive Noise Cancelling
ASA	Auditory Scene Analysis
BAEP	Brainstem Auditory Evoked Potential
BEM	Boundary Element Method
BCG	Ballistocardiogram
BOLD	Blood Oxygen Level Dependent
CNS	Central Nervous System
CSF	Cerebrospinal Fluid
EC	Euler Characteristic
ECG	Electrocardiogram
EEG	Electroencephalography
EPI	Echo Planar Imaging
ERD	Event Related Desynchronization
ERP	Event Related Potential
ERS	Event Related Synchronization
ERSP	Event Related Spectral Perturbation
EPSP	Excitatory Postsynaptic Potential
EP	Evoked Potential
FDR	False Discovery Rate
FID	Free Induction Decay
FWE	Family Wise Error
FWHM	Full Width Half Maximum
GLM	General Linear Model
HRF	Hemodynamic Response Function

IC	Independent Component
ICA	Independent Component Analysis
IFG	Inferior Frontal Gyrus
IPSP	Inhibitory Postsynaptic Potential
ISI	Interstimulus Interval
ITPC	Intertrial Phase Coherence
LFP	Local Field Potential
LLAEP	Long Latency Auditory Evoked Potential
LSTG	Left Superior Temporal Gyrus
MEG	Magnetoencephalography
MLAEP	Medium Latency Auditory Evoked Potential
MMN	Mismatch Negativity
MR	Magnetic Resonance
MRI	Magnetic Resonance Imaging
OBS	Optimal Basis Set
PCA	Principal Component Analysis
PET	Positron Emission Tomography
RSTG	Right Superior Temporal Gyrus
RF	Radio Frequency
RFT	Random Field Theory
ROI	Region Of Interest
SEP	Somatosensory Evoked Potential
SNR	Signal to Noise Ratio
SPM	Statistical Parametric Map
STFT	Short Time Fourier Transform
SVC	Small Volume Correction
TDD	Template Drift Detection
TA	Time of Acquisition
TE	Time of Echo
TR	Time of Repetition
TTL	Transistor Transistor Logic
VB	Variational Bayesian
VBMEG	Variational Bayesian MEG
VEP	Visual Evoked Potential
VOI	Volume of Interest

Contents

List of Figures

List of Tables

Men ought to know that from the brain, and from the brain only, arise our pleasures, joys, laughter and jests, as well as our sorrows, pains, griefs and tears.

Hippocrates, Fifth Century B.C

1 Introduction

The brain is capable of reorganisation. Although firmly established recently, this concept was unthinkable 20 years ago. As new skills are learned or novel experiences acquired, brain cells alter the way in which they respond to the outer environment to reflect the circumstances of the changing. This is called plasticity.

There is an accumulating body of evidence indicating that neuronal functional specificity to basic sensory stimulation is mutable and subject to experience. One way to look at this plasticity refers to perceptual learning which is an improvement in sensory discrimination after a period of practice usually varying from days to weeks (Polley, Steinberg, and Merzenich, 2006; Moore, Amitay, and Hawkey, 2003; Demany, 1985; Watson, 1980). Behavioral studies show that the effects of perceptual learning can be highly specific to the trained stimulus features, suggesting that the lack of generalization is taken as evidence that learning might be mediated by cells in sensory areas (Polley, Steinberg, and Merzenich, 2005). Although it is well accepted that neuroplasticity occurs following extended training, there is still much to investigate about the neural substrates underlying early and rapid improvements in task performance taking place within the first hour of training (Alain, Snyder, He, and Reinke, 2007). Hawkey, Amitay, and Moore (2004) showed that perceptual learning can be assessed in rapid early performance rather than procedural learning as someone might argue. van Wassenhove and Nagarajan (2007) also show that enhanced perceptual discrimination is predicted to result in greater brain ac-

tivity in the modality specific cortex of the perceptual event as well as in frontal areas responsible for modulating selective attention.

When discussing learning, it is important to understand whether attention based training may play an important role in irrelevant distractor suppression. Several studies have provided evidence of its role in perceptual learning (Yotsumoto and Watanabe, 2008; Paffen, Verstraten, and Vidnyánszky, 2008; van Wassenhove and Nagarajan, 2007) while others have shown evidence of passive learning (Seitz and Watanabe, 2003; Watanabe, Nanez, and Sasaki, 2001) suggesting that attention may not be necessary in learning experience. Although recent findings may seem contradictory at first sight, Seitz and Dinse (2007) gave some insights about how these learning models can operate in parallel with each other.

One way of looking at attentional demands during perceptual learning is through selective attention. Attending to a sound selectively requires a person to listen to targets embedded in complex auditory events. Auditory frequency discrimination has been extensively explored in attention studies especially for its importance in the auditory process underlying complex auditory tasks, such as comprehension and understanding (Petkov, Kang, Alho, Bertrand, Yund, and Loods, 2004; Kiehl, Laurens, Duty, Foster, and Liddle, 2001b). Frequency discrimination requires the identification of a sound with a different frequency among a sequence of "standard" tones and it is questioned whether focused attention enhances this discrimination. Leek and Watson (1984) studied the influences of experimental context and pattern structure on frequency discrimination. They showed that perceptual learning improves frequency discrimination and may even overcome uncertainty effects although high signal uncertainty can decrease performance as stated by Green (1961). Perceptual learning has been extensively investigated in the visual system and is stimulus specific (Schoups, Vogels, and Orban, 1995; Shiu and Pashler, 1992). However, little is known about the mechanisms that initiate this learning, especially in other modalities.

1.1 Scientific question

This work aims to investigate the mechanisms initiating perceptual learning in the auditory system based on two hypothesis: (i) enhanced perceptual discrimination results in greater brain activity in modality specific cortex to the perceptual event and (ii) frontal regions are involved with prediction and top-down modulation of auditory selective attention that gives rise to auditory perceptual learning. The main contribution of the work consists in using multimodal imaging to show the importance of attention in irrelevant stimuli suppression during perceptual learning.

1.2 Study design

The simultaneous recording of electroencephalography (EEG) and functional magnetic resonance imaging (fMRI) and the correspondence between both signals on a trial by trial analysis can be used to provide better understanding about cognitive functions of the human brain. Processing of sensory stimulus features is essential for humans to determine their responses and actions. Therefore, it is important to understand the brain mechanisms of sensory information processing. As a tool for human brain mapping of cognitive functions, the goals of functional brain imaging are mainly to localize groups of neurons involved in some simple cognitive tasks, such as those dealing with perceptual processes, and identifying dynamic links between these groups in order to better understand how signaling is performed in the brain. For this purpose, areas such as physiology, psychology and engineering are brought together to investigate brain functioning.

EEG has long been used as a standard noninvasive technique to study brain functioning. It consists of electrical potentials recorded from electrodes placed over the scalp and gives a temporal resolution on the order of miliseconds. However, its spatial resolution is poor but other neuroimaging methods aim to overcome this lack of information. fMRI is the most established one with a spatial resolution on the order of two milimeters. These techniques can be used as a window of observation for the electric and hemodynamic changes related to cognitive processes. Recording EEG and fMRI simultaneously has the advantage of allowing the comparison of both modalities in the exact same state. As Chapter 2 will discuss, it is of particular interest in terms of habituation, learning and vigilance. Differences in preparation time and task experience can also affect participant's behavior, which can be reflected in brain activity as demonstrated by Ullsperger and von Cramon (2001). Simultaneous fMRI/EEG protocols not only guarantee identical sensory stimulation, perception and behavior, but provide a unique way to study the interaction between intrinsic brain states and event-related processing (Debener, Ullsperger, Siegel, and Engel, 2006).

Moreover, due to spatiotemporal limitations of each technique taken alone, they can be combined (as they are complementary in temporal/spatial resolution) to solve the ill-posed problem of source localization. In this kind of problem, there are more activated sources than actual measurements (electrodes). With data from both modalities, EEG inverse solutions are constraint to regions where fMRI indicates large hemodynamic activation. For this purpose a variational hierarchical Bayesian method (VBMEG) was used (Sato, Yoshioka, Kajiwara, Toyama, Goda, Doya, and Kawato, 2004) in this thesis. This method overcomes problems such as false positive incorporating fMRI information as a hierarchical prior on the current variance distribution, rather than on the variance itself. In this method, the strength of the fMRI constraint can be controlled by the hyperparameters of

the hierarchical prior (Yoshioka, Toyama, Kawato, Yamashita, and Nishina, 2008).

In contrast with the combination of independent measurements of fMRI and EEG (or MEG) data, the simultaneous measurements of fMRI and EEG data carried out in this work form a more realistic setup to combine high spatial resolution data with high temporal resolution data in cognitive experiments. A major difficulty in this procedure is the complexity of the design and the artifacts that happen in both modalities (Yan, Mullinger, Brookes, and Bowtell, 2009; Mullinger, Debener, Coxon, and Bowtell, 2007). The impact of the electrophysiological recording system in the MR image is seen especially in the quality of the image when electrodes or electronic equipment are placed inside the MR scanner. On the other hand, EEG data are highly affected by the image acquisition process. The most prominent artifacts are caused by the alternating magnetic fields of the MR scanner. Besides that, the quality of the EEG is affected by the ballistocardiogram (BCG) which is an artifact predominantly caused by cardiac-related body movement. Robust algorithms for physiological and mechanical artifacts removal have to be implemented. Allen and coleagues developed a template based artifact removal method (Allen, Josephs, and Turner, 2000; Allen, Polizzi, Krakow, Fish, and Lemieux, 1998) from which a variation is used in this work and compared to independent component analysis (ICA) implementations.

The thesis is organized in seven chapters. Chapter 1 contains the introduction and purposes of this thesis. In Chapter 2 the basic theory of the techniques implemented as well as a brief description of the cognitive processes investigated are presented. Chapter 3 describes how electroencephalography is used to investigate neuronal communication as well as the processing done on this type of data. In Chapter 4 fMRI data pre-processing is showed as well as the statistical parametric mapping adopted for testing whether an activation exists in a specific area. Chapter 5 shows the methodology used in the experiments, describing the design of fMRI studies and its combination with EEG recordings. Chapter 6 presents and interprets the results obtained with the tests carried out. Finally, Chapter 7 concludes the study pointing out the main results and giving suggestions of research directions that still need to be investigated. At last, Appendix A describes the hierarchical Bayesian method used in the source estimation procedure.

2

Theoretical Background

An fMRI experiment depends on techniques and methodologies coming from different fields of expertise, making it interdisciplinary. In this introductory chapter, the main issues concerning the theory of magnetic resonance and functional magnetic resonance will be discussed. The principal kinds of noise present in the environment will be briefly introduced as well as how the resultant images are analyzed. Besides fMRI, we will address recent views about the role of brain oscillations, recorded with electroencephalography, specially in attention and perceptual learning.

2.1 Magnetism

The magnetic resonance imaging system includes a superconductive magnet which provides a static magnetic field with high homogeneity inside the bore where the object to be imaged is positioned. The magnetic properties of some nuclei are the key of this technique: biological tissues have water as one of its constituents and most of them have high concentrations of lipids and hydrogen nuclei in it. These nuclei have a magnetic moment due to their spin. The magnetic field of the system makes the magnetic moment of a small percentage of these hydrogen nuclei align with the main magnetic field vector (Mansfield, 1988). Therefore, if a person is lying inside the magnet, each point within his body will have a certain number of protons aligned with the main magnetic field.

These aligned spins produce a bulk magnetization that precesses around the direction of the magnetic field with a specific frequency (the Larmor frequency) which is dependent on the magnitude of the magnetic field and characteristics of the nucleus being imaged according to Equation 2.1.

$$\omega = \gamma B_0, \tag{2.1}$$

with ω units in radians per seconds and magnetic field in Tesla (1T=10^4gauss). γ is a gyromagnetic constant specific to each nuclear species which for the hydrogen is 2.675x10^8 rad/s/T ($\gamma = \gamma/2\pi = 42.576$ MHz/T) (Bernstein, King, and Zhou, 2004).

By applying a radiofrequency (RF) pulse with a frequency matching the precession frequency, the orientation of the spins can be changed until their magnetic moments are perpendicular to the main magnetic field. The process can be seen in Figure 2.1. Removing the RF pulse, the nuclei relax and their magnetization return to the original orientation (equilibrium state). This process induces a voltage in a surrounding electrical circuit which is detected by a coil placed around the area of the object being imaged (perpendicular to the static field). The detected signal (called Free Induction Decay - FID) can be assigned to a specific position by making magnetic field gradients to vary the strength of the magnetic field (and resonance frequency) from point to point. Moreover it depends on the interaction between the spins and the environment (relaxation time) which determines the rate that the signal decays. The strength of the signal depends on the number of spins involved. T_1 and T_2 are characteristic constants defining the longitudinal and transversal relaxation, respectively. T_1 relaxation is the time course for the magnetization to return to its original longitudinal orientation. T_2 relaxation corresponds to the breakdown of the transversal magnetization due to spin-spin interactions (Liang and Lauterbur, 2000).

Two parameters are very important in determining an MRI (Magnetic Resonance Imaging) sequence. The time of repetition (TR) is the time between two RF pulses, that limits the relaxation of the magnetization to occur. The other parameter is the time of echo (TE), which is the time between the application of an RF pulse and the maximum peak of the signal induced in the coil.

Image contrasts are defined according to the T_1 and T_2 times of the tissues involved. A short TR allows shorter T_1 substance to recover its signal between repetitions to a much greater extent than a longer T_1 substance. The contrast in short TR and TE sequences is based on differences in T_1 and are called T_1-weighted images. Increasing TE increases the differences in the T_2 decay curves between substances, increasing the T_2-weighting. Images obtained with long TR and TE are called T_2-weighted.

A gradient echo sequence allows a flip angle lower than 90°, decreasing the amount of

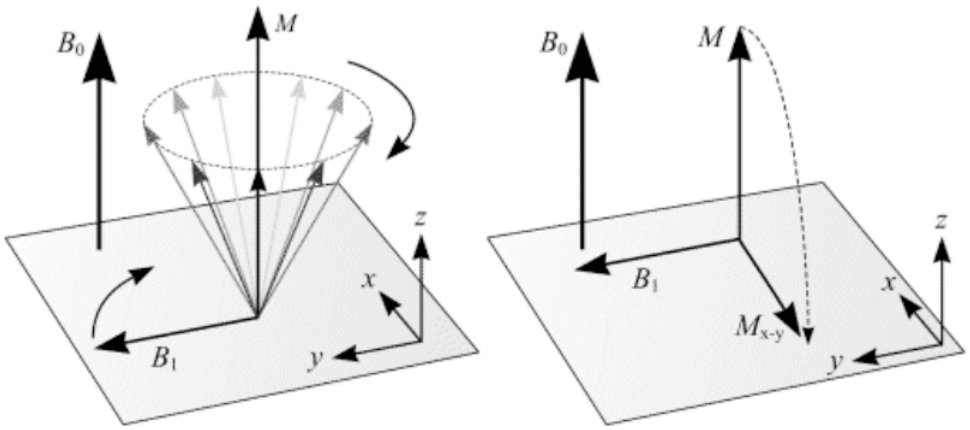

Figure 2.1: Precession of the system with the Larmor frequency after the application of the static field. The magnetization net is aligned with the main field B_0 and precesses with the Larmor frequency. A radio frequency pulse B_1 is applied perpendicularly to B_0, tipping the magnetization to the xy direction.

magnetization tipped into the transverse plane. The consequence is a faster recovery of longitudinal magnetization which allows shorter TR and scan time. This type of sequence is used in the echo planar imaging (EPI) data acquisition strategy. This method acquires the entire MR image rather than a single image line in the k-space (space of coding) after the preparation phase of the pulse sequence. It requires the time to read a single image line to be much smaller than T_2^* (real T_2 plus field inhomogeneities), thus, many lines can be read before the exponential has decayed to half its peak value. For this purpose the system needs to deliver strong gradient fields with fast switching. Coding is done varying the gradient fields in x, y and z directions, which allows plane selection as well. More information about the technique can be found in Liang and Lauterbur (2000); Stehling, Turner, and Mansfield (1991).

2.2 Functional Magnetic Resonance Imaging

The most used imaging method to produce information related to brain function is the BOLD (blood oxygen level dependent). In this method MR images are sensitive to changes of the state of oxygenation of the hemoglobin (Krüger, Kastrup, and Glover, 2001; Ogawa, Lee, Nayak, and Glynn, 1990). As this molecule has different magnetic properties according to the concentration of oxygen it can be used as a "natural contrast". It is a diamagnetic substance when full of oxygen (oxyhemoglobin) and becomes paramagnetic when the amount of oxygen is decreased (deoxyhemoglobin). During a neural activity there is an increase of the consumption of oxygen and it would be expected an augment of the amount of deoxyhemoglobin in the blood and a consequent decrease of the MR

signal. However it is seen an enlarged signal and a decrease of deoxyhemoglobin. This is due to the increase in blood flow and glucose consumption during the neural activity which is higher than the consumption of oxygen. Glucose is being broken down by an anaerobic process, the glycolisis, and as a result there is an increase of the amount of oxygen in the blood nearby (Raichle, 2001). Accordingly, the proportion of deoxyhemoglobin relative to oxyhemoglobin dictates how the MR signal will behave in a BOLD image: areas with high concentration of oxyhemoglobin appear as a brighter signal than areas with low concentration. The events that occur during a neuronal activity produce a complex signal function related to the neuronal stimulus: the hemodynamic response function (HRF). It is a complex signal not related to one specific physiological parameter but to a mix of cerebral blood flow, volume, and cerebral metabolic rate of oxygen (Logothetis, Pauls, Augath, Trinath, and Oeltermann, 2001). The HRF can be modeled as the four main steps below:

1. following a stimulus there is a dip caused by a transient increase of deoxyhemoglobin concentration;

2. it is followed by an increase of the oxy/deoxyhemoglobin ratio leading to high MR signal;

3. if the stimulus is sustained, the signal reaches a plateau;

4. after the cessation of the stimulus, the MR signal returns to the baseline and an undershoot might occur. This is because the regional blood volume normalizes at a slower rate than the changes in blood flow leading to more deoxyhemoglobin concentration.

The signal cited in item 2 is believed to be proportional to the neural activity in a specific area. A sketch can be seen in Figure 2.2. On the other hand it is still unclear how tight this signal is related to the neural activity, but Logothetis and Wandel (2004) and others have shown with electrophysiology measures close correlations between the BOLD signal and local field potentials (LFP). The latter are lower-frequency electrical measures summed over many neurons (Logothetis, Pauls, Augath, Trinath, and Oeltermann, 2001). In their pioneer work they measured the brain electrical activity in monkeys using fMRI and other electrophysiological methods. The experiment consisted in monkeys sitting in a scanner while they watched some checkerboard patterns. The authors saw an increase in the fMRI signal on a small area (in this case the visual cortex) as a direct reflex of the increase in neural activity. This and other studies (Schicker, Muckli, Beer, Wibral, Singer, Goebel, and Röder, 2005) in fact suggest that BOLD may originate less in neuronal spiking and more in low frequency potentials.

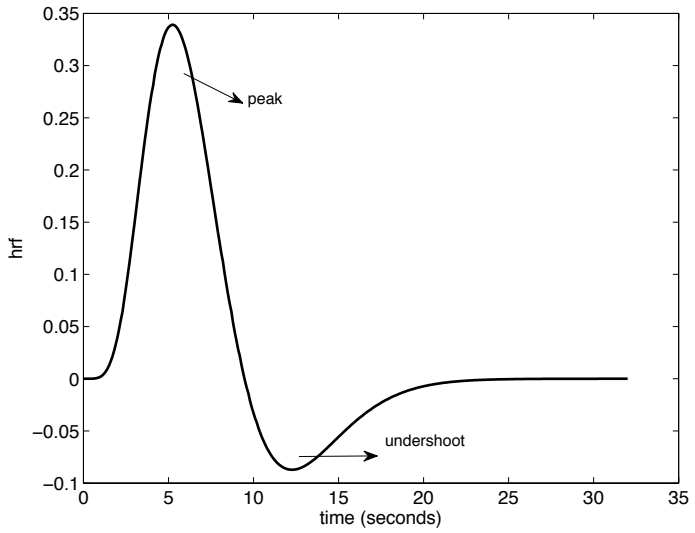

Figure 2.2: An example of an HRF as a response for a brief stimulation.

An important change in human brain mapping happened with the combination of the endogenous contrast mechanism (BOLD) and the rapid imaging technology available (Ogawa, Tank, Menon, Ellermann, Kim, and Merkle, 1992; Bandettini, Wong, Hinks, Tikofsky, and Hyde, 1992). These works showed that the changes in MRI signal intensity within activated cortical areas could be measured by high sensitivity equipments and the dynamics could be accompanied with signal changes occurring only seconds after the neuronal activity onset.

The MRI experiment starts when the subject performs a task inside the scanner while BOLD images of the brain are collected. A brain volume is a set of these images covering the whole brain acquired during 2 to 3 seconds. At the end an image of pixel intensities is formed and compared to a model of the BOLD response relative to the paradigm implemented. The signal changes are statistically tested for significance and viewed as statistical parametric images.

2.3 Paradigms

In fMRI, paradigms are strategies implemented to provoke a response to some kind of stimulation. The brain can be viewed as a system whose impulse response is the HRF. If the system is assumed to be linear (Boynton, Engel, Glover, and Heeger, 1996) and the hemodynamic response to an instantaneous impulse stimulus is found, the real paradigm can be seen as a combination of many stimuli and the hemodynamic response linearly summed (superposition theorem illustrated in Figure 2.3).

To define a paradigm, the experimenter needs to define in advance what he expects

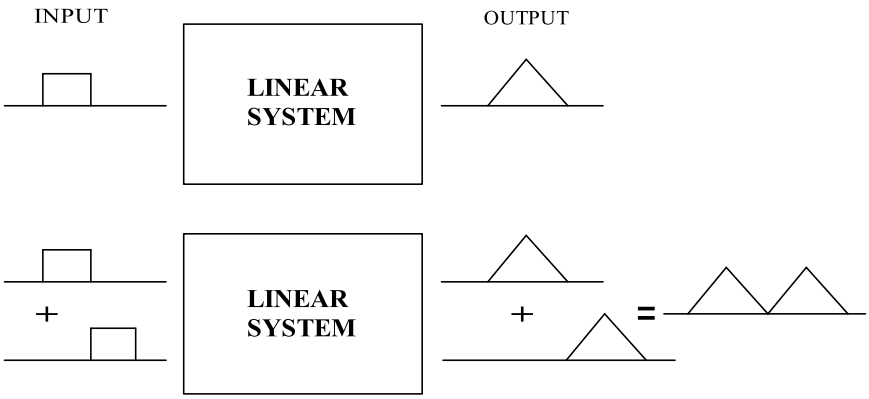

Figure 2.3: A schematic of a linear system. A linear system is one that exhibits the property of superposition: the outputs of a linear combination of input signals is the linear combination of the output of each input isolated.

from the experiment, i.e. the behavioral predictions of cognitive tasks performed by the subjects in the scanner based on the hypothesis under investigation. In this sense, the paradigm is the temporal organization structure of the whole task.

2.3.1 Block Designs

Block designs can implement the subtraction strategy. The origin comes from early PET (Positron Emission Tomography) studies where measurements were taken over periods of time up to 1 min (Amaro Jr. and Barker, 2006) using extended periods of "on" and "off" activations. In this strategy "activity" conditions are contrasted with a "control" condition. The images are analyzed assuming that any BOLD difference, above some statistical level, represents the brain regions involved in a particular task. The block paradigm is still implemented in many situations where the subject maintains a cognitive state in response to the presentation of a sequence of stimuli within a condition (Narayan, Kimberg, Tang, and Detre, 2005). This state is alternated with other moments (or epochs) when a different condition (or a control condition) is presented as shown in Figure 2.4. This paradigm is easy to implement as it does not require randomization of stimuli and careful selection of spacing between stimulus categories. Besides, this technique has advantages such as robustness of results, increased statistical power and relatively large BOLD signal change related to baseline (Amaro Jr. and Barker, 2006; Friston, Zarahn, Josephs, Henson, and Dale, 1999). A scheme is shown in Figure 2.5. Block designs have superior statistical power compared to other experimental designs. This is because the

fundamental frequency of the boxcar can be positioned at an optimal location with respect to the filtering properties of the hemodynamic response function and the low-frequency noise (Aguirre, 2010).

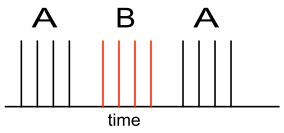

Figure 2.4: Stimuli type A are delivered first followed by stimuli type B.

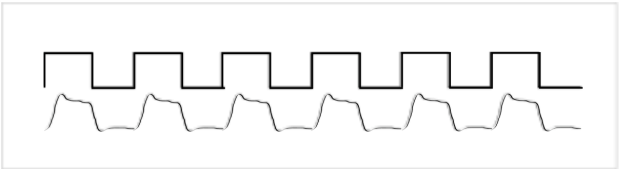

Figure 2.5: Block design: stimuli of the same condition are presented in blocks followed by a control (baseline) condition. The BOLD response is composed of individual HRFs from each stimulus (bottom graph). Adapted from Amaro Jr. and Barker (2006).

2.3.2 Event-Related Designs

Changing from the block design was gradual with studies exploring fMRI responses to brief stimuli. As an example, Ozus, Liu, Chen, Iyer, Fox, and Gao (2000) showed brain activation due to visual stimulus presentation of one second for stimulus rates varying from 1 to 20Hz.

The main characteristic of the event-related paradigm is to allow more flexibility of the design, modelling signal changes associated with individual trials, as opposed to blocks of trials. Hence, it can be used to probe primary sensory and higher-level neuronal function and also permit the linkage with electrophysiological techniques such as EEG. Some practical effects are the randomization of the order of conditions presented (which is very important for learning, memory and other studies) as well as the time between stimulus presentation (Interstimulus interval - ISI). The latter is important to reduce subject's ability to predict the occurrence of a new stimulus (Rosen and Dale, 1998). Whereas BOLD fMRI is insensitive to the particular high frequency alternation between one trial and the next, it is still sensitive to the low frequency envelope of the design. With closely spaced, randomly ordered trials, one is detecting the low frequency consequences of the random assortment of trial types (Aguirre, 2010). A scheme is shown in Figure 2.6.

Event-related designs have been used in studies investigating the responses of infrequent events (McCarthy, Luby, Gore, and Goldman-Rakic, 1997), working memory (Kim,

Matthews, and Park, 2010), attention (Luck, Woodman, and Vogel, 2000) and others.

Figure 2.6: Event related design: each stimulus is detected. The stimuli are presented on the top and the HRFs are shown on the bottom. Adapted from Amaro Jr. and Barker (2006).

A mix of block and event-related designs is also possible. This technique is a mixture of the characteristic block design measurement of repetitive sets of stimuli and the transient responses detected by event-related designs. The researcher have to deal with issues associated with poorer HRF shape estimation (Figure 2.7) although statistical power might be increased.

Figure 2.7: Mixed design: events closely presented are combined with control conditions (top). On the bottom HRF functions. Adapted from Amaro Jr. and Barker (2006).

2.4 Image Acquisition Techniques

The most common imaging technique is the echo planar imaging (EPI) that allows for rapid acquisition where all the information is collected after a single pulse of RF excitation. This technique has a high temporal resolution on the order of a few milliseconds (Stehling, Turner, and Mansfield, 1991). The parameter that controls temporal resolution is the time of repetition (TR) and corresponds to the time between two excitation pulses or the time to collect one brain volume (composed of many slices). However there is a compromise with the spatial resolution. The shorter the TR, the lesser the number of slices collected by TR. Besides, the temporal limit is also imposed by the temporal characteristics of the HRF (Amaro Jr. and Barker, 2006).

The spatial resolution unit in the 3D image is the voxel (volume element) that represents the minimum unit of brain tissue in an image. Ideally speaking, the smaller the

size of the voxel the better the resolution. However, there is a trade-off with background noise. Bigger voxel sizes (lower resolution) allow more signal to be detected as active. Reducing voxel size lowers the signal to noise ratio of the images and consequently the sensitivity of BOLD signal detection, but improves spatial specificity. A larger voxel in the cortical boundary may also include the cerebrospinal fluid (CSF) resulting in less signal originating from the gray matter (Amaro Jr. and Barker, 2006). The voxel size in the imaging acquisition can be defined based on the anatomical structure of the brain. The cortical thickness of 2 to 4 mm (Kandel, Schwartz, and Jessell, 2000) guides the optimum voxel size to something between 3 to 4 mm. Accordingly, it is important to keep in mind the three main variables of image acquisition: spatial resolution, temporal resolution and amount of brain tissue sampled. Thus, increasing the spatial resolution but maintaining the temporal resolution will reduce the covered area (number of image slices). There is also the option of increasing spatial resolution but keeping the coverage of the whole brain. In this case temporal resolution needs to be decreased. Another approach to deal with temporal resolution and time consumption is the jittering. It refers to varying the timing of the TR relative to the stimulus presentation or just varying the interstimulus interval (ISI) keeping TR fixed. If TR is fixed and the stimulus is presented always at the same fixed time, then the same point in the subject's BOLD response is going to be sampled many times. But points in between may be missed. Varying TR or ISI allows several other points in the response to be acquired (which offers a better characterization of the HRF shape) at the expense of sampling each of them fewer times. Varying the ISI is a strategy to increase the efficiency of the estimates at the expense of power reduction (Dale, 1999; Friston, Zarahn, Josephs, Henson, and Dale, 1999) - the same point is being sampled less times and consequently the accuracy of a given estimate is smaller. But there are also more points to sample and more confidence about the shape of the HRF in the condition. As already mentioned, from a behavioral point of view, an advantage of this strategy is that it is more complicated for the subject to guess what is happening and anticipation effects are reduced.

The last issue concerning image acquisition is the plan in which the images are acquired. If adopting total coverage, the whole brain is imaged. Another option is to cover only a specific area which is assumed to respond to the paradigm. In this case the coronal acquisition is usually implemented. For the whole brain coverage acquisitions are parallel to the bicommissural plan (a line connecting the upper part of the anterior commissure to the lower part of the posterior commissure). These are axially oriented images.

2.5 Scanner Acoustic Noise

One of the main drawbacks of fMRI acquisition is the loud acoustic noise inside the scanner. This noise can be up to 120 dB SPL which obscures the quality of the auditory stimulus presentation (Schmidt, Zaehle, Meyer, Geiser, Boesiger, and Jancke, 2008). One approach is to work directly on the source of the noise, more specifically the mechanical parts of the gradient coils (Mansfield, Haywood, and Coxon, 2001; McJury and Shellock, 2000). However, it requires hardware modifications and different paradigms of stimulation. A simpler solution is to present stimulus during a "silent" period inserted in the paradigm (Figure 2.8). The counterpart is the increase of the amount of time necessary for the whole experiment.

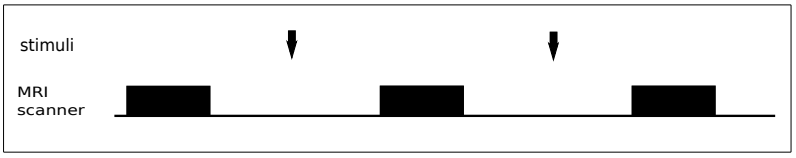

Figure 2.8: A schematic of a sparse design with TR=6 s. The black bars correspond to the time of acquisition and the arrows the stimuli delivered during "silent" periods.

2.6 Image Analysis

The last step of an fMRI study is the image analysis technique adopted. Although it is defined by the hypothesis of the experimenter, there are some common steps usually implemented. The data are first preprocessed, which means movement correction, realignment and smoothing to allow for intra subjects comparison. Then the HRF has to be modeled to represent the fMRI signal evolution according to an activated area. The last step is to test the statistical significance of the results. Cluster level analysis and correction for multiple comparisons (Friston, Ashburner, Kiebel, and Nichols, 2006) can also be included.

The final output is an activation map of a single subject where the areas whose statistical power is above some predefined level are presented in a color scale. This is the "first level analysis". There is a "second level analysis" where results are related to group statistics. For this step it is necessary to normalize and registrate all brains to a standard model to allow for comparisons.

2.7 New Approach in Neuronal Signal Measurements

In the previous sections it was shown that the neuroimaging field has gained significant results with fMRI and more specifically the endogenous BOLD contrast. Although spatial resolution is high, its temporal resolution is poor when compared with the electrophysiological techniques. EEG (or MEG) reflects large scale measures of neocortical dynamic function and has the same timescale of the ongoing electrical signaling (Nunez and Srinivasa, 1981). fMRI is linked to the energy consumption of the neuronal populations and records a signal on a timescale of several seconds. However, as stated before in this chapter, many studies have shown that cognitive processes modulate hemodynamic responses measured with BOLD contrast (Logothetis, Pauls, Augath, Trinath, and Oeltermann, 2001; Raichle, 2001). The simultaneous recording of EEG with fMRI can be combined to achieve high spatial and temporal resolutions of brain function.

The recording of EEG and fMRI in separate sessions is preferred by many scientists who want to avoid the difficulties of the simultaneous recording. Even small disturbances such as a nearby electromechanical device in EEG or metals in the MRI room may result in severe artifacts and corrupted signal quality. Recording EEG in an MRI scanner also involves a challenging post-processing step of signal cleaning (Debener, Mullinger, Niazy, and Bowtell, 2008; Vanderperren, Ramautar, Novitski, Vos, Mennes, Vanrumste, Stiers, van den Bergh, Wagemans, Lagae, Sunaert, and van Huffel, 2007; Ritter, Becker, Graefe, and Villringer, 2006). Herrmann and Debener (2008) made an extensive review about the integration of these techniques. According to them, the first approaches combining electrophysiology with hemodynamic responses come from positron emission tomography (PET) studies with EEG. In a visual attention study, Heinze, Mangun, Burchert, Hinrichs, Scholz, Munte, Gos, Scherg, Johannes, and Hundeshagen (1994) investigated location and timing of the earliest effects. For the spatial localization they subtracted PET images from the two conditions (attended and unattended) and saw that the same area was activated using a dipole localization of the ERP (Event Related Potential) component. With such result the authors suggested that the combination of both measures yield more information about the process under investigation. Many other studies used PET and more often fMRI (Liu, Ding, and He, 2006; Schreckenberger, Lange-Asschenfeld, Lochmann, Mann, Siessmeier, Buchholz, Bartenstein, and Gründer, 2004; Dale, Liu, Fischl, Buckner, Belliveau, Lewine, and Halgren, 2000).

It is also doubtful whether the subject can reproduce tasks in the same way if the recordings are done separately. Specially for cognitive studies, mental process is not going to be the same and even the most basic perceptual and cognitive operations may also show adaptation over time. In this case, session order or knowledge about the task makes a significant difference. Small changes in the setup such as the different positions

of the subject when inside a scanner (usually standing) or during the EEG recordings (usually seated) can influence the measurements. Of course, this can be solved just lying the subject down. Of more importance is the acoustical noise of MR scanning. Recordings of EEG done in an sound-attenuated room are significantly different. To attenuate this problem the experimenter can include an "artificial" or previously recorded background sound. These problems don't really impair the usage of this protocol but the experimenter needs to be aware of the differences that he may encounter.

To work around all the mentioned problems arising from separate recordings several studies have implemented the simultaneous approach. The first equipment for this purpose was described in 1993 in Ives, Warach, Schmitt, Edelmann, and Schmoer (1993) work using an analog cable telemetry equipment. Since then, event related potentials (ERPs) have been extensively explored (Herrmann and Debener, 2008). They are electrical fluctuations originated from the spontaneous EEG but time locked to a specific stimulus. The components of the ERP waveforms are extracted from spontaneous EEG by averaging the potential at each scalp location over the evoked stimuli. In this case the spontaneous EEG is assumed to be "noise", uncorrelated to ERP processes. However, there are contradictions about this assumption and single trial approaches are becoming widely used (Nunez and Silberstein, 2000). Because of the extensive work in hardware and software it is now possible to read ERPs and single-trial event-related EEG amplitudes from recordings inside an MRI scanner (Eichele, Specht, Moosmann, Jongsma, and Quiroga, 2005; Liebenthal, Ellingson, Spanaki, Prieto, Ropella, and Binder, 2003).

An approach of EEG and fMRI integration is to apply parametric variations of a stimulus and correlate the influence on ERPs with those of BOLD signal (Mayhew, Dirckx, Niazy, Iannetti, and Wise, 2010). Liebenthal, Ellingson, Spanaki, Prieto, Ropella, and Binder (2003) have done this in an auditory mismatch paradigm, where the ERP data were used to identify areas in which the BOLD signal varied with the magnitude of the negativity. The image results also gave information about the main generators of the mismatch negativity (MMN) response. This approach is also used to constrain EEG inverse solutions to regions where fMRI indicates activations in dipole localization problems.

Although most studies refer to the time locked ERP, event related EEG signals that are not phase-locked to a time-locking event are now on research focus. In this approach time domain average can not be used and an analysis on a single trial basis needs to be carried out as shown in Debener, Ullsperger, Siegel, and Engel (2006) and Jung, Makeig, and Westerfield (2002).

2.7.1 Technical Issues Concerning the Integration of EEG and fMRI

The technical problems that arise from the integration of EEG and fMRI can be divided in: magnetic field related effects, EEG artifacts induced by gradient switching, radio frequency (RF) pulses and the noise caused by the magnet pump and the operating gradient coils. Another source of noise can be explained using Faraday's induction law. The usage of amplifiers with long wires can induce an electric current caused by the movement of conductors. Thus, newer amplifiers with non ferromagnetic material have short cables connected to the electrodes cap and are placed inside the scanner as shown in Figure 2.9.

Figure 2.9: The amplifier system placed close to the subject's head inside the scanner (Herrmann and Debener, 2008). The signal is transmitted via optical fiber to a recording room to avoid electromagnetic interference.

Artifacts in EEG recordings

The *Gradient Artifact (GA)* consists of strong perturbations of the EEG signal due to time-varying magnetic field gradients. Therefore it is limited to the time required to acquire the images (i.e. TR). Under the unrealistic assumption of no head movement, this artifact is invariant over time. In this case an artifact template procedure can be implemented for its removal (Allen, Josephs, and Turner, 2000). Some other considerations

can be implemented to take into account the movement of the head. This issue will be addressed in Chapter 4.

There is another relevant kind of artifact present in the EEG recording: the *Ballistocardiogram Artifact (BCG)*. It is related to the cardiac activity and can exceed 150 μV at 1.5 T field strength which is one to two orders of magnitude greater than most ERPs (Garreffa, Bianciardi, Hagberg, Macaluso, Marciani, Maraviglia, Abbafati, Carni, Bruni, and Bianchi, 2004) and scales in amplitude with the magnetic field strength. Besides, the artifact varies within and between subjects. Temporal fluctuations of autonomic nervous system properties such as heart beat and blood pressure can impact the BCG. Its removal is not a simple task and is source of enumerable works (Debener, Mullinger, Niazy, and Bowtell, 2008; Vanderperren, Ramautar, Novitski, Vos, Mennes, Vanrumste, Stiers, van den Bergh, Wagemans, Lagae, Sunaert, and van Huffel, 2007; Ritter, Becker, Graefe, and Villringer, 2006). However, there is a close temporal relation between the BCG and the electrocardiogram (ECG) and because of this, ECG is recorded simultaneously to allow for the correct, at least partial, removal of the artifact.

2.8 Sensory Information

The processing of sensory stimulus features is essential for humans in determining their responses and actions. Thus, it is important to understand the brain mechanisms of sensory information processing (sensory prerequisites of cognition). In turn, the techniques described in the previous sections play an important role in understanding the brain dynamics of the cognitive processes which will be discussed in the next topics.

2.8.1 Selective Attention

Attention is a central nervous system (CNS) process that enables perceptual or motor responses to be made selectively to one stimulus category or dimension in preference to others (Kandel, Schwartz, and Jessell, 2000). Irrelevant stimuli are partially or completely rejected from perceptual experience (Basar, 2004). Selective attention enhances the responses of neurons in many brain areas. Neurons in the frontal cortex and superior colliculus discharge more intensely when the animal attends to the stimulus (Kandel, Schwartz, and Jessell, 2000). This kind of sensory processing is essential for planning movement and self defense. Activation of the thalamus and cerebellum has also been correlated to attention (Frith and Friston, 1996). Since attention refers to selective aspects of sensory processing, it follows that all experimental investigation of attention must measure the responsiveness of the individual to more than one category of stimulus. The

differential response to attended versus unattended stimuli provides the operational basis for this analysis.

As stated before, ERPs reflect changes of ongoing EEG activity evoked by the stimulus and are used to investigate responsiveness and cognition. Many neurophysiological studies confirmed the effects of auditory attention through some well known components such as N1 which peaks 100 ms after stimulus and P300 (around 300 ms after stimulus). It is usually assumed that N1 reflects automatic stimulus processing influenced by early attention and orientation processes (Luck, Fan, and Hillyard, 1993). P300 is thought to reflect electric activity associated to cognitive top-down processes such as attention and activation of immediate memory (Polich and Kok, 1995; Brandeis and Lehmann, 1986).

Auditory attention allows the rapid and precise directioning of the "acoustic mental environment" towards sounds of interest. Attention can be bottom-up (sound based) or top-down (voluntary or task-dependent) (Fritz, Elhilali, David, and Shamma, 2007). Top-down attention is linked to enhanced information processing, behavioral sensitivity and shortened response latencies, while bottom-up attention reads the acoustic scene and selectively gates incoming "different" signals. Attention modulated auditory responses were first demonstrated by Hubel, Henson, Rupert, and Galambos (1959) who showed that some cat auditory cells were activated only when attention conditions were met. Selective attention has also been extensively studied in humans either with evoked potentials (Mueller, Brehmer, von Oertzen, Li, and Lindenberger, 2008) or fMRI responses (Altmann, Henning, Döring, and Kaiser, 2008; Petkov, Kang, Alho, Bertrand, Yund, and Loods, 2004; Grady, van Meter, Maisog, Pietrini, Krasuski, and Rauschecker, 1997). It is known that the magnitude of attentional modulated responses changes according to task difficulties (Fritz, Elhilali, David, and Shamma, 2007). The results are usually inferred from the combination of task design and subject's performance. Thus the "raw" access of attention is difficult to measure, making comparison between studies a subjective task.

One focus of interest in attention research is how to extract auditory cues from the real world such as in the *cocktail party* effect or when focusing on a single instrument in an orchestra. The so called auditory scene analysis (ASA), the process of segregating and grouping sounds from the mixture of sources that makes our acoustic environment, is an essential step in auditory processing. The extraction of the signal from noise seems to be a multi-stage process that relies on our expectations of the auditory incomings, attention and other forms of top-down control (Alain, Snyder, He, and Reinke, 2007). The ability to detect "deviant" sounds in a sound stream is essential in human and animal survival. There is evidence that the brain has evolved a sophisticated novelty detection system that includes an automatic, pre-attentive component in the processing of important information (Molholm, Martinez, Ritter, Javitt, and Foxe, 2005; Winkler, Czigler, Sussman,

Horvath, and Balazs, 2005). Recent investigations about the novelty detection system include the *mismatch negativity (MMN)* component. Its role on the neural mechanisms of auditory attention is still unclear, but it can also serve as a powerful tool to understand perceptual deviations in certain kinds of patients as well as to investigate cortical plasticity (Näätänen and Alho, 1995).

2.8.2 Perceptual Learning

There is an accumulating body of evidence indicating that even at the earliest stages of sensory processing, neuronal functional specificity is mutable and subject to experience. Long after most aspects of brain development have ceased, repeated exposures or trainings improve our perception of a stimulus and cause neural reorganizations in the brain (Yotsumoto and Watanabe, 2008; Mueller, Brehmer, von Oertzen, Li, and Lindenberger, 2008). This induced improvement based on experience is called perceptual learning and the neural changes that follow are defined as neural plasticity. It is one aspect of learning very specific for low-level attributes of the stimulus learned (Fahle and Poggio, 2002). Perceptual learning seems to modify the neuronal pathways active during processing of the task and not to require an intermediate consolidation storage such as the hippocampus. Memory is a consequence of learning which implies the coding, storage and retrieval of information. Perceptual learning is certainly based on some form of information storage but differs from memory as it is stored implicitly by changing the way the stimuli are analyzed. Together with neural plasticity it has been studied in all sensory modalities such as vision (Fahle, 2005; Schoups, Vogels, and Orban, 1995), auditory (Demany, 1985) and somatosensory (Pleger, Foerster, Ragert, Dinse, Schwenkreis, Malin, Nicolas, and Tegenthoff, 2003) although vision is, probably, the sensory system most investigated.

Recent findings show that some forms of perceptual learning are highly specific and suggest that perceptual learning involves structural or functional changes in primary sensory cortices such as V1, in the visual system. It has already been demonstrated that perceptual tasks improve with practice and it was generally thought that improvements in discriminative power were not attributed to changes on early levels of sensory but were exclusively cognitive, i.e., high-level changes of visual information processing. However, electrophysiological experiments put new information into this interpretation suggesting that even the adult primary sensory cortices have more plasticity than first believed (Buonomano and Merzenich, 1998). The lack of task generalization is taken as an evidence that learning might be mediated by cells in early sensory areas. Recanzone, Merzenich, Jenkins, Grajski, and Dinse (1992) were the first to demonstrate evidence of alterations of low-level cortical processing showing that the gain in training-induced performance was correlated with the amount of expansion of the cortical map that represented the trained

skin area.

Given that learning occurs in developing and adult systems, an important question for understanding perceptual learning is how does a neural system know which information is behaviorally relevant and which is not. It has been suggested that attention based training plays an important role in irrelevant distractor suppression. Several studies have provided evidence of its role in perceptual learning (Yotsumoto and Watanabe, 2008; Paffen, Verstraten, and Vidnyánszky, 2008; Mukai, Kim, Fukunaga, Japee, Marrett, and Ungerleider, 2007; van Wassenhove and Nagarajan, 2007) while others show evidence of passive learning (Watanabe, Nanez, and Sasaki, 2001; Seitz and Watanabe, 2003) and are used against attentional needs in learning experiments. Although recent findings may seem contradictory at first sight, Seitz and Dinse (2007) give some insights about how these learning models can operate in parallel with each other.

Paradigms implementing attended versus non-attended discrimination tasks show improvements in visual abilities after extensive training. Schoups, Vogels, and Orban (1995) trained subjects with a circular noise field task an showed that these subjects improved in sensitivity to contour orientation of the trained position. They also observed a lack of generalization of stimulus discrimination. In another study Li, Piëch, and Gilbert (2004) saw that monkey V1 cells assumed novel functional properties when trained in a shape discrimination task. These properties depended on the perceptual task being performed showing the specificity. Trying to understand the role of attention in perceptual learning Seitz and Watanabe (2005) discussed a potential link between perceptual learning and the alerting system noting that the latter is associated with the right frontal and right parietal regions.

Auditory perceptual learning

Perceptual learning research is dominated by studies of vision but recent studies of auditory learning suggest that it may differ considerably from the visual modality (King and Nelken, 2009). Karmarkar and Buonomano (2003) showed that the lack of generalization when task difficulty is increased in a visual experiment is not seen in an auditory learning. In auditory perceptual learning, the trained perceptual dimension and the task difficulty determine the efficacy, rate, and specificity of learning. For example, training on a frequency discrimination task leads to rapid and robust learning although optimal learning may depend on task difficulty (van Wassenhove and Nagarajan, 2007).

Many investigators of the human ability to detect small differences in frequency between sine tones have noted that this ability could improve with training. Weeks of practice and many trials may be necessary to reach an individual asymptotic discrimination threshold (Demany, 1985). However, little is known about the process involved.

Many studies search for this answer and Demany (1985) investigated the frequency generalization between different frequency ranges. They observed that frequencies up to 2500 Hz influenced the discrimination of a standard 200 Hz tone. According to the results they hypothesized that frequency discrimination is mediated mainly by a temporal coding process up to 5000 Hz and beyond this value it is mediated exclusively by a tonotopic coding.

Substantial perceptual learning may occur in the very first trials, as evidenced by the improvements made early in learning by participants. Moore, Amitay, and Hawkey (2003) pointed out the need to incorporate early trials into perceptual learning experiments rather than just ignoring them. An interesting study conducted by Atienza, Cantero, and Dominguez-Marin (2002) showed differences in time evolution during perceptual learning supporting the hypothesis that fast and slow neural changes underlie the acquisition of improved performance. Differences in time course had been observed in neural and/or behavioral modifications spanning from short time after presentation of several trials to days (van Wassenhove and Nagarajan, 2007). The improvement of perceptual sensitivity within the training session is assumed to occur as a result of fast neural changes while slow behavioral improvements still take place in the period between sessions. The early neural changes are thought to affect pre-attentive and attentive processing after training and also some time later when there is no additional stimulation. The slower changes are thought to be the result of the reorganization of cortical representations (Gilbert, 1994).

Although slow perceptual learning is accepted to be accompanied by enhanced stimulus representation in sensory cortices, the neural substrates underlying early and rapid improvements are still not fully understood. This research area is of great interest of those aiming to understand how fast and slow perceptual learning interact and make a substrate for other types of learning and memory. It seems that this fast learning is highly dependent on attention as observed by Alain, Snyder, He, and Reinke (2007). During an experiment about with vowels phonetically different they observed an early evoked response around 130 ms after stimulus onset localized in the right auditory cortex and a late evoked response approximately 340 ms in the right anterior superior temporal gyrus and inferior frontal cortex. These results showed enhancement of ERPs amplitude while improving in task performance. There seems to be a sharpening on auditory neurons responsiveness guided by attention happening on the early moments of learning. It is worthy to say that fast perceptual learning can also be questioned as procedural learning as the latter accounts for the fast improvement in performance that results from learning the response demands of the task. Hawkey, Amitay, and Moore (2004) refuted this hypothesis assessing the contributions of both types of learning to improvement in an auditory frequency discrimination task and showing that the perceptual learning contribution was

higher than 75% of the rapid early performance improvement.

2.9 Summary

In this chapter the basic steps of functional magnetic resonance recording were presented as well as the acquisition techniques and paradigms commonly adopted. We also discussed the advantages of recording EEG and fMRI simultaneously, specially in the study of cognitive processes. The chapter is concluded pointing out how these tools can be used to help understanding the processing of sensory information.

3

EEG Data Processing

In order to understand the advantage of the simultaneous recording of EEG and fMRI as well as its drawbacks, this chapter will briefly discuss the source of the electric activity recorded in the scalp and how these signals are analyzed in order to study neural communication. Moreover, the main steps of the EEG data processing are presented.

3.1 EEG as a Measurement of the Cellular Electromagnetic Field

In 1875, Richard Caton, a British scientist, published the first report of his experiments with measurements of the electric activity of the brains of rabbits and monkeys (Malmivuo and Plonsey, 1995). They are believed to constitute the discovery of the electroencephalogram. In 1924, the German psychiatrist Hans Berger made the first recording of the EEG on a human being. Since then, electroencephalography has been an intensively used technique in clinics and research laboratories (Vullemoz, Rodionov, Carmichael, Thornton, Guye, Lhatoo, Michel, Duncan, and Lemieux, 2010; Michel, Murray, Lantz, Gonzalez, Spinelli, and de Peralta, 2004; Miranda de Sá and Felix, 2002). It can be considered the standard technique on neurophysiology for the diagnosis of brain pathology such as epilepsy, sleep disorders and disorders of the central nervous system (CNS). EEG measurements consist of registering electric potential differences between

pairs of electrodes in the scalp of the individual as shown in Figure 3.1. These potentials are the result of volumetric currents flowing from postsynaptic cortical neurons to the scalp through a conductive medium (pia mater, arachnoid, dura mater, skull and scalp) (Nunez and Srinivasa, 1981).

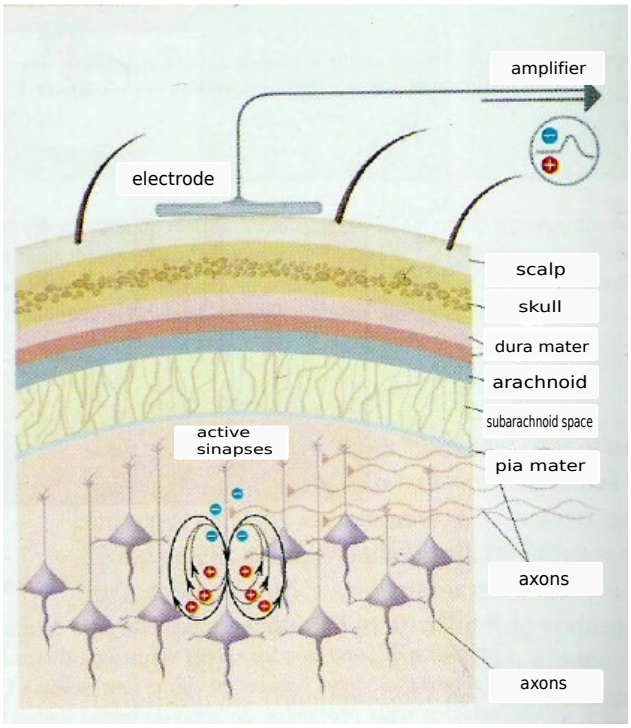

Figure 3.1: Scalp electrode and the tissues involved in electric conductivity.

To understand the technique itself it is important to understand how and where the bioelectrical signals are generated. Basically, the brain is a gelatinous mass encased by three meninges (dura mater, arachnoid and pia mater), the cerebrospinal fluid (CSF), the skull and the scalp as shown in Figure 3.2. It is composed of the cerebellum, brainstem and cerebrum (Figure 3.3). The outer part of the cerebrum is a cellular shell of gray matter, the cerebral cortex. Phylogenetically it is divided in archicortex, paleocortex and neocortex, the latter composed of pyramidal and non-pyramidal cells. Pyramidal cells have triangular cell bodies with the apex directed toward the cortical surface. It has been shown that the vertically oriented pyramidal cells with their long apical dendrites placed parallel to each other are the major contributors to the signal registered in the EEG (Nunez and Srinivasa, 1981).

The principal generators of EEG fields measured on the surface of the brain are excitatory and inhibitory postsynaptic potentials of the pyramidal cells located in cortical layers III, V and VI. Because of the attenuating properties of the skull, spatial summation of cortical activity is critical for producing a voltage field recordable from the scalp. The current flowing across the external resistance of the cortex sums with the loop currents

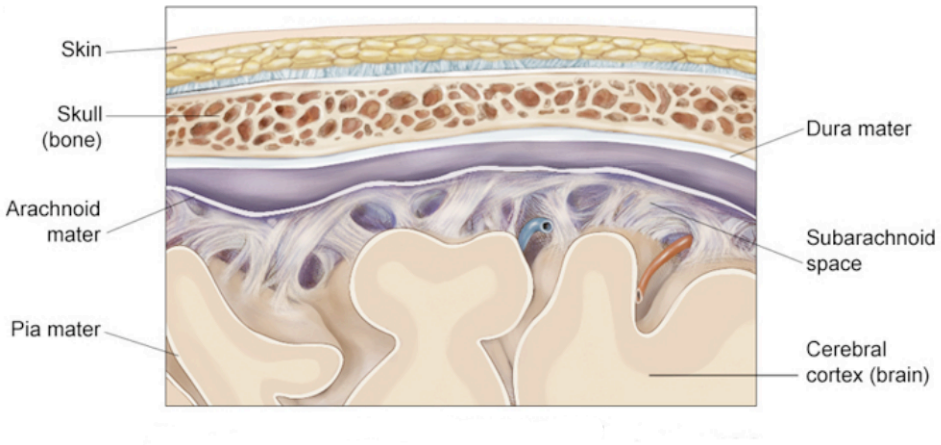

Figure 3.2: Crossectional view of the meninges. Adapted from the American Society of Clinical Oncology.

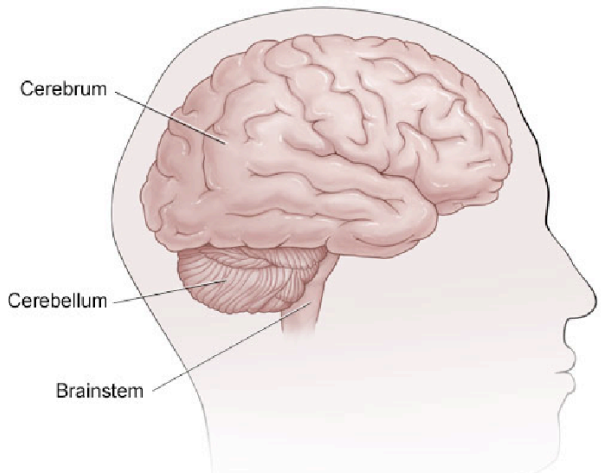

Figure 3.3: The brain and its parts. The cerebrum is composed of the right and left hemispheres. The brainstem includes the midbrain, the pons and the medulla while the cerebellum is located at the back of the head.

of the neighboring neurons to constitute a local mean field. Viewed from outside the cells, membrane areas where current flows in or out of the cells are called respectively sinks and sources. Excitatory currents, involving Na^+ or Ca^+ ions, flow inward toward an excitatory synapse and outward away from it. The outward current is referred to as a passive return current. Inhibitory loop currents, involving Cl^+ and K^+ ions, flow in the opposite direction (Olejniczak, 2006). In this way, a tiny dipole is set up as shown in Figure 3.4. A dipole from a single neuron is very small and cannot be seen from distant electrodes, but if the dipoles from many neurons summate, the resulting voltage can be measured at the scalp. Moreover, if neurons have a similar orientation and receive the same type of input, their dipoles will summate and may be measurable at the scalp. This

is most likely to occur in cortical pyramidal cells, which are aligned perpendicular to the surface of the cortex. Because current is conducted throughout a medium until it reaches the scalp, the voltage that will be present at any point on the surface will depend on the position and orientation of the generator dipole and on the resistance and shape of the various components of the head as well.

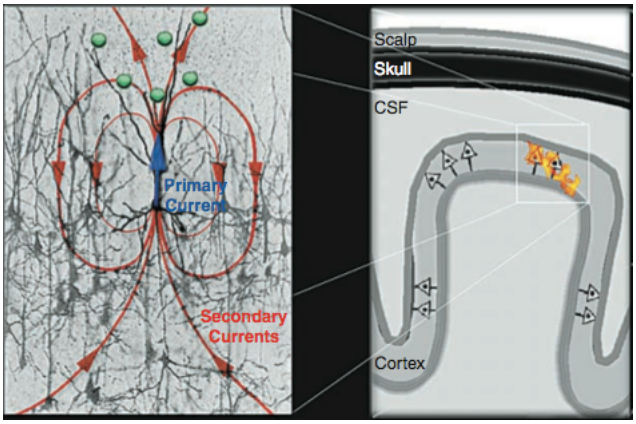

Figure 3.4: Excitatory postsynaptic potentials generated from cortical neural cell assemblies. On the left, excitatory postsynaptic potentials are generated at the apical dendrites of a pyramidal cell and trigger the generation of a current that flows through the brain. Conservation of electric charges imposes that the current loop be closed with extracellular currents flowing even through more distant parts of the conductor. On the right, cortical pyramidal cells are organized in assemblies with dendrites normally oriented to cortical surface.

Usually, EEG is recorded according to the international standardized 10-20 electrode position system (Sharbrough, Chatrian, Lesser, Lüders, and Picton, 1991; Klem, Lüders, Jasper, and Elger, 1999). The reference points are the nasion (in the front) and inion (in the back) of the head. From them the skull perimeters are divided into 10% to 20% intervals, where the electrodes are positioned as shown in Figure 3.5. In addition to the original 21 electrodes, intermediate 10% electrodes can also be placed.

By placing electrodes on the scalp it is possible to record the electrical activity of the brain which can be triggered by an external stimulus or not. The spontaneous potentials are electrical activity coming up spontaneously such as alpha rhythms and sleep states (Stroganova, Orekhova, and Posikera, 1999; Roth, Achermann, and Borbély, 1999). Event related potentials (ERP) are a change in the brain activity time-locked to an event. These responses will be discussed in the next paragraphs.

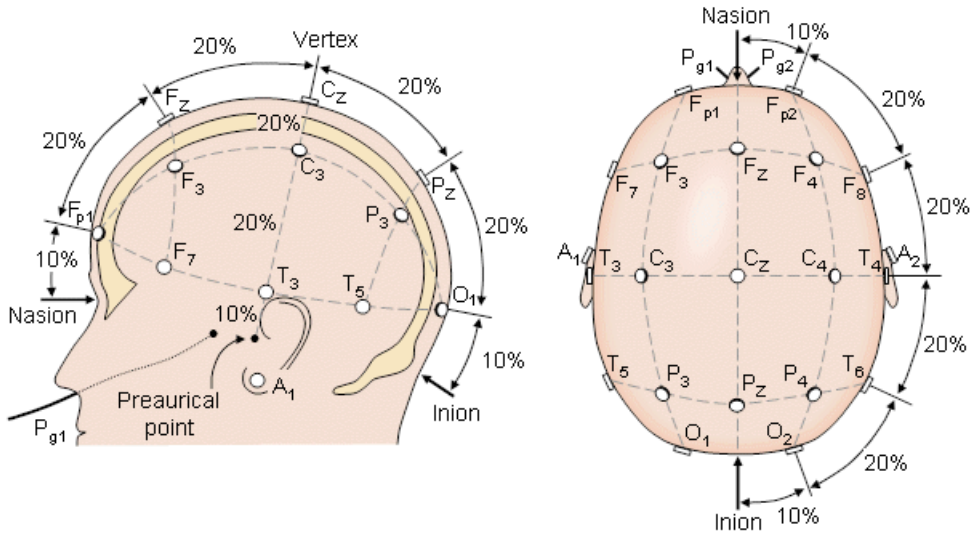

Figure 3.5: Electrodes positions according to 10-20 international system (Sharbrough, Chatrian, Lesser, Lüders, and Picton, 1991).

3.2 Evoked Potentials - EP

The term evoked potential is a general term for evoked oscillations phase locked to a sensory stimulus. Given a stimulus presented to a subject during EEG recording there will be a voltage change in response to that stimulus. Since the amplitude of this signal is extremely small (on the order of microvolts), the most common way of extracting information is averaging a significant number of EEG epochs (or segments), each time locked to the stimulus. EP averaging makes use of the fact that the EPs are time-locked to the stimulus but the background EEG is not.

It is, thus, possible to quantify the response of a specific sensory pathway to one particular stimulus type. As shown in Figure 3.6 EPs can be used to assess conductive properties of the auditory pathway following a specific stimulation. The wave patterns are characterized by their polarities (negative or positive) and latencies, which are the moment of peak occurrence after stimulus presentation. In the auditory system, they are usually recorded from the scalp when clicks, tone pips or more complex stimuli are delivered. Auditory evoked potentials (AEPs) can be divided into short latency components (brainstem evoked responses - BAEP), medium latency components (MLAEP) and long latency components (LLAEP) (Burkard, Eggermont, and Don, 2007). Medium latency components can be associated to the primary cortex while later ones are generated in brain areas related to cognitive processing: the temporal and frontal cortices (Thornton and Sharpe, 1998). Many of the long latency waveforms are thought to reflect processes that come from cognitive demands and are usually called event-related potentials.

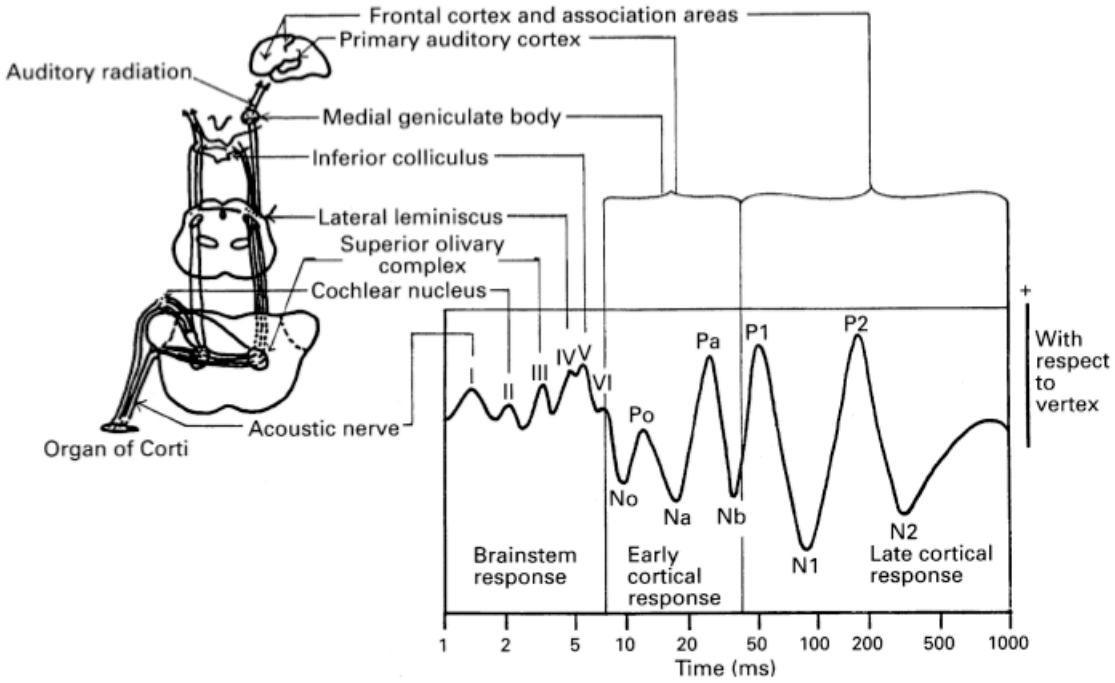

Figure 3.6: Auditory evoked potentials. In the brainstem, the response has a tight relationship with the anatomy of the auditory pathway.

3.3 Event Related Potential - ERP

The term event related potential designates a broader class of potentials that display time relationships to some physical or mental occurence. They are usually associated with endogenous brain state (Bressler and Ding, 2006) which was not originally covered by the EP definition. ERPs allow the investigation of basic functional pathways by the recording of early ERPs or "evoked potentials" (EPs) in response to clicks or tones (auditory EP - AEP), flashes (visual EP - VEP) or electrical stimulation (somatosensory EP - SEP). Cognitive pathways are investigated as well by the recording of ERPs related to the execution of attention, emotion or memory tasks (Luck, 2005).

As an example, the N100 is a negative peak at about 100 ms after stimulus onset in which novel and deviant stimuli produce enhanced amplitudes. Another component, the mismatch negativity (MMN), is a response that appears only if there is a mismatch between the prediction and the real incomings of a sensory pathway. This negative peak has been extensively investigated since it is considered to operate a pre-attentive process on the acoustic environment (Pakarinen, Lovio, Huotilainen, Alku, Näätänen, and Kujala, 2009; Näätänen and Alho, 1995). The positive peak P300 is another well known component appearing when a subject listens to a sequence of monotonous tones, randomly replaced by a deviant tone (Picton, 1992).

Like evoked potentials, ERPs are usually captured by averaging response epochs time

locked to a number of similar events. However, this procedure can average out what is not exactly synchronized but still a consequence of the stimulation. This view has gained large support by the evidence of a strong parallel processing in the whole brain (Basar and Karakas, 2006; Basar and Schürmann, 2001) where phase incoherent signals can also add to the EEG signal. Therefore, it is necessary to characterize phase incoherent event-related brain dynamics as well, also called induced responses. The difference between any single trial response and the average ERP can be modeled as a perturbation on the baseline EEG or a variance in the evoked response. This approach can give new insights into the dynamics of cortical networks (Delorme, Makeig, Fabre-Thorpe, and Sejnowski, 2002).

3.4 Event Related Spectral Perturbation - ERSP

EEG has also been described by its rhythmic activity which is divided into frequency bands noted to have different distributions over the scalp (Nunez and Srinivasa, 1981). They are known as *delta* (up to 4Hz), *theta*(4-7Hz), *alpha*(8-12Hz), *beta*(12-30Hz) and *gamma*(30-70Hz).

In 1977, Pfurtscheller (1977) derived a term to show that cortical arousal within the alpha band involves "desynchronization" of relatively slow and spatiotemporally coherent cortical rhythms, and their replacement by faster and more spatially differentiated activity, what was called the event related desynchronization (ERD). A more general measure, the event related spectral perturbation (ERSP) was derived by Makeig (1993) to measure induced dynamic changes in amplitude of the EEG spectrum as a function of time relative to the stimulus. Recently, many cognitive studies are interested in understanding the event-related oscillations involved in perceptual and attentional demands. The event-related synchronization and desynchronization (ERS/ERD) are different responses of neuronal structures in the brain that are highly frequency band specific. This new manner of understanting brain dynamics shows that oscillations are induced because their self-organized emergence are not evoked by only the stimulus itself but induced through other mechanisms in conjuction such as arousal and nonlinearities. In an auditory experiment, Makeig (1993) showed that some electrophysiological responses were not fully covered by the ERP but phase incoherent responses could be seen in the ERSP.

Quantification of ERS and ERD in time and space has been extensively investigated showing that these responses are functionally related to cognitive processing (Basar, 2004; Basar and Schürmann, 2001; Pfurtscheller and Lopes da Silva, 1999). It has been shown that alpha band rhythms (7-10Hz) appear as a desynchronization (ERD) in attention, learning and memory tasks (van Winsum, Sergeant, and Gueze, 1984). Attention-related

40 Hz responses were reported in humans, specially over the frontal and central areas (Tiitinen, Sinkkonen, Reinikainen, Alho, Lavikainen, and Näätänen, 1993). In Deiber, Pascal, Olivier, Gold, Fazio-Costa, Ibanez, and Giannakopoulos (2007), induced theta activity was recorded in the frontal region for a detection task, but not for the passive task, suggesting its dependency on focused attention to the stimulus. Perceptual learning has also been manifested as enhancement in the power of induced high gamma band activity (62-98 Hz) located in the left inferior frontal gyrus (van Wassenhove and Nagarajan, 2007).

The computation of ERD and ERS implies that the EEG power within identified frequency bands is displayed relative to the power of the same EEG derivations recorded during the baseline period (few seconds before the stimulus onset) (Pfurtscheller and Lopes da Silva, 1999). The calculation is as follows: baseline spectra are calculated from the EEG immediately preceeding each event. The epoch is divided into overlapping data windows to create a moving average of the amplitude spectra. These spectral transforms are normalized with respect to the mean baseline. The ERSP is created averaging normalized response transforms of many trials.

3.5 Neuronal Sources of Activation

Llinas (1988) has shown in 1988 that neurons can act as oscillators or resonators and the precise timing of their activity may represent information. These resonators are thought to have functional roles such as determining the "awareness" state which defines attentional states, timing in motor coordination and also the rhythm of thalamo-cortical circuits. The synchronous activity of oscillating networks is now on focus again since it can relate single-neuron activity to behavior.

Animal recording studies have stimulated research in humans proposing that synchronised neural activity is the key neural mechanism mediating the brain's ability to "bind" different features of a perceived object together to form an integrated percept. This is a relatively new approach to investigate high frequency responses, which are not time-locked to stimulus onset. It extends the view gained by more traditional approach such as those involving ERP studies of learning, memory and attentional visual information processing as well as other higher cognitive functions. It is well known since Berger's study that brain oscillations govern brain state. At that time alpha waves were seen in the EEG recordings. As alpha power was larger with eyes closed than with eyes opened, it was thought that it reflected a relaxed state. However, a decrease in alpha power has been linked to increasing demands of attention and task load. Theta power on the other hand tends to increase in memory tasks (Amabile, 2008; Klimesch, 1999).

The recent interest in neuronal network is because understanding the neuronal organization might give us an insight about how the brain develops and coordinate emotions, perceptions, thoughts and actions coming from distributed regions across the brain (Basar, Schürmann, Demiralp, Basar-Eroglu, and Ademoglu, 2001b). In the brain, the emergence of a specific neuronal assembly is thought to underlie the operation of every cognitive act. Assemblies can be seen as distributed local networks of neurons temporarily linked by reciprocal dynamic connections (Ward, 2003; Wickens and Miller, 1997). There are reciprocal connections within the same cortical area or between areas situated at the same level of the network. Moreover, studies showed that there are also connections that link different levels of the network in different brain regions to the same assembly. As an example, synchronism was observed in a 2 mm scale between excitatory and inhibitory interneurons (Gray, 1999). But this kind of interconnection was also observed in larger patches of neural tissue as in columns of the primary visual cortex of cats, separated by 2-7 mm. Large scale synchronization with neural groups which are further apart in the brain ($>$ 1 cm) are also observed. In this case the synchronism cannot be linked to local cytoarchitecture but to other forms of distant connections (Phillips and Singer, 1997). Results from local field potential (LFP) recordings in humans with surgical resection for epilepsy revealed gamma band power enhancement in oscillations showing large scale synchronism between temporal and frontal lobes during a discrimination task (Varela, Lachaux, Rodrigues, and Martinerie, 2001).

In cognition, Kaiser, Lennert, and Lutzenberger (2007) investigated neural oscillations using MEG in order to understand the temporal dynamics of cortical mechanisms underlying auditory perceptual decision making. They observed spectral enhancement in beta range during easy decisions while activation was higher in frontoparietal for more complex patterns. Basar, Basar-Eroglu, and Schürmann (2001a) made an extensive survey arguing that selectively distributed delta, theta, alpha and gamma oscillatory systems act as resonant communication networks through large populations of neurons suggesting that these processes might play an important role in functional communication specially for integrative functions.

3.6 Source Localization: the Inverse Problem

Electroencephalography can also be used for estimating the location of the EEG generators within brain space, which is known as the inverse problem. The EEG inverse problem is an ill-posed problem because the solution is non-unique (there are more sources than measurement voltages). Besides, it is unstable as the solution is sensitive to small changes in noisy data.

There are different options to solve the inverse problem and one strategy is to calculate an equivalent dipole (Kiebel, Daunizeau, Phillips, and Friston, 2008; Scherg and von Cramon, 1986; Cuffin, 1985). A dipole is a mathematical abstraction that is assumed to generate a potential on the scalp. By changing the parameters of the dipole (position and orientation), *forward solutions* can be calculated in order to get a possible scalp potential distribution. The forward solution is then compared to the original scalp potential to check the validity of the model. In general, this strategy is applicable in situations with a small number of active sources (e.g. epileptic spikes) (Scherg, Bast, and Berg, 1999). Another way to accomplish the problem is through a distributed source model, using minimal prior information about the nature of the generators apart from anatomical constraints, which usually limit the solution space to the grey matter. For grey matter extraction, subject-specific MRI scans can be used (Hamalainen and Ilmoniemi, 1994).

Besides specific assumptions concerning the method of solving the inverse problem, additional assumptions have to be made related to the physical, geometrical and anatomical properties of the generator, conductive media and recording electrodes. Head models can be made of concentric spheres but, recently, more realistic head models using MRI information have been used (Mulert, 2010).

3.7 EEG Data Processing

This section discusses the main issues regarding EEG data processing from data recorded in an MRI environment, which is the focus of this study. As already stated, simultaneous EEG and fMRI provide a powerful tool to study spontaneous and evoked brain activity because of the complementary temporal and spatial resolutions the two techniques provide. The principal problem which affect the analysis of EEG data is the artifact removal. Artifacts can come from two main sources: *gradient artifact* and *ballistocardiogram artifact*.

3.7.1 Artifacts Removal

The first class of artifacts are induced by gradient switching and radio frequency (RF) pulses. They induce a critical electric noise that obscures all the EEG traces. These artifacts are due to electromotive forces related to wire loops perpendicular to the direction of the gradient field (Debener, Ullsperger, Siegel, and Engel, 2006). It has been shown that the gradient artifacts and EEG have spectral content in the same range, hence, the former cannot be removed by simple low-pass filtering (Allen et al., 2000; Felblinger, Slotboom, Kreis, Jung, and Boesch, 1999). Several techniques to reduce imaging artifact have been reported. Laudon, Webster, Frayne, and Grist (1998) made a study with ECG electrodes.

The induced electromotive force in these electrodes was recorded and subtracted from the ECG signal. However, it is not practical for multichannel recording (in the case of EEG applications) and the artifact reduction is on the order of 20% what is too small for the milivolt artifacts superposed to the microvolt EEG signals. Although some methods seem to work well for animals or for ECG signals, the reduction is still insignificant to human EEG (Felblinger, Slotboom, Kreis, Jung, and Boesch, 1999; Sijbers, Michiels, Verhoye, Auderkerke, van der Linden, and van Dyck, 1999).

As investigated by Allen, Polizzi, Krakow, Fish, and Lemieux (1998), this artifact has no substantial intervolume variability and thus can be subtracted from the recorded EEG by using an average template. Probably the most used removal technique is the artifact template subtraction method proposed by Allen, Josephs, and Turner (2000). In this method, the shape of the gradient artifact is considered constant over time and additive to the physiological signal. Thus, a template is built with the average of many artifacts and is subtracted from the ongoing EEG signal. This method is implemented in this thesis and because of this it will be treated here in more detail.

The amplitude of the induced gradient artifact is given as

$$V_{GAMax} = (dB/dt)_{max} A_{max} \tag{3.1}$$

where V_{GAMax} is the maximum amplitude of induced gradient artifact, $(dB/dt)_{max}$ is the maximum rate of change of the gradient field, and A_{max} is the maximum loop area.

When calculating the average artifact, the first five epochs of each session are always included. Subsequent epochs are included only if the cross correlation function between the epoch and the current average exceeds 0.975. The objective is to avoid espurious signals (such as subject movement) to corrupt the template. In a periodic (or sparse) design an epoch is defined as the time between volume scans (TR) and the average is computed over 25 epochs. To optimize the calculation of the average artifact, a 25 - coefficient *sinc* function is used to interpolate the EEG values synchronously with the slice timing signal. After subtraction an anti-aliasing filter is applied and the signal is downsampled to a typicall EEG sampling rate (200-250 Hz). At this stage most artifacts are removed but some residual can be found synchronized to slice-timing signals. This residual signal is removed using adaptive noise cancelling (ANC) as shown in Figure 3.7. This method uses a *primary* input containing the corrupted signal and a *reference* input containing noise correlated with the primary noise. The reference is adaptively filtered and subtracted from the primary input to obtain the signal estimate (Widrow, Glover, McCool, Kaunitz, Williams, Hearn, Zeidler, Dong, and Goodlin, 1975).

The second significant artifact is the ballistocardiogram (BCG), which is caused by the cardiac electric field which propagates throughout the body and can be measured at

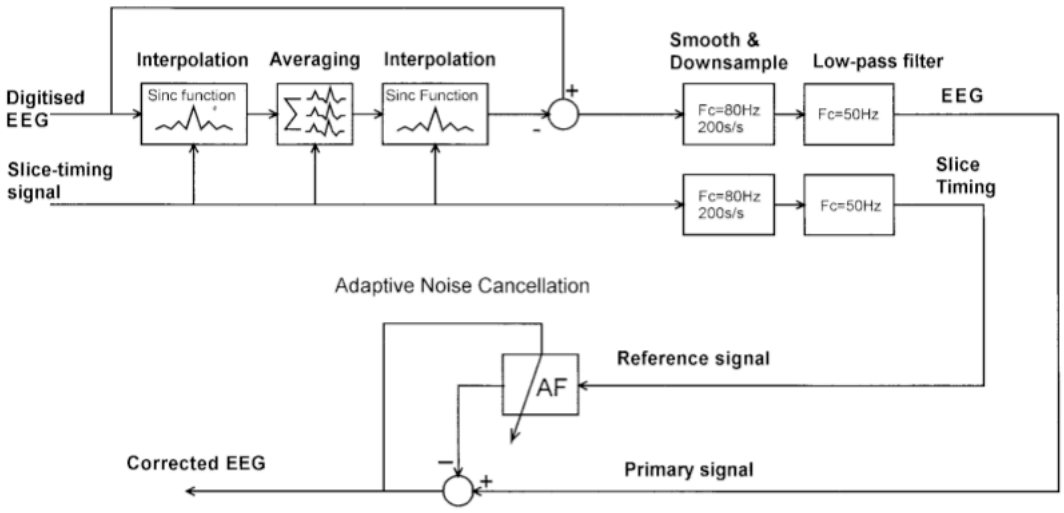

Figure 3.7: Schematic of the artifact removal method proposed by Allen, Josephs, and Turner (2000).

any location on the body surface, including the scalp (Dirlich, Vogl, Plaschke, and Strian, 1997). The problem of the cardiac field artifact in EEG averaging has been reported in many studies (Debener, Mullinger, Niazy, and Bowtell, 2008; Vanderperren, Ramautar, Novitski, Vos, Mennes, Vanrumste, Stiers, van den Bergh, Wagemans, Lagae, Sunaert, and van Huffel, 2007). It is most prominent in the QRS complex and during the T wave. This is probably the most challenging artifact and many factors contribute to its generation. The fundamental mechanism underlying the BCG is stated by Faraday's law of induction, which says that any movement of an electrical conductor in a static magnetic field results in current induction. What many authors advocate is that this motion can have many origins. One of them is the pulsatile movement of the scalp and electrodes motion caused by the expansion and contraction of adjacent blood vessels. Bonmassar, Purdon, Jaaskelainen, Chiappa, Solo, Brown, and Belliveau (2002) measured this motion from an artery and used it with an adaptive filter resulting in BCG removing. Blood flow itself can be a source of this artifact as blood is a conductive medium and induces electrical potentials in the presence of a magnetic field (Allen, Polizzi, Krakow, Fish, and Lemieux, 1998).

The removal of this artifact is usually accomplished by two main approaches. The first one is the implementation of independent component analysis (ICA). This technique was succesfully applied for recordings at 1.5T (Mancini, Perrucci, Cugini, Ferretti, Romani, and Gratta, 2006). Debener, Mullinger, Niazy, and Bowtell (2008) reported that at higher fields, its topographical variability is more pronounced and therefore fixed spatial topographies are not well suited. They also showed that correlation approaches between independent components (IC) and the electrocardiogram (ECG) channel does not perform

well alone. The reason is that ECG has prominent features not seen in the EEG, such as the QRS complex. Despite these observations ICA has been succesfully implemented in many studies (Mantini, Perrucci, Cugini, Ferretti, Romani, and Gratta, 2007; Srivastava, Crottaz-Herbette, Lau, Glover, and Menon, 2005).

A second method for BCG removal uses its temporal correlation with the pulsatile movements of the heart - the ECG. Therefore, an ECG is usually recorded together. Allen, Polizzi, Krakow, Fish, and Lemieux (1998) developed a method that subtracts an average pulse artifact waveform from the referential EEG signals at the time instants synchronized to the ECG peaks. A brief explanation of the method will be given here and more information is found at their paper. The method uses the 10 previous seconds of EEG and ECG signals to build an artifact template. A peak corresponding to the QRS complex is identified in the ECG signal by detecting a turning point following an amplitude threshold crossing. The average waveform is calculated for the period ± half the R-R interval time locked to the ECG peaks. This template is subtracted from the penultimate second of the 10 seconds segment and the corrected segment is shown. In order to have a robust peak detection method, the mean value of the template is compared to the incoming EEG signal to avoid another peak artifact to be incorporated into the template. Besides, a cross-correlation between the ECG waveform at each peak and the average ECG waveform is calculated. The validity of the ECG peaks can then be tested with this procedure. To calculate the averaged waveform the algorithm searches for four sucessive ECG peaks with a predefined R-R interval variability (to be sure it contains a QRS complex and not an artifact). A slightly different approach proposed by Niazy, Beckmann, Iannetti, Brady, and Smith (2005) uses optimal basis set (OBS) instead of simple averaging to build the pulse artifact template. The pulse artifacts are aligned in a matrix to calculate the principal components of the artifact residuals using principal component analysis (PCA). They form a basis set which is then fitted and subtracted from each artifact.

Ocular and movement artifacts contaminate EEG data as well. The removal of these artifacts had been extensively explored and information can be found in He, Wilson, Russell, and Gerschutz (2005); Haas, Frei, Osorio, and Pasik-Duncan (2003) for regression analysis, Kierkels, Riani, Bergmans, and van Boxtel (2007) for Kalman filter approach and Callan, Callan, Kroos, and Vatikiotis-Bateson (2001); Jung, Makeig, Humphries, Lee, and Mckeown (2000) for ICA techniques.

3.7.2 Time-frequency Analysis

The traditional method to study and visualize events in the EEG signal is to average epochs time-locked to the stimuli. The results are positive or negative voltage deflections

coming out from the spontaneous activity in the EEG. The "background" signal is canceled out, approaching zero as the number of trials increases (Burkard, Eggermont, and Don, 2007). The peaks revealed (the ERP components) reflect deviations from a period previous to the stimulus (the baseline). Their peak amplitudes and latencies are used to measure or index a sensory, motor or cognitive response.

The recent interest in studying event-related EEG comes from the suggestion that neural oscillations and synchronization represent important mechanisms for interneuronal communication between distributed brain regions (Basar, Schürmann, Demiralp, Basar-Eroglu, and Ademoglu, 2001b). One approach to study event-related EEG oscillations is the time-frequency analysis which involves the decomposition of single trial EEG signals into magnitude and phase information. They can tell which frequencies have the highest power at specific points in time and space and how their phase angles change across time. In time-frequency decomposition, a complex number is estimated at each time point yielding both time and frequency domain information as summarized below:

- Each trial is convolved with a Morlet wavelet transform centered on a segment of the epoched EEG. By sliding this windowed function across the entire time series (one point at a time), a complex number at the window's center point is calculated for each time point as shown in Figure 3.8.

Figure 3.8: Example of an EEG time series convolved with a Morlet function, containing real and imaginary components.

- For each time point there will be complex numbers calculated for all trials. The mean power for a given frequency at a particular time point is calculated squaring and averaging the magnitude length of these complex vectors.

- The phase information is revealed after removing the magnitude information (normalizing it) from the complex values. As in the mean power case, phase angles from all trials are averaged to produce the phase locked information.

- Doing these steps for all trials, time and frequency points yield a time-frequency matrix of total power values and a matrix with phase locked values (also known as *intertrial phase coherence - ITC*).

Although this work focused on wavelet based decomposition (using the Morlet function) this is not the only option adopted in the analysis of brain dinamics. Short time Fourier transform (STFT) has also been adopted in many studies and a comparison between the techniques can be found in Bruns (2004); Muthuswamy and Thakor (1998). In fact, the STFT was tested but the results obtained with wavelet decomposition yielded results with better resolution.

3.8 Summary

The millisecond temporal resolution of the EEG makes it well suited to the noninvasive study of cortical activation dynamics. Although these electrophysiological approaches have the potential to reveal the activation sequence of cortical areas, their spatial resolution is too coarse which highlights the importance of the simultaneous acquisition. This chapter discussed the main approaches in EEG data analysis.

4

FMRI Data Processing

A rapid improvement has been happening in imaging technology and methodology which has an enormous impact on how the brain is seen and its functioning interpreted. Detailed anatomical images combined with functional images obtained with PET and fMRI techniques help investigating issues concerning normal and abnormal brains. A functional imaging study involves the collection of one or more functional scans of each subject. The necessary steps to access signal changes related to brain activation will be addressed in this chapter.

4.1 Conventions

Before starting an MRI study it is necessary to be familiar with conventions and the terminology that describes orientation. The basic directions are right, left, anterior, posterior, inferior and superior as shown in Figure 4.1. The nose is referred to as the anterior end and the opposite to it is the posterior. By drawing a line connecting these two points we define the anteroposterior axis. From left to right ear there is the left-right axis. The top and the bottom are other extremes used as reference: the head end is the superior end while the feet is the inferior end, forming the superior-inferior axis.

Besides orientation, there are three reference planes (also called views) used in anatomy. The *saggital* plane divides the head into left and right portions (y-z plane); the *coronal*

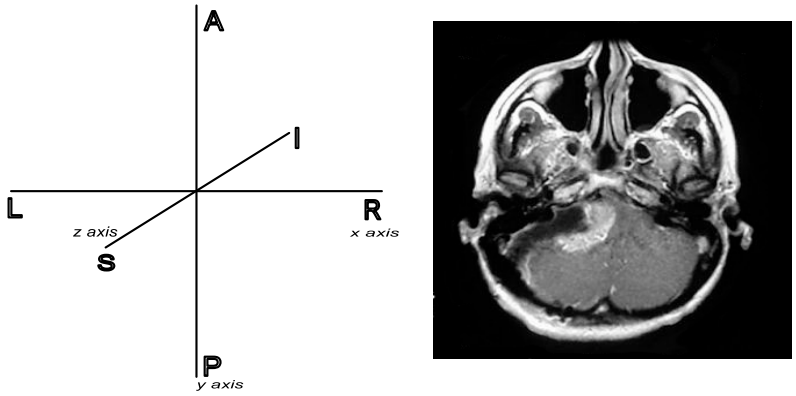

Figure 4.1: Slice orientation. R: right - L: left - S: superior - I: inferior - A: anterior - P: posterior. On the right, an axial view of a brain image.

plane divides the head into anterior and posterior portions (x-z plane); and the *axial* plane separates the superior portion from the inferior (x-y plane). Images of the three views are shown in Figure 4.2.

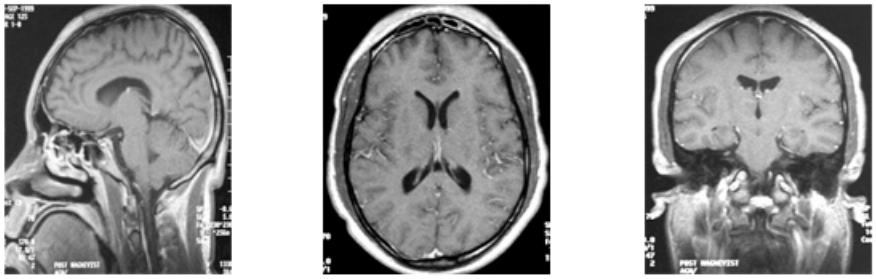

Figure 4.2: Anatomical views of the brain. From left to right: sagittal, axial and coronal.

Images output from scanners are stored in the ANALYZE [1] format using radiological convention. This means that looking at a 2D axial slice and taking a row from one ear to the other, pixel "1" is on the right side of the image and pixel "N" on the left side. Pixel numbers increase from right to left with zero at the center. However, SPM (statistical parametric mapping) stores data in neurological convention. It means that x increases from left to right, y increases from posterior to anterior and z increases from inferior to superior. SPM uses a spatial transformation matrix to transform ANALYZE data (**.hdr*, **.img*) into neurological format. It also keeps a MATLAB data file **.mat* with

[1] ANALYZE TM is a file format for storing MRI data. The data set consists of two files:

- Header file (.hdr): Provides image dimension, identificação and some processing history information;
- Image file (.img): uncompressed voxels whose datatype and ordering are described by the header file.

(Mayo, 1986-1995)

all spatial transformations. A 2D image is stored in an **.img* file as a continuous data stream (8 bits/pixel/voxel). Data is stored as M rows and N columns. They are often of sizes 64x64, 128x128, 256x256. All images of all subjects must be oriented in the same direction, with the origin set to the same point. This point is used by SPM to align each fMRI image with the anatomical one.

4.2 Preprocessing

In order to associate an observed response to a particular brain structure, the data is usually mapped onto an anatomical space. There is no convention about the preprocessing procedure although some "classical" analysis can be carried out. Some experimenters say that data acquired in interleaved mode should begin with slice timing correction and then realignment. Next, coregistration of functional and anatomical images can be performed followed by normalization and smoothing. If sequential mode is used for scanning, slice timing can be used just before normalization and smoothing.

4.2.1 Slice Timing Correction

Functional volumes are usually formed one slice at a time but the capture of these slices is spread out in time over the few seconds of the total volume capture (Donaldson and Buckner, 2001). Therefore, the BOLD signal is sampled at different layers of the brain at different time points although it would be good to have the signal for the whole brain from the same time point.

When fitting a model to each voxel's time series (at a later step) it is assumed that the data of each time point was taken at the beginning of the corresponding volume's scan time. But, if the points were scanned at even small different times, the model fitting may not be good. Henson, Büchel, Josephs, and Friston (1999) address this problem and show the different images that can be acquired if a poor model is assumed. Slice timing correction is thus used to correct the acquisition time delay between slices of a volume, which is done shifting the data in time. This can be achieved by applying the Fourier transform to each voxel's time series, phase shifting the data and then applying the reverse Fourier transformation. At the end each time series has the values that would have been obtained if the slice had been acquired at the same time as the reference slice (Ashburner, Chen, Flandin, Henson, Kiebel, Kilner, Litvak, Moran, Penny, Stephan, Hutton, Glauche, Mattout, and Phillips, 2009).

4.2.2 Image Registration

In imaging neuroscience, signal changes due to any hemodynamic response can be much smaller than signal changes due to subject motion, particularly at tissue boundaries or at the edge of the brain. In this case it is necessary to eliminate systematic variation before statistical modelling. First, the acquired images must be aligned so that the information contained in each one may be consistently observed in physical structures or regions (Figure 4.3). Furthermore, head movement inside the scanner cannot be completely eliminated (even with the head cage there is some motion), making motion correction a necessary preprocessing step of the image data analysis. This is probably the most common application of within-modality registration in functional imaging.

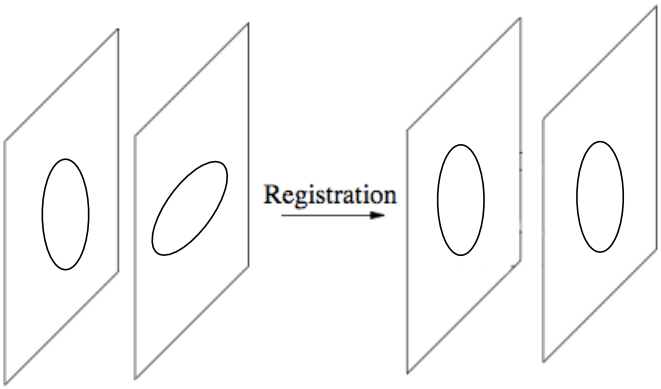

Figure 4.3: Registration applied to images for alignment.

Image registration (or realignment) is about determining a spatial transformation, or mapping, that relates positions in one image to corresponding positions in one or more other images (Maintz and Viergever, 1998). The most common algorithms for movement correction consider the head a rigid object, which is reasonable since the skull is a rigid body. The algorithm determines the parameters of a rigid body transformation that optimize some criteria (e.g. sum of squared differences) for matching each image with a reference image. The reference can be either the first image in the series or an average over all images being coregistered. There are two classes of registration methods: the realignment, also known as mono-modal (between images of the same modality) and the coregistration, known as multi-modal (between different modalities like anatomical and functional MRI).

For realignment in three dimensions (3D), six parameters are needed to define a rigid body transformation (three translations: x,y,z and three rotations: pitch, yaw, roll) as shown in Figure 4.4. For each point (x_1, x_2, x_3) in the image, an orthogonal mapping is done onto the coordinates of another space (y_1, y_2, y_3). This can be expressed as a matrix $\mathbf{y} = \mathbf{Mx}$:

$$\begin{pmatrix} y_1 \\ y_2 \\ y_3 \\ 1 \end{pmatrix} = \begin{pmatrix} m_{11} & m_{12} & m_{13} & m_{14} \\ m_{21} & m_{22} & m_{23} & m_{24} \\ m_{31} & m_{32} & m_{33} & m_{34} \\ 0 & 0 & 0 & 1 \end{pmatrix} \begin{pmatrix} x_1 \\ x_2 \\ x_3 \\ 1 \end{pmatrix}.$$

where m_{14},m_{24} and m_{34} are translation parameters.

Considering ϕ, φ and ψ, the pitch, roll and yaw angles respectively, a rotation matrix can be defined as the product of three orthogonal matrices each of which corresponding to the rotation around an axis (Teixeira, 2009):

$$\mathbf{R} = \begin{pmatrix} 1 & 0 & 0 & 0 \\ 0 & cos\phi & sin\phi & 0 \\ 0 & -sin\phi & cos\phi & 0 \\ 0 & 0 & 0 & 1 \end{pmatrix} \begin{pmatrix} cos\varphi & 0 & sin\varphi & 0 \\ 0 & 1 & 0 & 1 \\ -sin\varphi & 0 & cos\varphi & 0 \\ 0 & 0 & 0 & 1 \end{pmatrix} \begin{pmatrix} cos\psi & sin\psi & 0 & 0 \\ -sin\psi & cos\psi & 0 & 0 \\ 0 & 0 & 1 & 0 \\ 0 & 0 & 0 & 1 \end{pmatrix},$$

and the translation matrix as

$$\mathbf{T} = \begin{pmatrix} 1 & 0 & 0 & x_t \\ 0 & 1 & 0 & y_t \\ 0 & 0 & 1 & z_t \\ 0 & 0 & 0 & 1 \end{pmatrix}.$$

The homogeneous transformation matrix can then be parameterized as:

$$\mathbf{M}=\mathbf{TR}$$

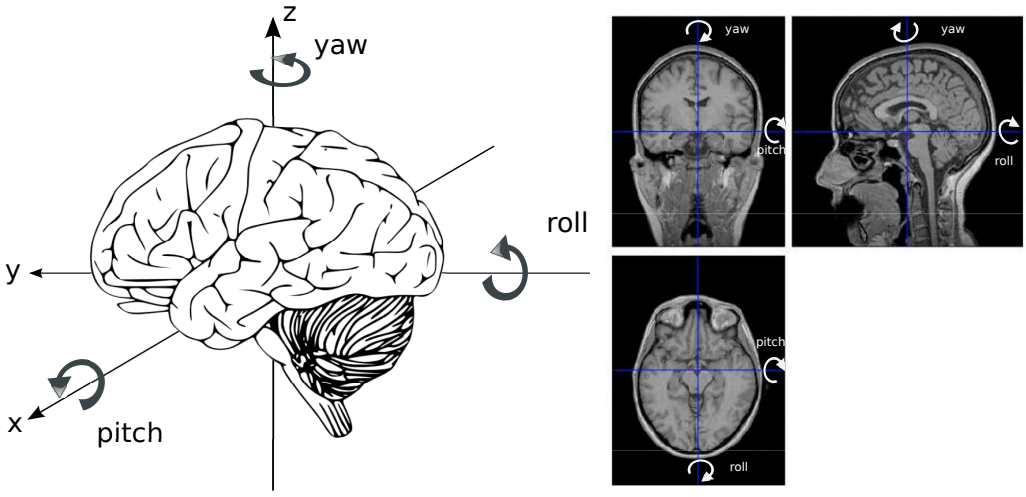

Figure 4.4: Transformations performed on each subject's image for motion correction.

However, according to Friston, Williams, Horward, Frackowiak, and Turner (1996), in fMRI time-series, much of the variance can be accounted for by the effects of movement-related artifacts still left over after the realignment procedure: interpolation artifacts,

nonlinear distortion due to magnetic field inhomogeneities and spin-excitatory history effects. They showed that movement-related changes are a complex function of position and scan to scan movement. Therefore, they suggest an autoregressive-moving average model for the effects of previous displacements on the current signal.

4.2.3 Coregistration

For studies of a single subject, the sites of activation can be accurately localized by superimposing them on a high resolution structural image (collected separately) of the subject (typically a T_1-weighted MRI). In this case the functional image is registered to the structural image. The structural scan may have a different field of view, voxel size or orientation, so that it will need to be coregistered to the functional images using an automated matching algorithm. Again, this is a rigid body registration but, because the structural image is acquired in a different modality to the functional images, there is no linear relationship between the image intensities and the registration cannot be simply performed by minimizing the residual sum of squares.

The most recent voxel-similarity measures used for inter-modal registration are based on information theory. These measures are based on joint probability distributions of intensities in the images, usually represented in the form of 2D joint histograms (Ashburner and Friston, 2003). After realignment of T_2^*-weighted images, structural (high resolution T_1-weighted image) and functional (low resolution T_2^*-weighted) images are coregistered to maximize the mutual information between these different modality data such as those shown in Figure 4.5.

The mutual information between images $\mathbf{f}$ and $\mathbf{g}$ is given by

$$I(\mathbf{f},\mathbf{g}) = H(\mathbf{f}) + H(\mathbf{g}) - H(\mathbf{f},\mathbf{g}), \tag{4.1}$$

where H(**f,g**) is the entropy of the joint probability distribution

$$H(\mathbf{f},\mathbf{g}) = -\int_{-\infty}^{\infty}\int_{-\infty}^{\infty} p(\mathbf{f},\mathbf{g}) log_2 p(\mathbf{f},\mathbf{g}) d\mathbf{f} d\mathbf{g}, \tag{4.2}$$

and H($\mathbf{f}$) and H($\mathbf{g}$) are the marginal entropies. The mutual information is a measure of the dependence of one image on another, and can be considered as the distance between the joint distribution p(**f,g**) and the distribution assuming complete independence (p($\mathbf{f}$)p($\mathbf{g}$)),

$$I(\mathbf{f},\mathbf{g}) = \int_{-\infty}^{\infty}\int_{-\infty}^{\infty} p(\mathbf{f},\mathbf{g}) log_2 \frac{p(\mathbf{f},\mathbf{g})}{p(\mathbf{f})p(\mathbf{g})} d\mathbf{f} d\mathbf{g}. \tag{4.3}$$

When both images are coregistered, this distance is zero and the mutual information is maximum. With such approach functional activations can be overlaid with individual's

anatomy or group-level functional activations with an average structural image.

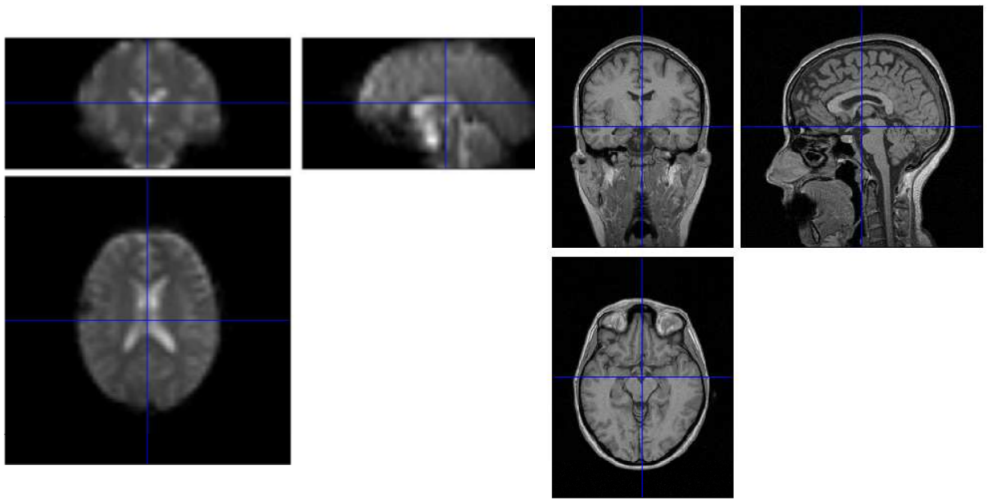

Figure 4.5: Functional and anatomical images are coregistered to provide a better localization of sites of activation. On the left, functional images of a subject are displayed. On the right, the anatomical images.

4.2.4 Spatial Normalization

Spatial normalization is the process of warping images from different participants onto a standard brain (also known as a template) (Frackowiak, Friston, Frith, Dolan, Price, Zeki, Ashburner, and Penny, 2003). During an fMRI experiment, data is collected for several subjects. However, each individual's brain differ in orientation, size and shape relative to others in the group. For comparisons, size and shape of all brains need to be changed to match a standard brain. Images can also be warped from a number of individuals into roughly the same standard space to allow signal averaging across subjects, as shown in Figure 4.6. Since it is most probable that different people have different strategies for performing tasks in the scanner, spatial normalization of the images is useful for determining what is invariant or not across individuals. In this case, activation sites can be reported according to their Euclidian coordinates within a standard space, the Talairach stereotaxic coordinate system (Talairach and Tournoux, 1988) or the Montreal Neurological Institute reference system (MNI) (Evans, Collins, Mills, Brown, Kelly, and Peters, 1993).

Normalization usually begins by determining the twelve-parameter affine transformation to register the brain with the template, *e.g.*, matching the orientation, size and shape (x-translation, y-translation, z-translation, roll, pitch, yaw, resizing in three dimensions and three shear deformations). These parameters are shown in Figure 4.7. The template is of the same modality as the image, so the optimization is done by minimizing

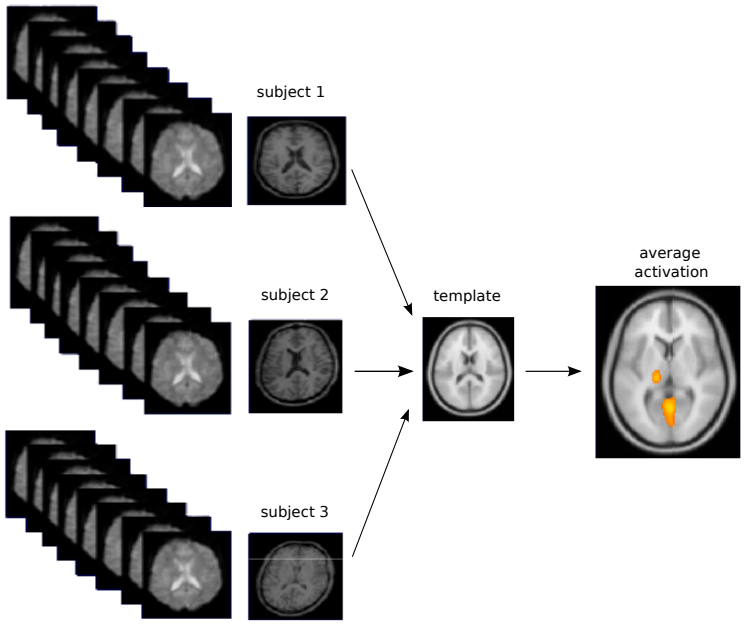

Figure 4.6: Images of three different subjects normalized to a template.

the residual of squares. In this step, variations in position and size are corrected in the whole image but local features usually do not precisely match. Because of that, nonlinear deformations described by a number of smooth basis functions (discrete cosine transform) are introduced to correct for deep differences.

The process is as follows. After realigning and coregistering the data, a mean image of the scanned series is used to estimate some warping parameters that map it onto a template that already conforms to some standard anatomical space (*e.g.* the one described by Talairach and Tournoux (1988)). Different models can be used for estimation such as spatial transformation matrix and discrete cosine basis functions. Putting them together in a Bayesian framework, one needs to find the deformation parameters θ that have the maximum posterior probability given the data y, $p(\theta \mid y)$, where $p(\theta \mid y)p(y) = p(y \mid \theta)p(\theta)$. As a result, the deformation is found by maximizing the probability of getting the data, given the current estimate of the deformation is true times the probability of this estimate being true (Frackowiak, Friston, Frith, Dolan, Price, Zeki, Ashburner, and Penny, 2003). Matching is done on a coarse scale and because of this, images are smoothed prior to the statistical analysis in a multi-subject study to allow for superimposition of corresponding sites of activation.

4.2.5 Smoothing

Smoothing is the operation of convolving image volumes with a Gaussian kernel of a specified width. At first glance smoothing seems blurring the image and, therefore,

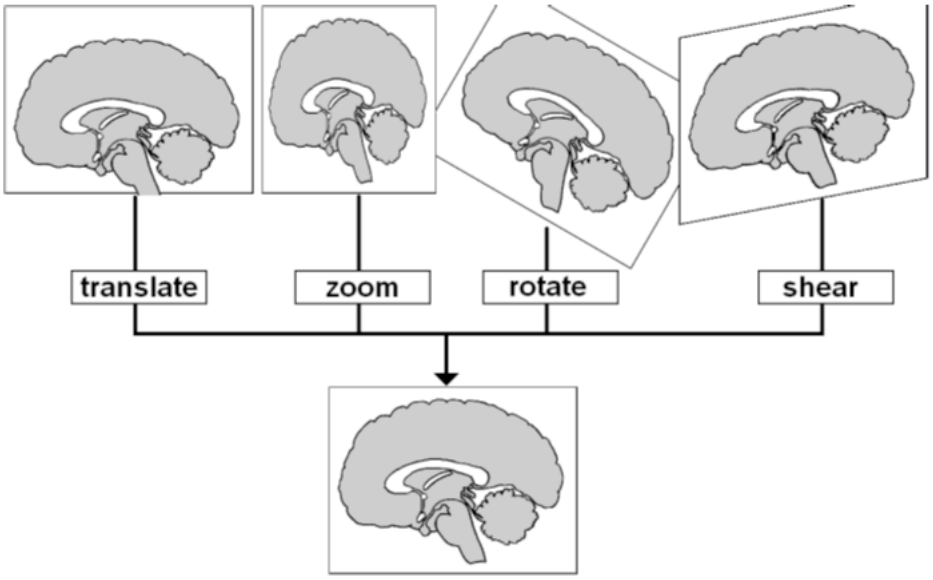

Figure 4.7: Linear transfomrs used for normalization as well as for realignment and coregistration steps. Images can be translated, zoomed, rotated and sheared to match a template.

degrading the spatial resolution. However, there is an increase of the signal to noise ratio (SNR) due to the removal of high frequency content that usually accounts for noise.

According to Frackowiak, Friston, Frith, Dolan, Price, Zeki, Ashburner, and Penny (2003) smoothing makes the data to have a more normal distribution and ensure the validity of inferences based on parametric tests. Besides, when making inferences about local effects using Gaussian random field theory, the assumption is that the error terms are some representation of a smooth Gaussian field. For this purpose smoothness needs to be greater than the voxel size. At last, in inter-subject averaging, smoothing is necessary in order to project the data onto a spatial scale where it is easier to see similarities among subjects. Thus, every data point will be multiplied by a curve in the shape of a normal distribution defined by the full width half maximum (FWHM), as shown in Figure 4.8. This is the width of the curve at half maximum and it is usually defined in milimeters. The FWHM chosen for the smoothing is typically two or three times the voxel size (around 8 mm) (Friston, Ashburner, Kiebel, and Nichols, 2006). An example of this step is shown in Figure 4.9.

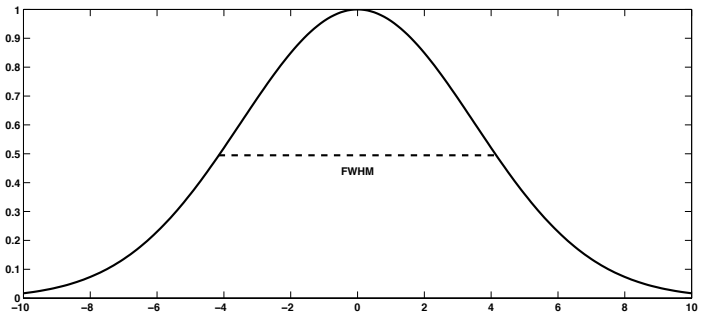

Figure 4.8: A gaussian distribution function with the FWHM highlighted.

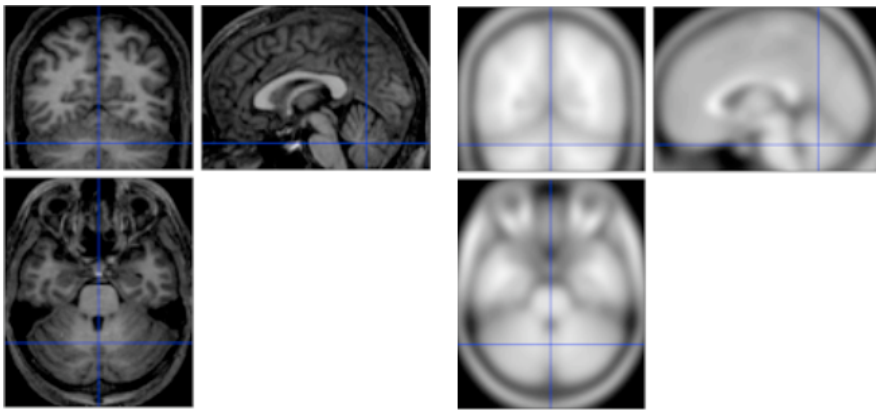

Figure 4.9: Coarse scale images after smoothing. On the left original anatomical images. On the right images after smoothing.

4.3 Statistical Parametric Mapping

In the previous section the preprocessing procedure necessary to prepare the data for the statistical analysis was explained. Now the statistical parametric mapping and the issues related to its computation and analysis are introduced.

As already explained in the introductory chapter, fMRI allows repeated measurement of brain activity at many voxels in the brain. Each voxel represents physiological responses of a small anatomical part of the brain (Figure 4.10). The analysis itself consists of determining which brain regions are activated following some task and, thus, the differences between two conditions need to be tested statistically since there is a lot of variability in subject's state as well as between subjects (Brett, Johnsrude, and Owen, 2002; Worsley, 2001). The computation and visualization of such statistical tests is known as *statistical parametric mapping*.

Statistical parametric mapping concerns the construction of maps that give a value for a certain statistic at each voxel in the brain used to test hypotheses about functional imaging data. These maps are modeled as continuous statistical processes to test hypotheses about local specific effects (Friston, Ashburner, Kiebel, and Nichols, 2006). They are

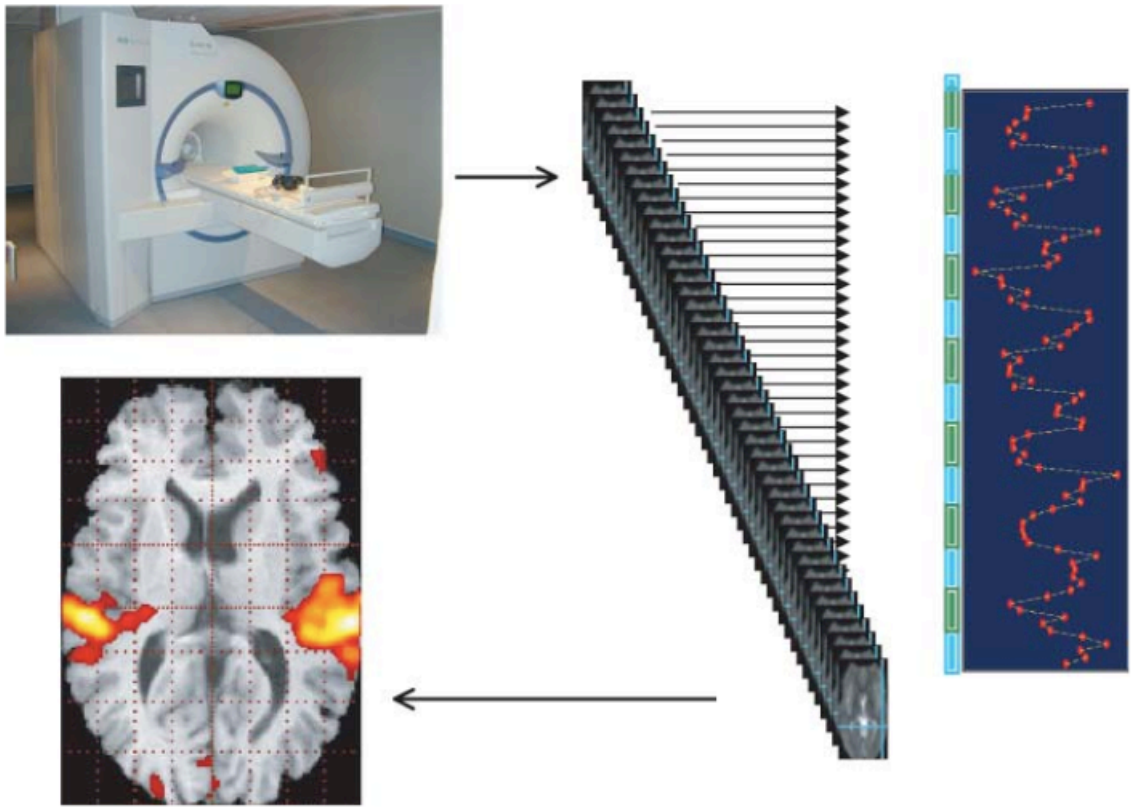

Figure 4.10: The responses of one point of each slice in the time series is shown as a function of time. Two conditions are evaluated indicated by the green and blue dashes on the right. After statistical processing a brighter area can be seen as a statistical parametric map overlaid on an anatomical volume.

image processes with voxels that are distributed according to a known probability density function, usually t-student or F distributions (T or F maps). Statistical parametric mapping refers to the use of the general linear model (GLM) and the random field theory (RFT) to analyze and make classical inferences about features of the statistical parametric maps (SPM). The GLM is used to estimate parameters that explain the continuous data whereas the RFT is used for the multiple comparison problem when one is interested in the analysis taken in the whole volume simultaneously. It adjusts p-values for the search volume and plays the same role for continuous data as the Bonferroni correction does for discrete statistical tests (Friston, Ashburner, Kiebel, and Nichols, 2006). In a multiple comparison problem, a given α value can be appropriate for each individual comparison, but not for the whole set of comparisons. In order to avoid too many false positives, the α value (which is usually around 0.05) has to be lowered. In the Bonferroni correction this is done by setting the α value to each comparison equal to α/n while the value to the entire set of n comparisons is α. More about this will be addressed in the next sections.

The null hypothesis for a particular statistical test will probably be that there is

no change anywhere in the brain. For example, in a comparison of activation against rest, the null hypothesis would be that there are no differences between the scans in the activation condition and the scans in the rest condition. This null hypothesis implies that the volume of Z scores for the comparison will be similar to an equivalent set of numbers from a random normal distribution. The question is to decide whether some of the Z statistics in the statistic map are larger (more positive) than it would be expected in a similar volume of random numbers? If the number of independent observations were known, a Bonferroni correction could be used. But this is not the case for a smoothed image. The multiple comparison problem is thus concerned with how high one should set the Z threshold so that he can be confident that the remaining peak Z scores are indeed too high to be expected by chance.

4.3.1 The General Linear Model

The basic idea of statistical image analysis corresponds to model the observed physiological responses into components of interest and errors and make inferences about the interesting effects (Friston, Ashburner, Kiebel, and Nichols, 2006). The statistic can then be seen as an estimate of the response divided by an estimate of its standard deviation (t-statistics). The GLM includes simple t-tests on scans according to different conditions, correlation coefficients between observed responses and boxcar stimulus functions, inferences using multiple linear regression and selective averaging to estimate event-related responses (Frackowiak, Friston, Frith, Dolan, Price, Zeki, Ashburner, and Penny, 2003). The design matrix encodes different experimental designs according to the question of interest. The basic idea of the model is as follows.

The first step consists of fitting a model to a single voxel's time course. Thus, the data of interest is a 1D vector of intensity values. A linear model is of the form:

$$y(t) = \beta x(t) + e(t); \tag{4.4}$$

where $y(t)$ is the observed data with intensity values for each time point, $x(t)$ is the model (for example a boxcar function) and β is the parameter estimate for $x(t)$, i.e. the value that $x(t)$ must be multiplied by to fit the data. The error term accounts for the residual error between the fitted model and the data. If there are two types of stimuli (for example visual and auditory), the model would be

$$y(t) = \beta_1 x_1(t) + \beta_2 x_2(t) + e(t). \tag{4.5}$$

In this case there are two different model waveforms corresponding to two stimulus time-courses and two parameters (β_1 and β_2) to be estimated. Different model waveforms within

a complex model are often referred to as explanatory variables. For more realistic fitting, the stimulus function is convolved with the hemodynamic response function (Kiebel and Friston, 2004).

The general linear model is often equated in a matrix form

$$\mathbf{Y}=\beta\mathbf{X}+\varepsilon.$$

$\mathbf{X}$ is known as the design matrix corresponding to the model time courses. An example is shown in Figure 4.11. Two model time courses are displayed in two columns, for example visual stimulation on the left and auditory on the right. In this example, the first column will generate a high first parameter estimate in the visual cortex while the second column will generate a low second parameter, as the fitting won't be good for voxels in the visual cortex. This matrix, then, contains all effects that may have an influence on the acquired signal. Each column of the design matrix corresponds to some effect of interest built during the experiment (Smith, 2001).

To convert a parameter estimate into a useful statistic, its value is divided by its standard error resulting in a T value (t-statistic). If the parameter estimate is low relative to its estimated uncertainty, the fit is not significant. Thus, T is used to access whether or not a voxel is activated by a specific stimulation. The parameters β can be estimated using least squares as follows:

$$\hat{\beta} = (\mathbf{X}^T\mathbf{X})^{-1}\mathbf{X}^T\mathbf{Y}. \tag{4.6}$$

The fitted data $\hat{Y}$ are, therefore,

$$\hat{\mathbf{Y}} = \mathbf{X}\hat{\beta}. \tag{4.7}$$

After parameter estimation statistical inferences are made about the parameters by using contrasts. For this purpose, contrasts are defined as a linear combination of parameters. For example in a model with three parameters, one can ask if there is a linear increase by testing β_1 using the combination $1\beta_1 + 0\beta_2 + 0\beta_3$ with the contrast vector [100].

4.3.2 Random Field Theory

To decide whether a specific area is activated, the statistical map needs to be thresholded based on a given level of significance. Consequently, a significance level (p-value) is defined and applied to every voxel. The problem is that there are thousands of voxels in the image and in this case many of them are expected to be activated by chance even with small p-values. Therefore, the question now is about the volume or family of voxel statistics. The risk of error that the voxel values could have arisen by chance is

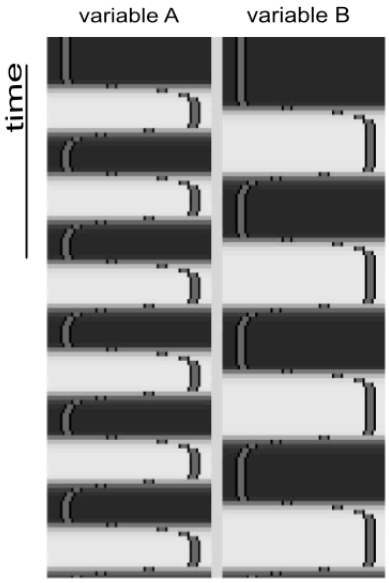

Figure 4.11: Example of a design matrix using two explanatory variables. Time is on the *y* axis and runs from top to bottom. Each column represents a predictor and the values are the results of the convolution of the box car function with the hemodynamic response function.

the family-wise error rate (FWE). This is a "multiple comparison problem" and it needs a correction to reduce the number of false positives. Typically a Bonferroni correction is used dividing the significance level at each voxel by the number of voxels. Obviously the resulting thresholds will be too small and thus rigorous. The FWE correction is based on probability rules to set the threshold above which values are unlikely to have arisen by chance. In an image with n voxels, the probability of each voxel to be greater than a threshold is α. The probability of all the tests being less than α is $(1-\alpha)^n$. Consequently, the family-wise error rate (the probability that one or more values will be greater than α is:

$$P^{FWE} = 1 - (1 - \alpha)^n. \tag{4.8}$$

For small α, equation 4.8 simplifies to

$$P^{FWE} \sim n.\alpha, \tag{4.9}$$

and the α for a single voxel level to have the requested P^{FWE} is

$$\alpha = P^{FWE}/n. \tag{4.10}$$

As an example, if a FWE rate of 0.05 is desired, then the required threshold for a single voxel would be $0.05/n$, where n is the number of voxels in the image. The Bonferrroni procedure gives a *corrected* p-value, in this case 0.05 corrected for the number

of comparisons, while the uncorrected p-value is $0.05/n$ (Brett, Penny, and Kiebel, 2003).

Although Bonferroni correction can be used to calculate FWE rates in some functional imaging analyses, it is too conservative. Most functional imaging data have some degree of spatial correlation (correlation between neighbor voxels) and the errors from the statistical model will tend to be correlated among neighbor voxels. Spatial correlation can come from the way the scanner collects and reconstructs the image, the actual physiological signal or spatial preprocessing applied to the data such as smoothing (Worsley, 2001). This means that the number of independent observations in the data is less than the number of voxels. The problem of using Bonferroni is that it assumes the individual probabilities being independent and, thus, uses multiplication for the probability of combined events. Figure 4.12 shows an example where the number of independent observations is difficult to detect when the data is smoothed.

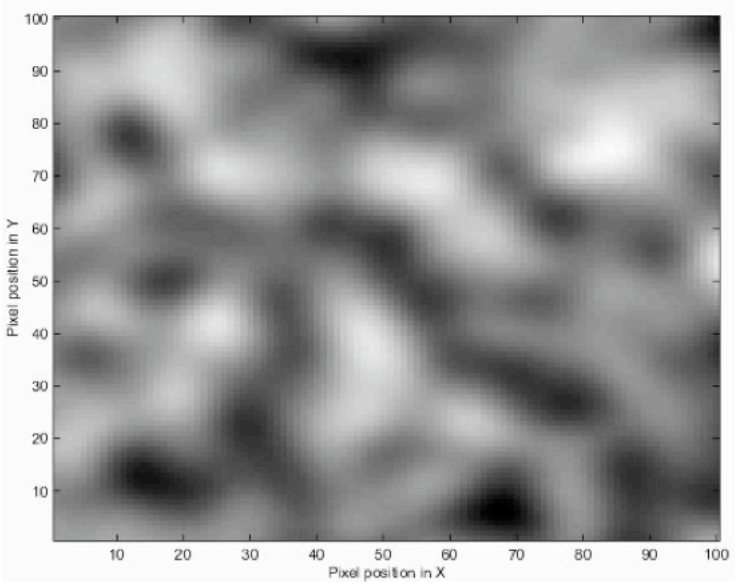

Figure 4.12: Example of an image smoothed with a FWHM of 10 pixels (Brett et al., 2003).

It is easy to see from Figure 4.12 that smoothing with a Gaussian kernel makes the problem of calculating the number of independent observation more complex. In this case Bonferroni correction can not be used and random field theory (RFT) needs to be applied. The theory of random fields provides a way to adjust the p-value that takes into account the fact that neighboring voxels are not independent. RFT can be used to find the height threshold of a smooth statistical map which gives the required family-wise error rate. The way that RFT solves this problem is by using results that give the expected Euler characteristic (EC) for a smooth statistical map that has been thresholded. It works as follows:

- estimate of the smoothness of the statistical map,

- calculate the expected Euler Characteristic (EC) which is used to find the expected number of clusters above a given threshold at different thresholds (Frackowiak, Friston, Frith, Dolan, Price, Zeki, Ashburner, and Penny, 2003),
- calculate the threshold at which we would expect 5% of equivalent statistical maps arising under the null hypothesis of containing at least one area above threshold.

In a functional image we use the smoothing kernel (FWHM) as a measure of the number of "independent" elements in the image. These are called *resels* (RESolution ELements), first introduced by Worsley, Evans, Marrett, and Neelin (1993). A resel is a block of pixels that is the same size of the FWHM. Hence, in a thresholded image, the EC can be used to get the probability of having one or more blobs with Z score greater than the critic value Z_t. The expected value of the Euler characteristic is the α value. Knowing the number of resels R and with a Z score threshold Z_t, the EC can be calculated using:

$$E[EC] = R(4 \ln 2 (2\pi)^{-\frac{3}{2}} Z_t e^{-\frac{1}{2} Z_t^2}) \tag{4.11}$$

This equation gives the probability of having one or more blobs where Z is greater than Z_t and can be used for thresholding.

4.3.3 The False Discovery Rate

There is another solution for the multiple comparison problem. Instead of controlling the chance of any false positives, the false discovery rate (FDR) controls the expected proportion of false positive among those voxels that show a significant result (Genovese, Lazar, and Nichols, 2002). This is a less stringent correction than FWE while letting some false positive detections.

Let N denote the total number of voxels being tested. Each voxel can be classified into one of four types, depending whether or not the voxel is truly active an whether or not it is declared active, as shown in Table 4.1.

Table 4.1: Classifications of voxels in N simultaneous tests.

	Declared Active	Declared Inactive	Total
Truly Active	N_{aa}	N_{ai}	Ta
Truly Inactive	N_{ia}	N_{ii}	T_i
Total	D_a	D_i	N

The FDR is given by the ratio

$$FDR = \frac{N_{ia}}{N_{ia} + V_{aa}} = \frac{N_{ia}}{D_a}, \tag{4.12}$$

that is, the proportion of declared active voxels which are false positives. The procedure for the calculation consists of computing the uncorrected p-value for each voxel and order them from the smallest to the largest. To control the FDR at level α, find the largest k so that $P_k < \alpha k/N$. This will be the corrected p-value. In this way, the resulting threshold, corresponding to the value of Z for P_k, depends on the amount of signal in the data, not on the number of voxels or smoothness. More information can be found in Worsley (2001).

4.3.4 The Small Volume Correction

When the statistics are carried out for the whole brain because nothing is known about an especific region of interest, the Euler characteristic does not depend on the shape of the object. However, factors such as volume, surface area and diameter of the search region influence the expected value of the EC, as they dictate how many resels the volume will contain. When making inferences about region activations in SPMs, if there is some hypothesis where the effect may be expected, a correction for the entire brain is not appropriate and a p-value that has been appropriately corrected based on the shape of the region must be used. To make inferences about regionally specific effects, the SPM is thresholded using some height and spatial extent thresholds. The p-values can be corrected based on the number of activated voxels comprising a particular region (*cluster level inferences*) or each peak within that cluster (*peak level inferences*).

4.3.5 Random Effects Analysis

The last step in a statistical mapping is the *random effects analysis*. It is very common to run an experiment several times with many subjects. This allows the comparison and generalization of conclusions to the population from which the subjects were drawn (Frackowiak, Friston, Frith, Dolan, Price, Zeki, Ashburner, and Penny, 2003). Random effects analysis is a statistical method to combine results across sections or subjects. In an experiment, a subject's response will vary from trial to trial. Further, this response will vary from subject to subject. These two sources of variability, within-subject and between-subject must be taken into account when making inferences about the population (Friston, Ashburner, Kiebel, and Nichols, 2006; Smith, 2001).

In statistical terminology, if one wishes to take the variability of an effect into account, the effect must be considered as a "random effect". Subject specific effects are estimated in a first level analysis and the contrasts of parameter estimates are then reentered into a GLM of a second-level SPM analysis (Penny and Holmes, 2004).

The difference relies on the fact that in the fixed effects analysis, the error variance

is estimated on a scan-to-scan basis assuming that each scan represents an independent observation. In this case the degrees of freedom are essentially the number of scans (Friston, Ashburner, Kiebel, and Nichols, 2006). In random effects analysis, the appropriate error variance is based on the activation from subject to subject where the effect constitutes an independent observation and the degrees of freedom fall according to the number of subjects. Therefore, which analysis should be done actually depends on the experimenter's question having in mind that although more conservative, random effects allows the inference to be generalized to the population from which the subjects were selected.

4.4 Summary

This chapter addressed the necessary steps to assess signal changes related to brain activation in a functional imaging study. The preprocessing constitutes an important step of this process and was discussed here. Moreover, the statistical parametric mapping used to make the statistical inferences about localized activation was presented.

5 Methodology

5.1 Experiment Design

The experiment consisted of simultaneously recording EEG and fMRI of 11 subjects (10 males) in an auditory frequency discrimination learning task. Subjects were 22 to 40 years old, with no auditory or visual complaints. Informed consent was obtained from each subject before the experiment, in accordance to the ATR Human Subject Review Committee. During the task, auditory and visual stimuli were delivered interleaved in an oddball paradigm.[1] The visual stimuli were used to control attention to the task. The task consisted of detecting a deviant stimulus on a sequence of standard stimuli. Each subject responded whether or not there was a deviant in the sequence by pressing the right or left bottom.

5.1.1 Auditory Stimulus

Each auditory stimulus was composed of five tones (400 Hz, 600 Hz, 700 Hz, 800 Hz and 1000 Hz) with a total duration of 150 ms (10 ms of rise and fall times). These pure sinusoids were summed to compose a complex sound used in the experiment (Figure 5.1). These frequencies were defined based on the frequency response of the tube phone used

[1] An oddball discrimination paradigm involves responding to stimuli that are dissimilar to the majority of stimuli presented.

to deliver the stimuli (Figure 5.2). The tube phones are MRI compatible and provides a fairly flat signal until around 1 kHz. The deviant stimulus differed from the standard one in the frequency of the fourth tone. Frequency deviations varied from 1Hz to 40 Hz with steps of 1 Hz. Stimuli consisted of sequences of five sounds with random interstimulus interval varying from 450 to 500 ms. Each sequence had at most one deviant sound in position 2, 3, 4 or 5 as shown in Figure 5.3. Stimuli were delivered binaurally through a plastic tube of 6.10 m attached to foam earplugs (ER-30 tube phone, Etymothic Research) inserted into the subject's ear. The tube introduced a constant delay of 64 ms in sound presentation to the ears.

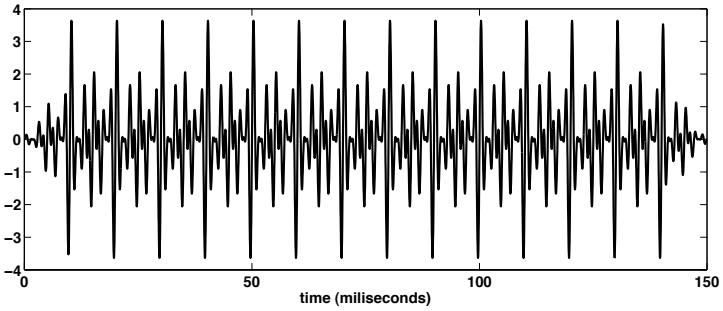

Figure 5.1: Auditory stimulus used in the experiment. Complex auditory stimulus delivered to the subject, with 150 ms length and 10 ms rise and fall times.

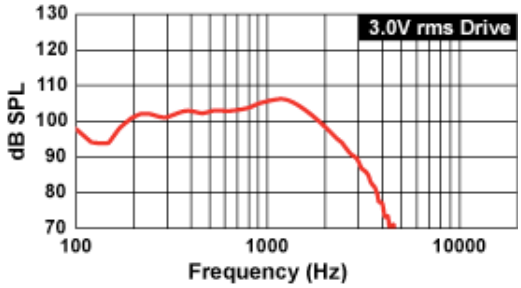

Figure 5.2: Frequency response of the tube phone used to deliver the stimuli (after Etymotic Research, 2002).

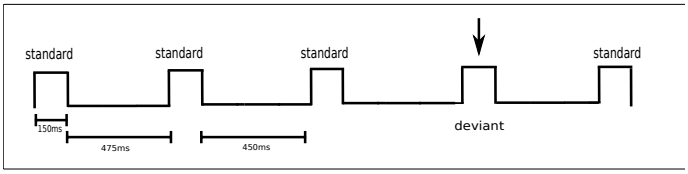

Figure 5.3: Auditory stimuli delivery. Auditory stimuli consisting of five complex sounds. The arrow indicates the deviant stimulus in position four.

5.1.2 Visual Stimulus

Visual stimulus followed a similar paradigm. Standard stimulus consisted of a white rectangular horizontal bar positioned in the center of a screen (40 cm from the eyes, viewed through a mirror). The deviant bars were also positioned in the center but rotated clockwise on steps of 0.2 degrees until 12 degrees as shown in Figure 5.4. Stimuli were delivered in sequences of five separated by 450 to 500 ms. As in the auditory stimulus presentation, in each sequence of five stimuli there was only one deviant bar and it was never in the first position.

(a) (b)

Figure 5.4: Visual stimulus used on the experiment. (a) Horizontal bar used as standard stimulus. (b) A bar rotated clockwise (deviant stimulus).

5.1.3 Stimuli Delivery: the Staircase Method

In a sequential experiment the course is determined by the preceding stimuli and responses, also known as an adaptive procedure. Up-down methods are examples of adaptive techniques that have received a lot of attention in psychoacoustic experiments. Adaptive techniques are widely used in psychoacoustics for rapid measurement of predetermined points in the psychometric function (Levitt, 1971). In a detection task they provide a method of estimating the signal level L that is required for the subject to obtain a particular proportion of correct responses P_c. In these methods the level of the signal is determined on each trial based on the responses of the subject on previous trials. Whether or not to change the signal level on a given trial is determined according to some previous rules which characterize the adaptive technique. The most used rules for changing the levels of the signal are the one-up one-down (1 step), the one-up two-down (2 steps) and one-up three-down rules (Paffen, Verstraten, and Vidnyánszky, 2008; Kollmeier, Gilkey, and Sieben, 1988; Levitt, 1971). In the one-up one-down method the stimulus level is decreased (or increased) after a positive (or negative) response as shown in Figure 5.5(a). When the stimulus level changes from decreasing to increasing or vice versa, the value at

which that change occurs is labeled a reversal. To finish the method it is necessary to define the maximum number of reversals allowed. The increments by which the stimulus is changed are known as *step*.

The one-up two-down staircase procedure was used in the present study as a *forced-choice tracking method* to track variations in auditory (or visual) detection. In this method the stimulus level is decreased after two positive responses or increased after one negative response in each trial, as shown in Figure 5.5(b). For positive response it means detecting a deviant in a sequence of five sounds or five bars. The amount of reduction or increase is determined by the step size. The end is reached after a predefined number of reversals or number of trials. Threshold estimation is done using the arithmetic mean of reversal values.

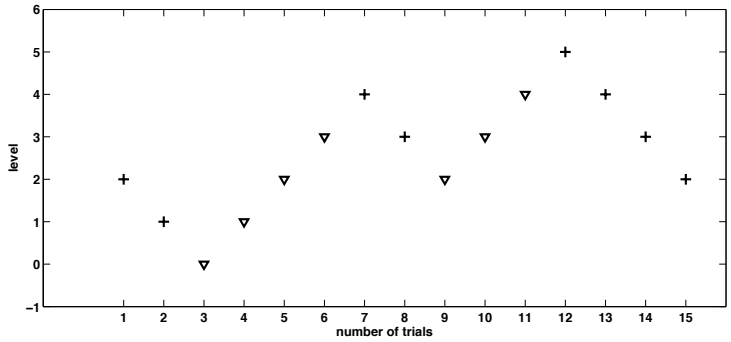

(a) One-up one-down staircase procedure. The stimulus level is decreased after one positive response (+) and increased after one negative response (▽).

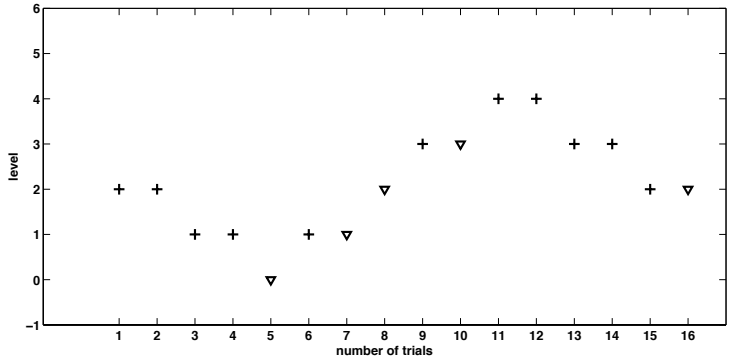

(b) One-up two-down staircase procedure (two alternative forced choice). The stimulus level is decreased after two positive responses (+) and increased after either a negative response (▽) or a positive response followed by a negative one in the next trial.

Figure 5.5: Examples of staircase procedures."+" represents positive response and "▽" represents negative response.

At first, the staircase was used in the behavioral test to find in which level the deviant stimulus would start for each subject. To avoid the subject guessing which stimulus comes

next, two staircases were implemented and run pseudo-randomly. The final level (the level that would be used to start the main experiment) was an average of both results. Following recommendations in Garcia-Perez (1998) the number of reversals was 15. A variation of the standard procedure was done halving the step size at each "down" run. This increased convergence without loosing accuracy. The starting values of frequency deviations for the two staircases used in the behavioral test were 18 Hz and 19 Hz and for the visual deviation it was 4 degrees for both staircases.

5.1.4 Behavioral Test

Frequency discrimination ability was tested behaviorally in a sound attenuation booth with attenuation level of 40 dBA. To deliver the sounds a notebook IBM lenovo 2.33 GHz was used with stereo headphones Sony MDR-CD180. The sounds were delivered on a pseudo-random sequence based on the one-up two-down double-interleaved staircase procedure described above. Subjects had to press the keyboard (/1/ or /2/) to indicate whether or not a deviant sound was present in the sequence. The ability to determine small variations in clockwise rotation of a rectangular bar from horizontal position was also tested behaviorally. The response was recorded in the same manner as in the auditory test. In both tests no feedback was sent to the subject. The discrimination level obtained in the behavioral test was used as a starting point for the staircase in the MRI experiment.

5.1.5 3D Scanning

After the behavioral test, the subject was placed with a 64 electrode cap as shown in Figure 5.6. The electrodes were pin type sensors placed inside a plastic holder mounted on the cap. All electrodes were made of pure sintered Ag/AgCl. The Ag/AgCl electrode is very well suited in biology for current-carrying applications (Grimmes and Grottem, 2000). It is usually made of silver covered by an AgCl layer. In general, products are considered safe in MRI if they are non-metallic (such as plastic or silicon based) or non-ferromagnetic (not including iron, nickel or cobalt). A three dimensional (3D) digitizer (FastScan hand-held laser scanner) was used to acquire subject's head shape and each electrode's position for the source localization procedure. An example is shown in Figure 5.7. The scanning rate is approximately 50 lines/second and the line-to-line resolution is 1 mm at 50 mm/second.

5.1.6 The Setup

The experiment setup is shown in Figure 5.8. A control unit was used to send and receive data from the scanner. Stimuli were delivered through an optic fiber to the MRI

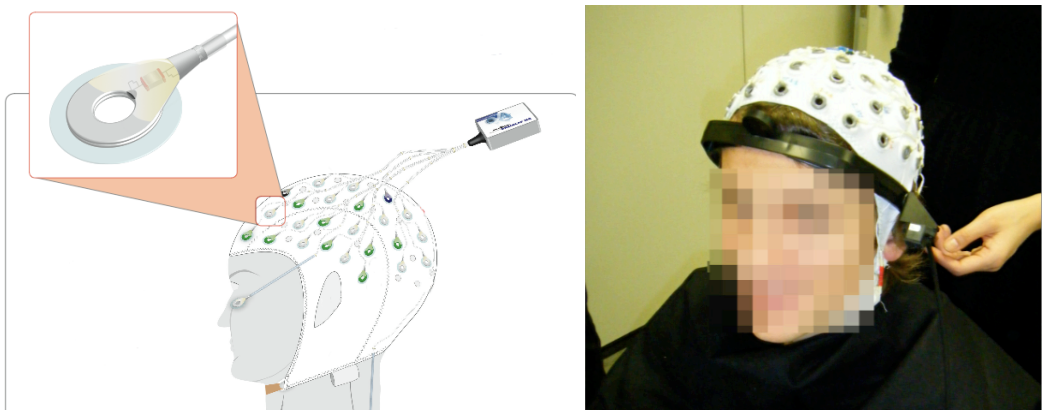

(a) Cap with 64 electrodes (including one ECG and one EOG) used in the experiment and how it is fitted to the subject's head.

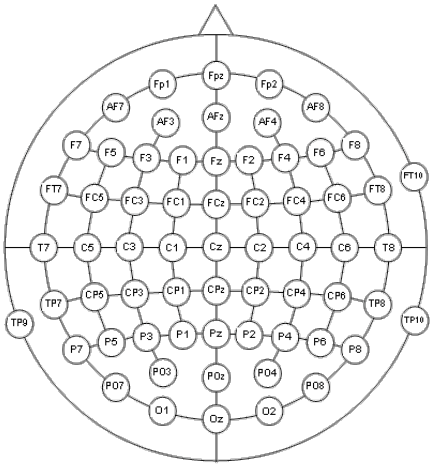

(b) Electrodes montage on a 64 electrode cap. Mastoid electrodes: TP9 and TP10.

Figure 5.6: 64-channel cap with standard layout.

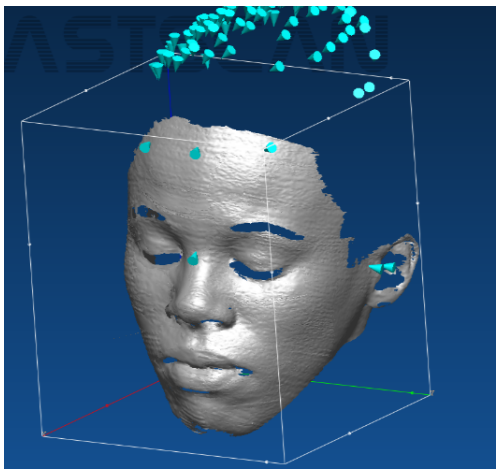

Figure 5.7: Scanned face of a subject with electrodes and markers in the fronthead and ears.

room. The EEG recording system was also connected to the amplifiers via an optic cable.

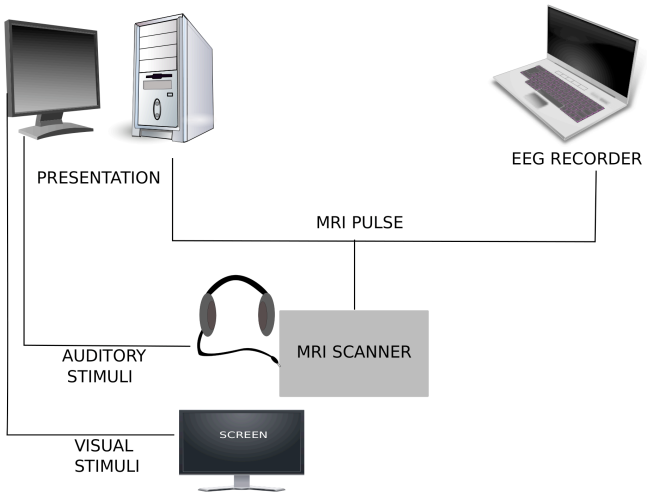

Figure 5.8: The experiment setup.

5.1.7 The Main Experiment: a Sparse Design

For the electrophysiological and functional measures the stimuli were delivered according to the staircase procedure used in the behavioral test, although in the main experiment only one staircase was used. For stimulus delivery we used Presentation Software (www.neurobs.com), a stimulus delivery and experimental control system for neuroscience. The stimulation protocol and hardware communication were implemented using the presentation control language (PCL). Auditory stimulation was delivered binaurally through a plastic tube attached to foam earplugs using the commercial system ER-30 Etymotic Research that is MRI and EEG compatible. A sparse image acquisition technique was applied to prevent contamination of the BOLD response by the acoustic noise of the scanner and to limit the epochs of contamination of the EEG by the gradient switching during the image acquisition. Functional MRI data were acquired using a Shimadzu Marconi's Magnex Eclipse 1.5T PD250 scanner. Functional data consisted of T_2^*-weighted, gradient echo, echo-planar imaging sequence (TE=48ms and flip angle 90 °). During each scan, 165 volumes were acquired over 16.5 minutes. The repetition time (TR) was 6 seconds and the scanning time (TA) was 2 seconds. Stimulus presentation was made during the "silent" 4 second period. Each volume was composed of 20 axially oriented contiguous slices with 4x4x5 mm voxel dimensions and 1 mm gap between slices. fMRI data from the first two volumes of each run were discarded to allow for magnetic saturation effects. At the end of the experiment a T_1-weighted structural scan was acquired to align functional data across multiple scanning runs to a subject's reference volume.

The experiment consisted of two types of task conditions: auditory and visual. Trials of a single condition were grouped together in blocks of 18 sequences of ten stimuli (five auditory and five visual) lasting 120 seconds in total. Auditory and visual stimuli were interleaved in a sequence separated by a pseudo-random interval ranging from 150 to 175 ms. Each block started with a visual instruction in the center of the screen 40 cm far from the subject's eye. Based on what was shown (<Picture of a ear for auditory condition> or <Picture of an eye for visual condition>) the subject had to pay attention to the auditory or visual stimuli. Each instruction lasted four seconds on the screen. Task order was counterbalanced across scanning runs and subjects. Stimuli were delivered during the four seconds of silence when there was no scanning. Before each group of five auditory and five visual stimuli there was a baseline ranging from 650 ms to 800 ms. After each sequence of 10 stimuli (visual and auditory) participants were asked to indicate, by pressing a button with the right hand (after a green cross appeared on the screen), whether or not a deviant was present in the sequences. A visual feedback (positive or negative) was sent after each response. If no response was detected after 1500 ms, a negative feedback was sent. There was a rest condition between each instruction and the start of the stimuli as well as at the end of each block. Figure 5.9 shows a scheme of the experiment. The whole experiment consisted of four runs of eight blocks each (four blocks of auditory attention and four blocks of visual attention), resulting in 144 trials acquired per condition per run. Each run lasted 16min30s. In the experiment, non-attention to stimulus was maintained drawing the subject's attention to the other modality (visual or auditory).

It is important to say that a decision was made when designing this experiment. The main objective was to investigate learning, and because of that it was important to use a variable-ISI design as it seems more "random" to the subjects. With a fixed ISI, anticipation effects can become quite substantial in subjects just before a stimulus appears, as they catch on to the timing of the experiment. However, the trade-off is a loose of detection power. Since each point of the HRF will be sampled fewer times there will be less confidence in the accuracy of any given estimate. Another issue was the choice of a sparse design to reduce the acoustic noise contamination in the cognitive state of the subject. Nevertheless, the experiment becomes long and the last run can reflect effects of fatigue.

5.1.8 Electroencephalography Recording

A 64-channel EEG was registered using the fMRI-compatible BrainVision recorder system (Neurobs) in a continuous mode using the BrainCap-MR 64 electrode cap (Brain-Products, Munich, Germany). Potentials recorded at each site were referenced to the

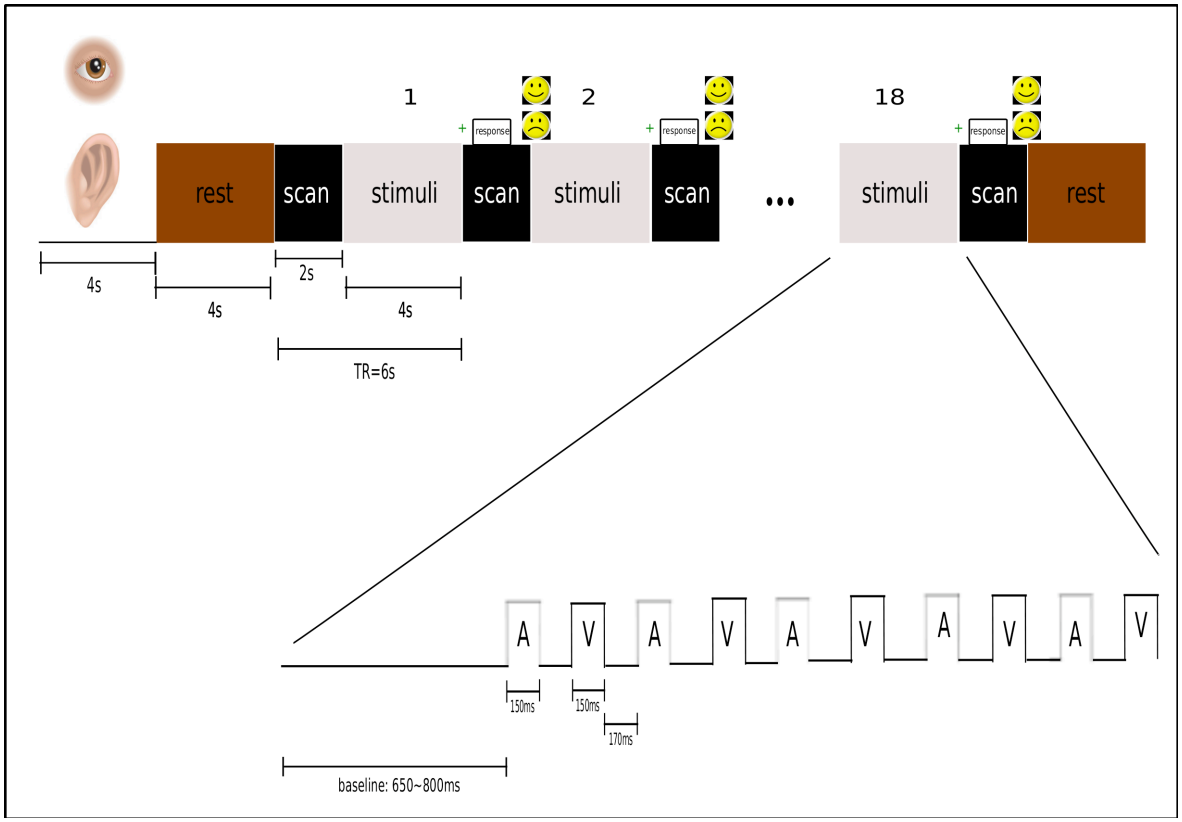

Figure 5.9: Scheme of the experiment. Auditory and visual stimuli are delivered interleaved.

center of the head (Cz). Eye movements were monitored with an electrode below the left eye. Electrocardiographic activity (ECG) was also recorded simultaneously. Electrode resistance was kept below 5kΩ, filling the holder with gel to reduce skin conductance. Data were sampled at 5 kHz per channel. The stimulus delivery system sent pulses to the ERP recorder system to tag the EEG at each stimulus and response event.

The amplifier

We used a shielded, non-magnetic, battery operated amplifier which was placed inside the scanner close to the subject's head. The short length cables minimizes loop current between electrode cap and amplifier. From the amplifier, the digitized signal was sent via optic cable to the USB interface in the control room. The specifications can be seen in Table 5.1. A 16 bits resolution is important to record signals without clipping and still resolve activity down to 0.5 mV approximately.

Table 5.1: A single amplifier specification.

Amplifier	
Number of channels per unit	32
Bandwidth (Hz)	0.016 to 250
High pass filter (Hz)	0.016
Input noise (μVpp)	<1
Input impedance (MΩ)	10
A/D-C (bit)	16
A/D rate (Hz)	5000
Max. sampling frequency (Hz)	5000
Resolution (μV)	0.5
CMRR (dB)	$\geqslant$90

5.2 Data Processing

Data processing consists of five steps. First, artifacts are removed from the EEG measurements. In sequence, fMRI was preprocessed to be used in the statistical parametric mapping. The section ends with the preparation of the data for the source localization procedure and the estimated current peak analysis.

5.2.1 EEG Artifacts Removal

As stated by Formaggio, Storti, Avesani, Cerini, Milanese, Gasparini, Acler, Mucelli, Fiaschi, and Manganotti (2008), a major problem in recording EEG during fMRI scanning is the removal of artifacts that arise from interactions between the subject, EEG electrode leads and the magnetic fields in the scanner. Movement of the leads within the static field of the magnet induces an electromotive force in a wire loop according to Faraday's law. This movement is also related to heart pulse that produces a ballistocardiographic artifact in the EEG which can be of the same order of magnitude of the brain signals. However, the problem here is that the artifacts do not have the same duration and shape of the ECG pulses as it usually happens when the subject is not inside a MRI scanner. Moreover, the switching magnetic fields applied during image acquisition may induce an electromagnetic force in the electrode leads and in a wire loop. This artifact is very large and obscures completely the EEG. The processes to remove these artifacts are described below.

Scanner gradient artifact removal

The artifacts generated by the switching of the movable gradient fields and by the radio frequency pulse generated in the scanner bore are expected to be time invariant since the generation of the MR and fMRI images demands that these gradient fields are

temporally accurate.

The Vision Analyzer algorithm (BrainProducts, Munich, Germany) incorporates an approach proposed by Allen, Josephs, and Turner (2000). This software was chosen rather than MATLAB-based plug-in fMRI Artifact Slice Template Removal (FASTR, Center for Functional MRI of the Brain, Oxford, UK) because of computational costs. According to Ritter, Becker, Graefe, and Villringer (2006) both methods lead to similar results. The algorithm offers template drift detection (TDD) and subsequent template drift correction. Template jitter is caused by imperfect synchronization between the EEG amplifier and the scanner clock. TDD finds temporal shifts between the average artifact template and the individual artifact. It adjusts the start of the scan marker such that the drift is shorter than one sampling interval. With the use of the drift information, a predefined number of different average-artifact templates is calculated. To each individual artifact is assigned one template. Artifact correction is obtained by subtraction of the corresponding template.

Although the scanner outputs a TTL signal (i.e. 5 V) at the time it starts a new slice or volume acquisition (which is recorded by the amplifier), the markers are not always set correctly at the same time point within the volume's time course. So, the first step consists of shifting the start markers so that the onset of each fMRI volume coincides with the time point at which the EEG data point is being acquired. In order to correct for the exact time of the onset of each artifact the volume start markers are shifted. However, they need to be shifted in increments smaller than the 200μs intervals given by the original 5kHz sampling rate. To achieve this, the data were upsampled to 50kHz using a spline interpolation. After this there are sufficient samples to do the markers alignment.

Most of the time the gradient does not begin at the same time of the marker the scanner sets. In practice scanners can set the marker some time after the gradient switch starts. Because of that, data were segmented from -25 to 20 ms around the volume the scan markers just aligned and the time before the marker during which the data was affected by the gradient activity was measured. In the present data, the gradient activity started approximately 20 ms before the marker. As the real TR output from the scanner was 6050.1 ms, the correction period became -20 to 6030.1 ms. The baseline period was set as the entire TR to avoid different DC offsets. After scanned intervals that would be used to build the template were selected. The first volume was included although some authors prefer dropping the initial volumes to avoid dummy scans being used in the calculation. Five volumes were used to build the initial correction template and the inclusion of more volumes depended on a correlation criteria ($r>0.975$). This method of template selection is in accordance with the results shown in Ritter, Becker, Graefe, and Villringer (2006). In the final step data were downsampled to 250 Hz and lowpass filtered

to 50Hz. Figure 5.10 shows a data set with and without gradient artifact.

Ballistocardiogram artifact removal

The data free of gradient artifact was visually inspected and highly contaminated trials were eliminated. The remaining trials were segmented in blocks of 3725 ms (650 ms of baseline period) and all epochs (trials) were concatenated before the removal of baseline period's mean from each epoch (trial). Subsequently, ICA was conducted over the epoched and baseline removed data (650 ms prior to and 3075 ms after stimulus onset) in order to extract ballistocardiogram, ocular and movement artifacts (Jung, Makeig, and Westerfield, 2002; Callan, Callan, Kroos, and Vatikiotis-Bateson, 2001; Jung, Makeig, Humphries, Lee, and Mckeown, 2000).

ICA was originally proposed to solve blind source separation on linear mixtures $\mathbf{x}$ of sources $\mathbf{u}$ that are temporally independent and spatially fixed. Its first applications date back to 1986 when Heuralt and Jutten (1986) introduced an adaptive algorithm in a simple feedback architecture to separate unknown independent sources. The method has wide application on speech processing systems, telecommunications and medical signal processing. The objective of ICA is to recover independent sources given only sensor observations that are unknown linear mixtures of the unobserved independent source signals (Lee, Girolami, Bell, and Sejnowski, 2000). Eight years later, Comon (1994) elaborated the concept of independent component analysis and proposed cost functions related to the approximate minimization of mutual information between the sensors. Bell and Sejnowski (1995) working on an information theory perspective demonstrated the separation and deconvolution of mixed sources using their infomax learning rule.

In EEG analysis, maximizing the joint entropy of the output of a neural processor minimizes the mutual information among the data projections. The rows of the input matrix $\mathbf{x}$ are the EEG signals recorded at different electrodes, the rows of the output matrix $\mathbf{u}$=$\mathbf{W}\mathbf{x}$ are time courses of activation of the ICA components, and the columns of the inverse matrix $\mathbf{W}^{-1}$ give the projection weights of the respective components onto the scalp sensors. Cleaned EEG signals can be derived as $\mathbf{x}' = (\mathbf{W}^{-1})\mathbf{u}'$, where $\mathbf{u}'$ is the matrix of activation waveforms, $\mathbf{u}$, with rows representing artifact components set to zero (Jung, Makeig, Humphries, Lee, and Mckeown, 2000). In ICA decomposition, the independent component filters are chosen to produce the maximally temporally independent signals available in the channel data. These are information sources in the data whose mixtures have been recorded at the scalp channels via volume conduction. For ICA usage the mixing process is considered passive and linear but it still obscures the functionally distinct and independent source contributions. These information sources may represent synchronous or partially synchronous activity within one or more cortical region (regions)

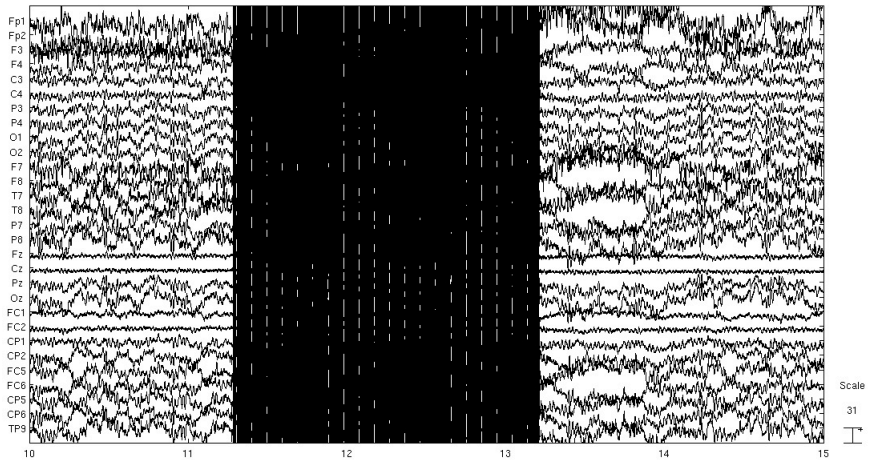

(a) Segment of an EEG data with gradient artifact.

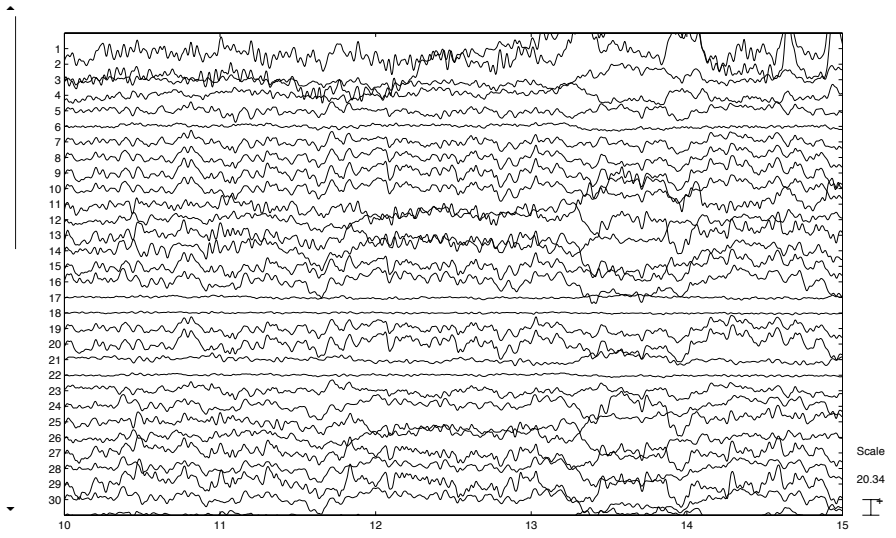

(b) Segment of an EEG data after gradient artifact removal.

Figure 5.10: Segments of EEG data with gradient artifact and after artifact removal.

and activity from non-cortical sources (e.g., potentials induced by eyeball movements or produced by single muscle activity, line noise, etc.).

In the present work the *runica* decomposition was used (Makeig, Bell, J., and Sejnowski, 1996) which implements the logistic infomax ICA algorithm proposed by Bell and Sejnowski (1995). This algorithm is part of the EEGLAB toolbox (Delorme and Makeig, 2004). The learning batch size was 66, and initial learning rate was 0.0001. This rate was gradually reduced to $4\text{x}10^{-8}$ during 95 training iterations. To determine the independent components (IC) that correspond to sources of artifacts, cross correlation analysis between each IC and EOG and ECG channels recorded simultaneously with neuronal data was performed (a component was arbitrarily considered an artifact if the correlation coefficient was greater than 0.3).

Other sources of artifacts

Slow baseline trends caused by the return to baseline after an artifact were rejected as well. These abnormal trends (linear drifts) cannot be rejected by averaging. To remove them, a first order polynomial calculated by linear regression was fitted to each section of the EEG. The data (in the components domain) is fitted to a straight line with a maximum acceptable slope (in our case 0.5 std.dev/epoch). In this case it corresponds to an epoch in which the straight line fit value might be 0μV at the beginning of the trial and 50μV at the end. The minimal fit between the EEG data and the line with minimum slope is determined using a standard R-squared (R^2) measure. Candidate epochs to be rejected should have R^2 greater than 0.2.

Another criteria was the detection of high amplitude data. As a threshold we defined a value equal to 10 times the mean of all components. The selection of the independent components to be removed was based on the three criteria described above and on the visual inspection of scalp maps as shown in Figure 5.11. The scalp map shows projections of the ICs on the electrode sites. Given the matrix $\mathbf{x} = (\mathbf{W}^{-1})\mathbf{u}$ which relates the recorded EEG signals to the sources of activation, the columns of $\mathbf{W}^{-1}$ are weight vectors which show the relation between the EEG data and the ICA component. The rows of the weight matrix represent the EEG channels location and its columns represent the ICs. Therefore, the value of the component can be used as an intensity value to fill the channel location on the scalp as illustrated in Figure 5.11. A typical example of ocular activity can be seen in component 1, while muscular artifact is highly localized as in components 58 and 59. These IC patterns were observed for component removal. After selecting the components relative to artifacts, they were subtracted from the EEG data.

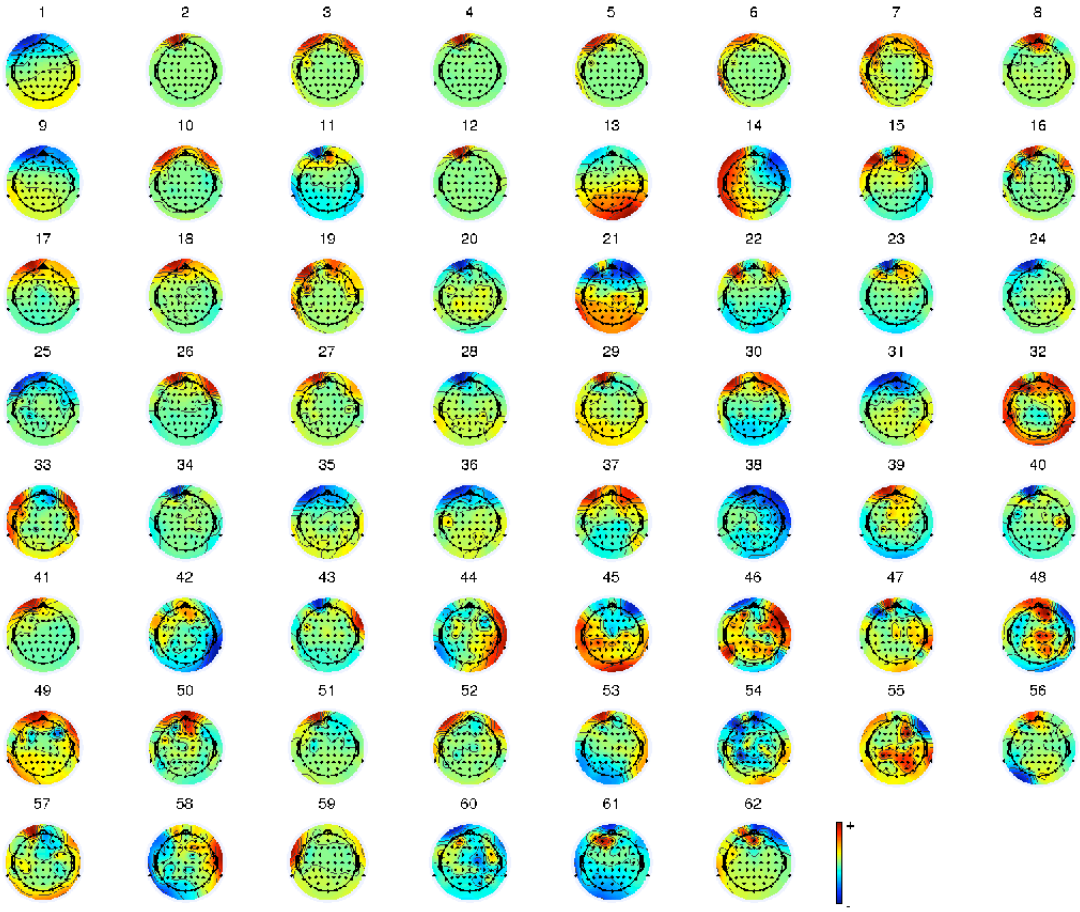

Figure 5.11: Topographical maps of the independent components.

5.2.2 fMRI Data Processing

SPM is a MATLAB package designed for the analysis of brain imaging data sequences (Ashburner, Chen, Flandin, Henson, Kiebel, Kilner, Litvak, Moran, Penny, Stephan, Hutton, Glauche, Mattout, and Phillips, 2009). As described in Chapter 4 the first step in a statistical parametric mapping of functional data is the preprocessing of the data. The first two volumes of each session were discarded to avoid data with unstable magnetization.

Preprocessing

Slice Timing Slice timing was done specifying the acquisition order (top to bottom, continuous), TR = 6 s and TA. In the case of a sparse design,

$$TA = scan\ time - \frac{scan\ time}{number\ of\ slices}. \tag{5.1}$$

where *number of slices*=20 and actual *scan time* TA=1.90 s. Slice number 10 was chosen as the reference slice. This is the midpoint of the 20 slices acquired per volume. Because top and bottom images show less structures they were not selected to be the reference.

Realign and Unwarp Realign is for motion correction. It works in two stages: the first files from each session are realigned to the first file of the first session and then within each session, the second, third and other images are realigned to the first image. After the whole process, the first image in a time series is used as a reference scan to which all subsequent scans are aligned. The *unwarp* operation was also used to model the residual movement related variance that can be explained by a model for susceptibility-by-movement interactions. Susceptibility artifacts are a consequence of the disturbances of the field caused by the presence of an object in its neighborhood. It is a property of the material. The varying field strength will affect different materials in a different way. These disturbances cause spatial misplacement of the RF signal. SPM assumes that the way deformations change when the subject changes his position is known (these are the derivatives of the deformations with respect to subject position). It means that for a given time series and a given set of subject movements it would be possible to predict the "shape changes" in the object and the subsequent variance in the time series. In this case the inverse problem can also be formulated: given the observed variance (after realignment) and known (estimated) movements, it is possible to estimate how deformations change with subject movement. The deformation field is formulated as small vectors at each position in space showing the direction that a particular location has been changed. The derivative is then the rate of change of these vectors with respect

to subject movement and is used to remove the variance caused by the susceptibility-by-movement interaction. Realignment produces the estimated parameters: the columns are the estimated translations in mm ("right", "forward", "up") and the estimated rotations in rad ("pitch", "roll", "yaw") that are necessary to shift a volume, as shown for the subject in Figure 5.12.

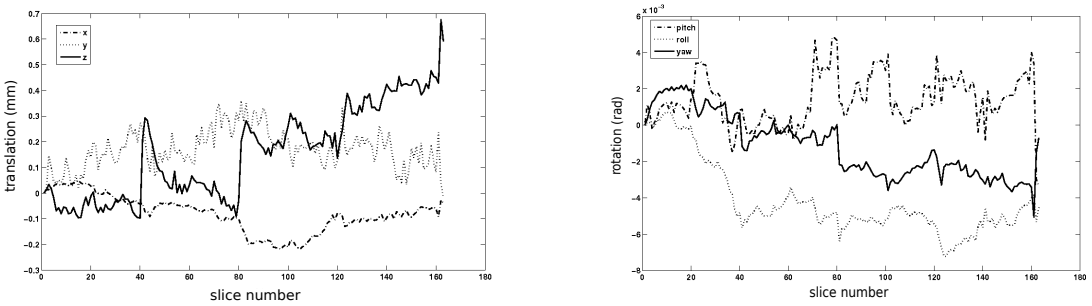

(a) Estimated translations in mm.

(b) Estimated rotation in rad.

Figure 5.12: Estimated movement parameters of one subject during the first session of the experiment.

Coregistration In order to see the locations of the activations in the subject's brain, it is necessary to coregister functional data to the high resolution structural image. This step also improves the later stage of normalizing to a template. Thus, coregister was used to align the mean functional volume (produced by the realignment step) specified as the *target image* to the higher resolution MRI specified as the *source image*. Since there is no deformation (as the images come from the same brain), coregistration is performed finding the three translations and three rotations parameters. It maximizes the mutual information between two images:

$$I(\mathbf{f},\mathbf{g}) = \sum_{y\in f}\sum_{x\in g} p(x,y) log\left(\frac{p(x,y)}{p(x)p(y)}\right), \tag{5.2}$$

where p(**x**,**y**) is the joint probability of images **f** an **g** and p(**x**) and p(**y**) are the marginal probabilities.

After alignment the two images have the same origin and axes, as in Figure 5.13.

Normalization Spatial normalization is the process of warping images from all the individuals into the same standard space to allow signal averaging across subjects. Once this step is completed, it is possible to refer to a given location in any single brain independently of the gyral anatomy, for example. The most used space in SPM is the MNI-Talairach referential and is defined by a T_2 template image (ideal model) as shown

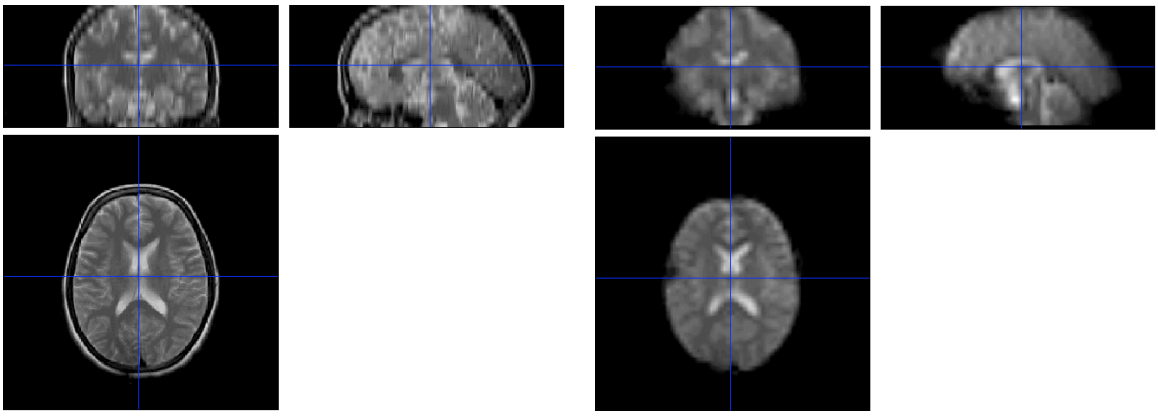

(a) Structural image. (b) Functional image.

Figure 5.13: Coregistration of anatomical and functional images. The crosshair is at the same point in both images.

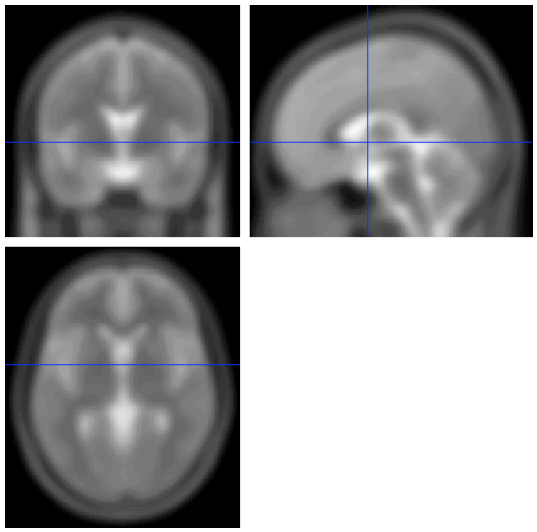

Figure 5.14: MNI Template with voxel dimensions 2x2x2 mm.

in Figure 5.14. This work used the T2.mnc anatomical image available in SPM2 package. All the other images are normalized to this reference. The algorithm works by minimizing the sum of squared differences between the images and the template. It uses an affine transformation with 12 parameters (three translations, three rotations, three scalings and three shears)(Ashburner and Friston, 1997). Images were spatially normalized by resampling every 3 mm using sinc interpolation.

Smoothing Functional images were convolved with an isotropic Gaussian kernel of 8 mm width. Smoothing is applied to compensate for residual between-subject variability after normalization as well as to permit application of Gaussian random field theory at the statistics inference step.

Model specification and parameter estimation

After preprocessing, the model for the statistical analysis was defined. First, the design was specified through the design matrix. This matrix of explanatory variables is made up of column vectors which predict physiological responses to different task conditions. Three sessions were specified with 163 scans each and two conditions: auditory and visual. Onset vectors with the onset times of each type of stimulation being studied on each condition were specified.

- standard auditory stimulus during auditory task;
- standard auditory stimulus during visual task;
- deviant auditory stimulus during auditory task (attention condition);
- deviant auditory stimulus during visual task (non-attention condition);
- rest condition (periods of no stimulation).

An onset vector is a vector with the onset time (seconds) of each stimulus. This is the vector to be convolved with the impulse response function. The standard stimulus position was selected based on the position of the deviant stimulus but in random order. In this case we assure we have the same amount of deviants and standards. The onsets for rest periods were selected from the two rest intervals in the experiment. For the first interval we took a random number after the instructions interval and for the second rest period we took a random value after the block of 18 stimuli. The design matrix for this experiment can be seen in Figure 5.15. Each column of the design matrix is the predicted fMRI signal that a voxel would show to a particular stimulus. Each row is a moment in time, with one row per MRI image-acquisition. Thus, reading down a column gives the response through time to a particular stimulus. As an example, in our case, the first column of the design matrix would be the vector "predicted signal that a standard auditory stimulus would evoke" and the second column would be the vector "predicted signal that a deviant auditory stimulus would evoke". Given a design matrix $\mathbf{X}$ and an fMRI signal measured from the scanner $\mathbf{y}$, the estimated parameter $\hat{\beta}$ is given by

$$\hat{\beta} = (\mathbf{X}^T\mathbf{X})^{-1}\mathbf{X}^T\mathbf{y}. \tag{5.3}$$

The individual subject analyses, low-frequency drifts or other physiological influences (e.g. changes in basal metabolism) were accounted for by using a high-pass filter (constructed by discrete cosine basis functions) in each voxel's timecourse. The cutoff parameter used was 128 s. Although it might be too conservative compared to the short trial interval, we have seen that this value is an arbitrary part of the process.

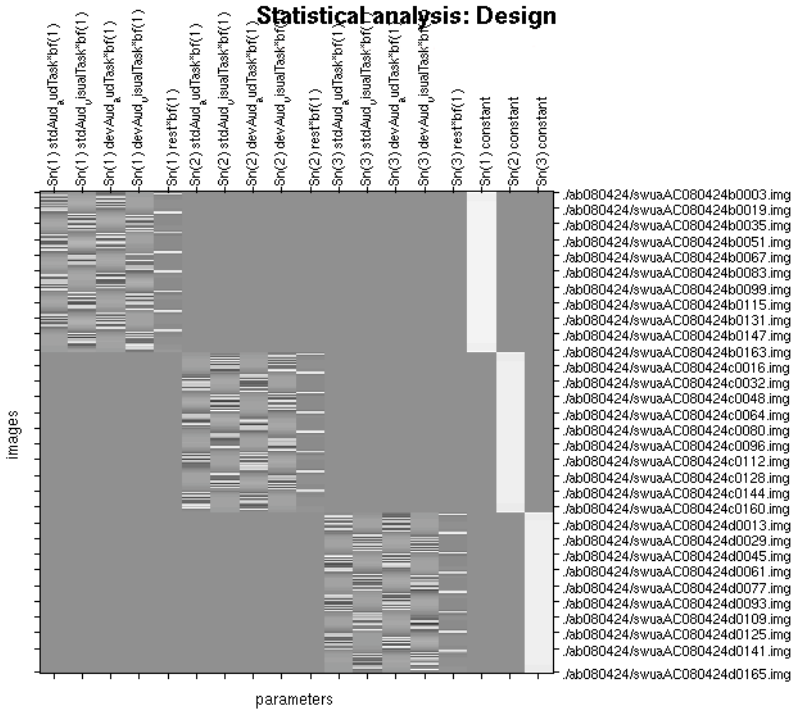

Figure 5.15: First level design matrix showing 3 sessions of one subject. The five columns for each session of the matrix represent the parameters estimated for the tested conditions. The last three columns are mean values of the whole brain activity.

In order to interrogate the results, we need to define the contrasts we want to analyze. Contrasts are conditions based on the parameter estimates of the predictor vectors created in the design matrix. t-tests were used to look at either positive or negative differences between parameter estimates. For example, when testing whether attention condition has increased activity compared to non-attention condition, for one single subject we have the representation shown in Figure 5.16. This contrast asks the question of which voxels showed increases in the first condition relative to the second. We also need to specify the p-value for the statistics test. Our questions were concentrated on the auditory task and consisted of:

- Where is auditory activation located?
- Where is visual activation located?
- What voxels showed increased activation in the auditory relative to visual condition? (testing attention)
- What voxels showed increased activation related to learning?

With these questions in mind we tested auditory and visual activations using the respective conditions against rest. To localize brain regions involved in the attentional

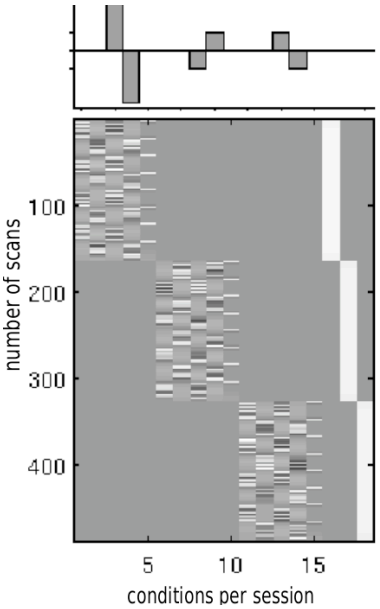

Figure 5.16: Design matrix of one subject and its weighted contrasts. Condition 3 (attention) is tested against condition 4 (non-attention) in each session. The contrasts at each session are weighted by the subject's performance in this session.

demands, activations in the attended and unattended conditions were directly contrasted. In addition, a measure of performance change indicating learning was assessed using the difference between beginning and ending thresholds for each session as a regressor in the design matrix.

Random Effects Analysis

In studies where it is desired to make inferences about an effect that extends to the population from which the subjects were drawn, it is necessary to employ a statistical model that explicitly accounts for multiple comparisons. These are called random effects and require two stages of analysis: analysis of individual subjects (intra-subject variability or fixed effects), as shown above, and an analysis of the group (inter-subject variability or random effects). The contrast images created in the first stage are used as the input for a between-subject variability analysis. To perform the t-test with multiple comparison we select the same contrast images for each subject. These analysis were done for 11 subjects. At last, we wanted to investigate the changes related to performance during the learning experiment. First, a mask was done with the union of two masks: contrast image of the auditory deviants stimuli against rest and the contrast image of the visual deviant stimuli against rest (Figure 5.17). Then, we ran the random effects analysis with the attention contrast (deviant auditory against deviant visual using the difference between consecutive sessions' threshold) under the mask created in which the design matrix was weighted with

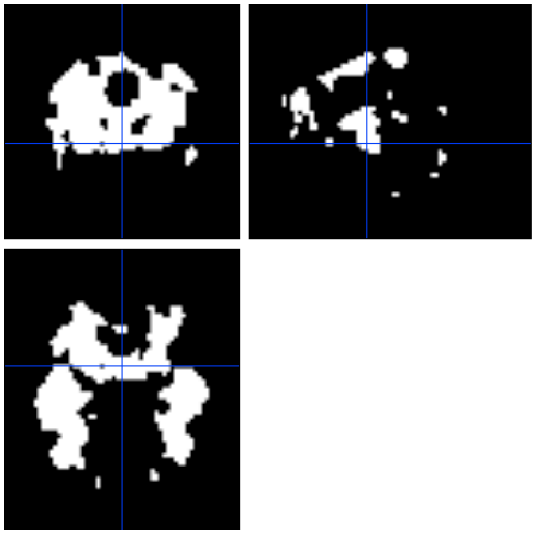

Figure 5.17: Mask used for the assessment of learning.

each subject's overall gain (difference between threshold of the last and first sessions).

The results of the statistical inference appear as significant activated voxels overlaid onto a segmented standard T_1-weighted brain used for spatial normalization (MNI template).

5.2.3 MRI Data Preparation for Spatial Localization

The source localization theory is detailed in Appendix A. The first step of the source localization procedure implemented in VBMEG (variational Bayesian MEG source estimation) was the coregistration between the MRI data (anatomical T_1 image) and the EEG data. Cortical surface extraction, mesh generation and coregistration of electrode locations with scalp surface are the main steps of head modeling and will be detailed in this section.

Cortical surface extraction

Each subject's individual cortical surface was reconstructed from structural MRI data using Freesurfer, an open source software from the Martinos Center for Biomedical Imaging designed for the study of cortical and subcortical anatomy (Dale, Fischl, and Sereno, 1999). The input of the segmentation step was a 3D saggital T_1-weighted MR image. A polygon cerebral cortex model of the boundary between white and gray matter was constructed for each subject as well as the pial surface. These surfaces were used later to constrain the solutions to the inverse EEG problem. First, intensity variations due to magnetic field inhomogeneities were corrected and a normalized intensity image from a high resolution anatomical T_1-weighted was created. In a skull-stripping procedure,

extra cerebral voxels were removed and the resultant image was segmented based on the geometric structure of the gray and white matters. The skull was stripped using a deformable template model. Voxels were then classified as white matter or not based on intensity and neighbor constraints. For the segmentation process, it is very important that the anatomical image have a good quality as shown in Figure 5.18. In sequence, the cerebral hemispheres were separated and disconnected from subcortical structures. These are called cutting planes as detailed in Dale, Fischl, and Sereno (1999). The resulting volume was covered with a triangular tessellation and deformed to produce a smooth representation of the gray/white boundary and the pial surface. A pial surface segmentation in shown in Figure 5.19.

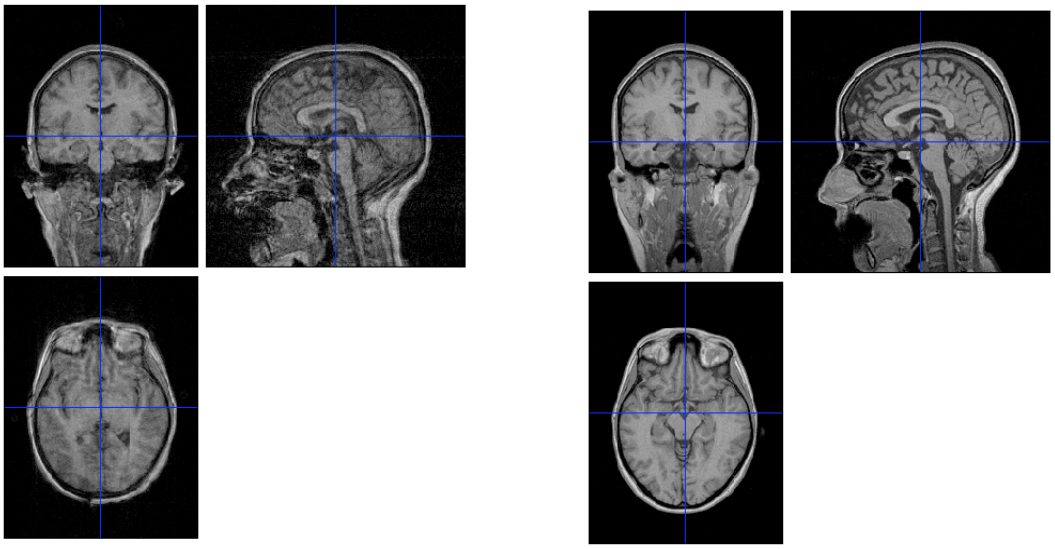

(a) Bad quality image with artifacts due to motion. (b) New image of the same subject, without motion.

Figure 5.18: Bad and good quality images. On the top of the head in (a) there are problems in the boundary.

Skull extraction and mesh generation

Although a spherical head model had been used in many reconstruction models to solve the EEG inverse problem (Spinelli, Andino, Lantz, Seeck, and Michel, 2000; Pascual-Marqui, 1999), recent methods are based on realistic models of the skull, scalp and brain that are suitable for electroencephalography source modeling. Modeling of the compartments in the head uses the boundary element method (BEM). Triangular meshes for the BEM were derived from the MR images using automatic segmentation techniques. The complete 3D model was obtained using a triangle net with approximately 95000 surface triangles (depending on the shape of the head) with side length of 1 mm. An example of

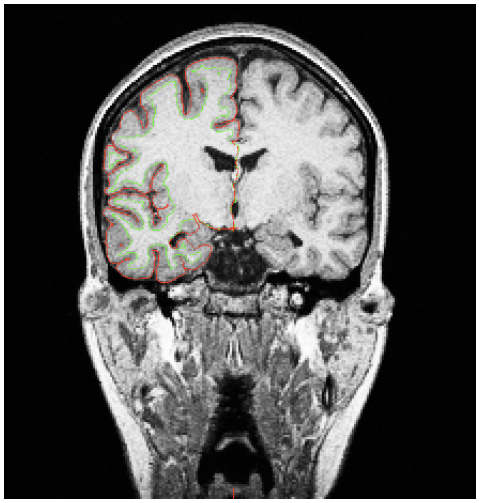

Figure 5.19: Pial segmentation.

a final model of the skull is shown in Figure 5.20.

Figure 5.20: Skin, scalp and skull (from the outermost to the innermost) extracted from a human T1-weighted MRI image.

For all subjects, the skull was extracted starting from a seed point in the middle of the brain. Threshold intensity values ranged from 80 to 160 (0 is black and 255 is white) and the maximum distance between pixels was 250 mm. After the BEM process was completed, morphology operations such as dilation and erosion were performed. Erosion was done with a 3 mm structure element and dilation with an 8 mm kernel. In BEM geometry setup, skull thickness was 3.5 mm and the minimum distance between the cortex and skull was 3 mm.

Coregistration of electrodes location and scalp surface

The electrode coordinates, measured by the digitizer, were mapped to the 3D volume coordinates. The landmarks (right and left preauricular and nasion) of the digitizing step were used as reference points. The fitting was done by finding the best translation

and rotation parameters that minimize the total distance between the sensors and scalp surface. A good fitting was reached with a quadratic error not greater than 2 mm and a mean distance between points of approximately 0.7 mm.

5.2.4 VBMEG Data

The steps described in the previous session are crucial to the source localization procedure. All the models: cortical surface, head and fMRI data were incorporated into the VBMEG algorithm. The cortical data, skull data and EEG data were coregistered and incorporated in the lead field matrix to the variational Bayesian estimation. The fMRI data were used to estimate the area of active dipoles.

Three shell head surface for the EEG model

The goal of EEG modeling is the relationship between a primary current source distribution and the data at the sensor array. The linearity of the model can be expressed as the inner product of a vector lead field and the primary current. The method employed follows Mosher, Leahy, and Lewis (1999) in which the lead field is partitioned into the product of a sensor matrix, a kernel matrix and the moment of the dipole. The sensor matrix models sensor orientation. The kernel matrices are functions of the sensor, source locations and the head geometry. The most used head models assume that it is made up of a set of concentric spheres, each with homogeneous and isotropic conductivity. Moreover, this method can be improved by using more realistic head shapes extracted from anatomical images. This approach was carried out in the present work, still assuming each region with constant conductivity. The conductivity ratios from the innermost to the outermost regions are 1.0, 0.0125, and 1.0 for CSF, skull and scalp, respectively. The cerebrospinal fluid of the cortical surface extracted from Curry software (Neuroscan Labs) was imported into VBMEG. The scalp surface was built from the intersection between the scanned face and dilated CSF. The third element of the head model, the outer skull surface was made by expanding the scalp surface using a spring model and subsequent erosion. An example is shown in figures 5.21 and 5.22.

Activity map

When running an fMRI analysis, the statistical maps of the desired contrast (their values and coordinate space) are stored in the MATLAB workspace. These thresholded statistical values were backprojected onto each subject's original space (without normalization) in order to be used in VBMEG and incorporate fMRI information in EEG current source estimation (Figure 5.23). The normalization procedure for the anatomical image

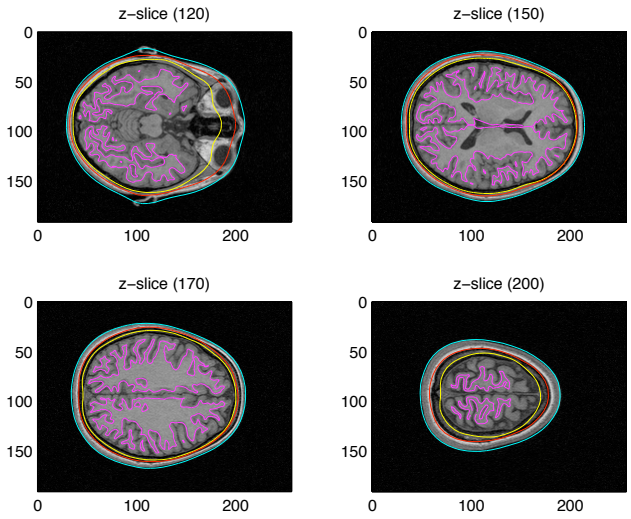

Figure 5.21: 3 shell head model for inverse method solutions.

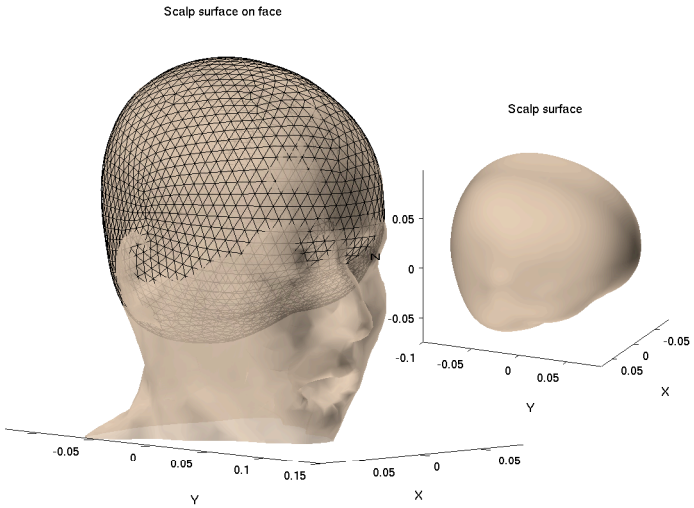

Figure 5.22: Scalp surface superimposed to the subject's face.

described in Chapter 4 finds the transformation that maps the actual anatomy (and anything coregistered to it) into the MNI template brain space. The output is, thus, a normalized anatomy file, and a MATLAB data file containing the transformation parameters. These parameters are then used to backproject from the normalized to each subject's space.

In sequence, the activation results of the fMRI analysis were stored in two structures: an area file, which has the areas of activation, and an activation file, with the values of the statistics. The fMRI data in the VBMEG structure is based on vertex indexes of the cortical surface and the results of the SPM analysis, defining the active dipole indexes. They are written as a new area file and the strengths are written in the activation file

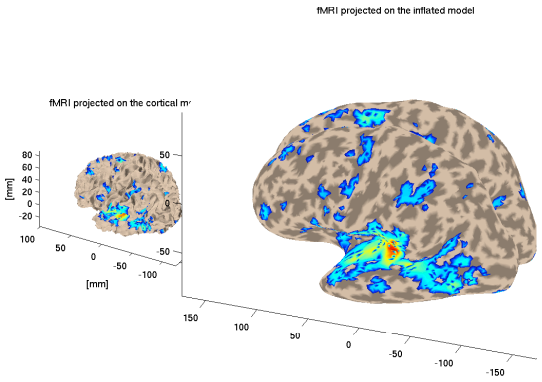

Figure 5.23: fMRI data projected onto the subject's individual surface.

as the Gaussian-average of the intensity values of the fMRI voxels in the neighborhood (the maximum distance for averaging was 6 mm). Three regions of interest (ROI) were selected according to the SPM results of the learning condition investigation: left frontal, left temporal and right temporal as shown in Figure 5.24. These areas were created using a mask with the "learning" contrast and extended voxels equal to 50 to clear out areas of no interest.

The lead field matrix

With information of dipole location from the brain model (cortex vertex indexes) and the position of the EEG sensors on the scalp, the EEG potentials for the multilayer model were calculated. First, EEG positions were mapped to the outermost surface of the 3 shell head surface, calculating the nearest vertex to an EEG sensor. The distance from the EEG sensor to the head vertex was used to interpolate the head potential to the sensor position. The lead field matrix is, therefore, a transform matrix to map the surface potential to the EEG data.

The current variance estimation was done using the time sequence of all trials. Each individual's activity of all conditions was used as a constraint (Figure 5.25). EEG data is shown in Figure 5.26. The parameters of the estimation model were:

- variance magnification(m_0): 100
- number of dipoles: 30000
- confidence parameter (γ_0): 100
- time range for observation noise estimation: -648 to -4 ms (baseline period)
- time window: -648 to 3076 ms

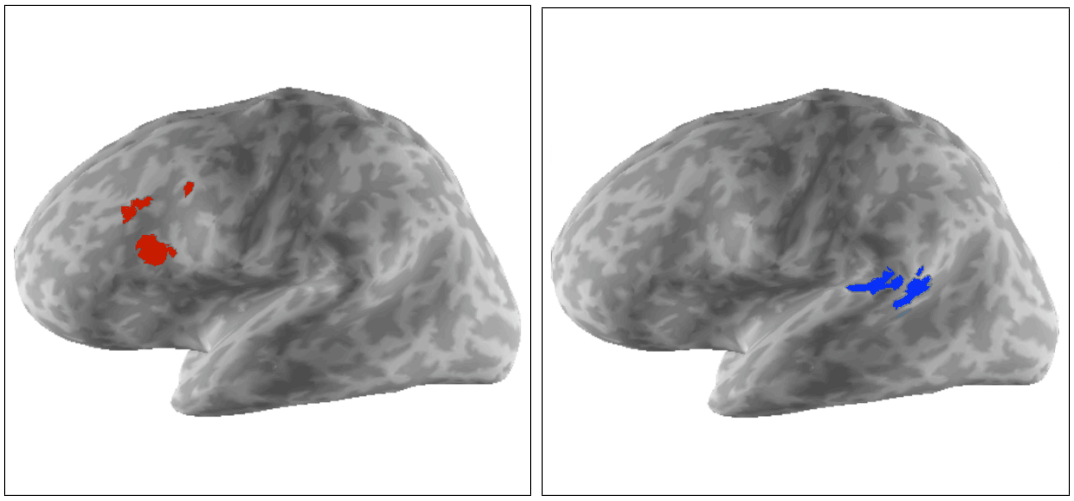

(a) Frontal ROI.

(b) Left temporal ROI.

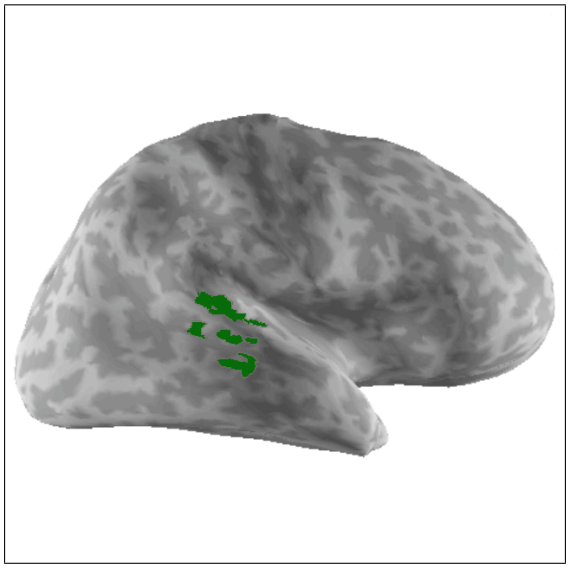

(c) Right temporal ROI.

Figure 5.24: ROI projected onto the subject's cortex.

Figure 5.25: Regions used as a constrain in the current variance estimation.

The active current area was found based on the estimated current variance. The last step was the reconstruction of the current in a specified area using the Bayesian inverse filter (Sato, Yoshioka, Kajiwara, Toyama, Goda, Doya, and Kawato, 2004).

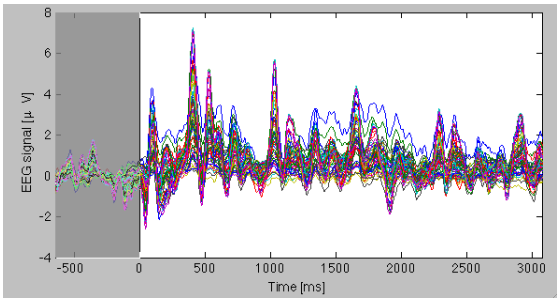

Figure 5.26: EEG data of 408 trials. Pre-stimulus data are shaded.

5.2.5 Current Peak Analysis

Current peak was selected for each area of interest: frontal, right temporal and left temporal. In each area, peak currents were chosen from a sphere of 6 mm in diameter. The current with greatest temporal mean value was selected for analysis. Current values were separated based on three conditions: auditory attended, auditory unattended (visual attended) and auditory standard.

Time frequency analysis was performed for each peak current and each subject at each trial. The signal was divided into windows and a wavelet transform performed on each window. The Morlet wavelet length starts at 3 cycles and increases by a factor of 0.5. By doing so, we explore the scaling characteristic of the wavelet by changing its width. As stated by Shyu and Sun (2002) the bigger the number of cycles the better the frequency resolution. Besides, as the Morlet wavelet transform is defined in the complex domain, the power spectrum can be interpreted in a similar manner as the Fourier spectrum. It is worth saying that a short time Fourier transform was also performed on the data but the resolution was too poor. We then have an estimate of the mean event-related spectral perturbation (ERSP) changes across event-related trials with mean baseline spectral activity subtracted. At last, a t-test was performed in the 11 ERSP images (Figure 5.27a). The analysis was done at each time-frequency bin to check if the mean distribution of 11 bins (from the distribution of 11 subjects) is different from zero. As a result there is an "image" of p values from the analysis of 11 subjects. The final result is obtained after masking out values greater than 0.05 (p>0.05).

Testing correlation between spectral results and detection threshold

In order to study the learning effect we checked whether there was a correlation between the threshold values reported by the subjects during the experiment and the signal registered. For each subject, at each time-frequency bin, the correlation between the power values of this bin over the trials and the threshold curve (frequency threshold over trials) were computed (Figure 5.27b). The correlation coefficient between two random

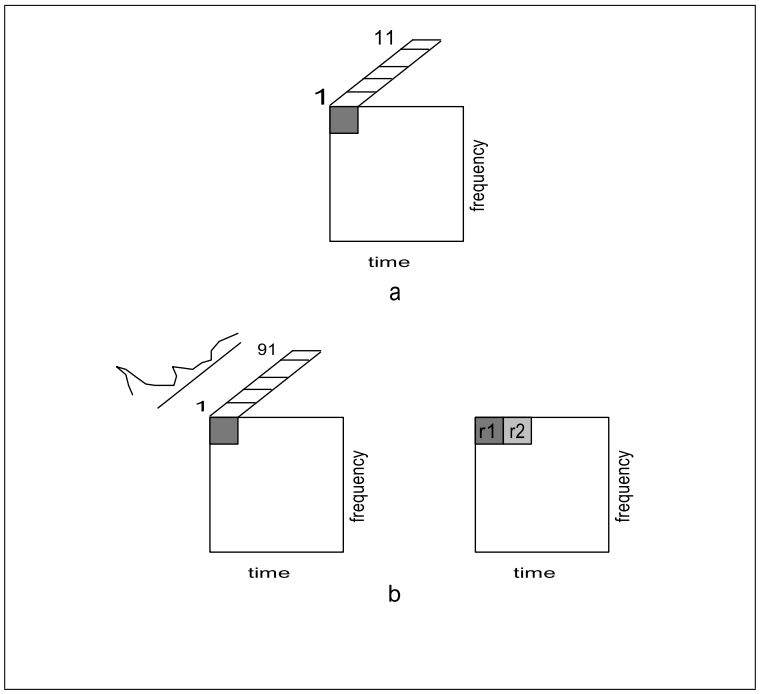

Figure 5.27: Schematic of time-frequency images of 11 subjects. a) 11 power values are taken from the same bin position and tested whether or not the distribution of 11 bins is different from zero. b) the correlation between frequency threshold values and power spectral analysis for each bin across trials is taken resulting in an image of correlation values.

variables is described by

$$\rho_{XY} = \frac{cov(X,Y)}{\sigma_X \sigma_Y} = \frac{E[(X-\mu_X)(Y-\mu_Y)]}{\sigma_X \sigma_Y}, \tag{5.4}$$

and calculated for a finite data set as

$$\rho_{XY} = \frac{\sum_{i=1}^{n}(X_i-\bar{X})(Y_i-\bar{Y})}{\sqrt{\sum_{i=1}^{n}(X_i-\bar{X})^2}\sqrt{\sum_{i=1}^{n}(Y_i-\bar{Y})^2}} \tag{5.5}$$

The result is an image of correlation values for each subject. Statistical t-tests verified the significance of the results over the 11 subjects and bins with significance values greater than 0.005 (p>0.005) were masked out.

5.3 Summary

This chapter presented the methodology carried out in the setup of the experiment as well as in the analysis of the fMRI and EEG data. The decisions about the sparse experiment design were also pointed out, explaining the compromise between the goal of the experiment (investigation of learning) and efficiency of the estimates. The results obtained are the topic of the next chapter.

6

Results and Discussion

This chapter presents some of the results obtained with the method described in the previous chapter. In the first section, the behavioral data are presented followed by the statistical analysis carried out in the fMRI data. In addition, the results of the artifact removal procedure in the EEG data are presented as well as the comparison of the performance of two ballistocardiogram artifact removal methods. The objective is to gain more insight about the particularities of each method. The chapter is finished with the source localization results. The results are very suggestive of the need of attention in rapid training performance improvement.

6.1 Behavioral Data

As explained in Section 5.1.4, the performance before and after training was recordered with the subject in a sound booth. Although the experiment was run in a different environment, these data can be used as a reference for the measurements carried out in the MRI scanner. The results are summarized in Table 6.1.

During the experiment, correct and incorrect responses were tracked and the results of four subjects are shown in Figure 6.1. Although the graphics show a performance improvement during the experiment, which suggests characteristics of learning, Figure 6.2 shows that some subjects did not improve during the three sessions. Four out of

Table 6.1: Performance before and after training.

subject	Auditory task		Visual Task	
	pre training (Hertz)	pos training (Hertz)	pre training (Degrees)	pos training (Degrees)
1	12	4	4	3
2	19	8	5	8
3	9	8	5	4
4	21	16	5	3
5	5	6	9	9
6	12	5	5	3
7	6	6	10	9
8	8	6	6	5
9	11	5	4	4
10	5	7	8	9
11	18	9	8	6

eleven subjects had this type of behavior.

The results of all subjects can be seen in Figure 6.3(a) with an exponential, quasi-linear and decreasing tendency in perceptual auditory frequency discrimination thresholds (r=0.9, p=0.004). Figure 6.3(a) shows the grand mean and the standard error of 11 subjects whereas Figure 6.3(b) shows the gain between sessions. These data give us evidence of learning behavior during the perceptual task.

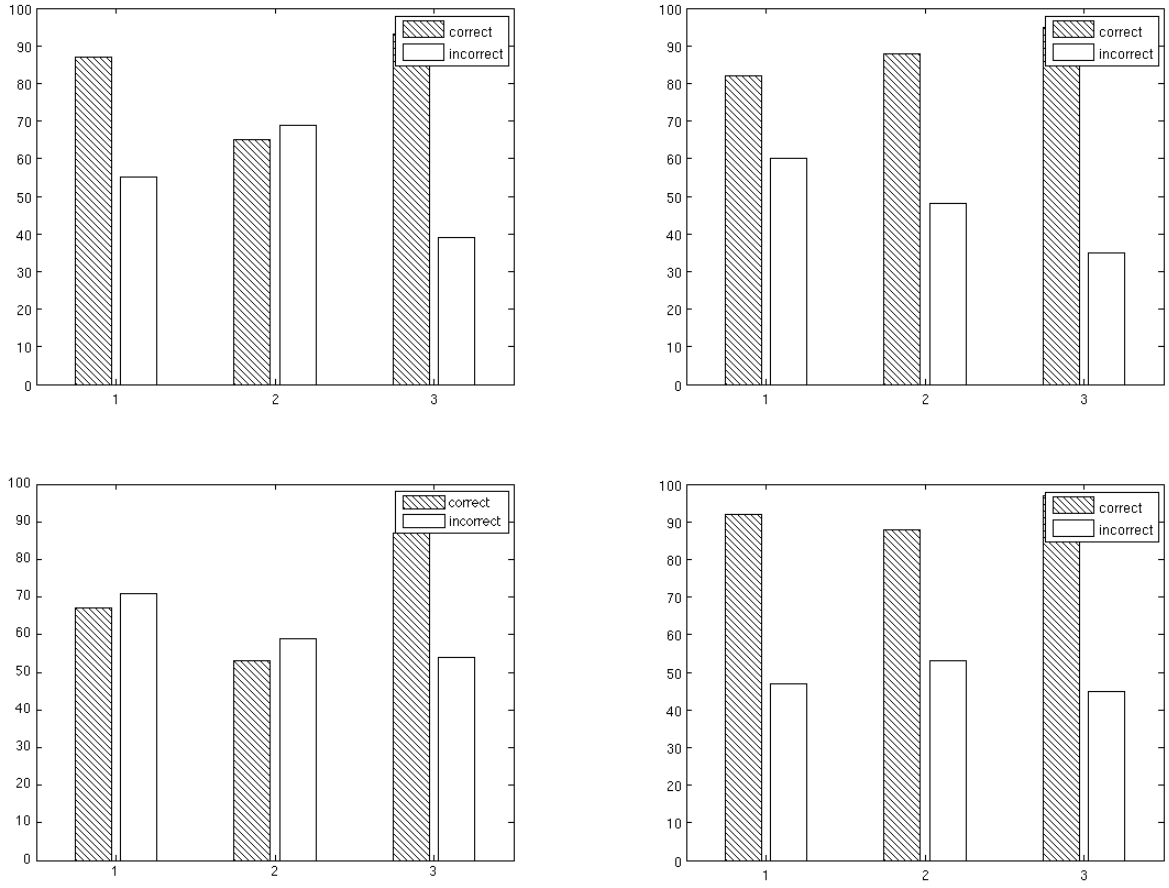

Figure 6.1: Correct and incorrect responses of four subjects. during the experiment for each session. Horizontal axis: sessions. Vertical axis: frequency of occurence.

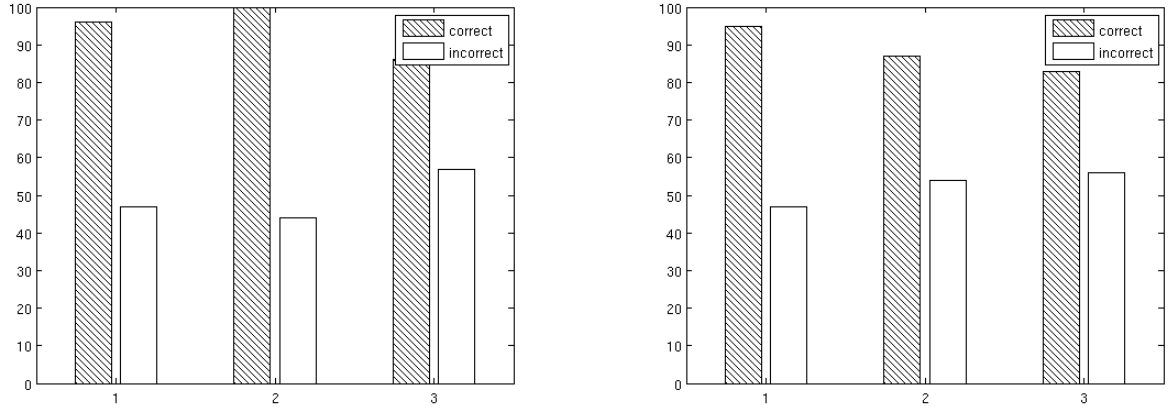

Figure 6.2: Correct and incorrect responses with no improvement during sessions. Horizontal axis: sessions. Vertical axis: frequency of occurence.

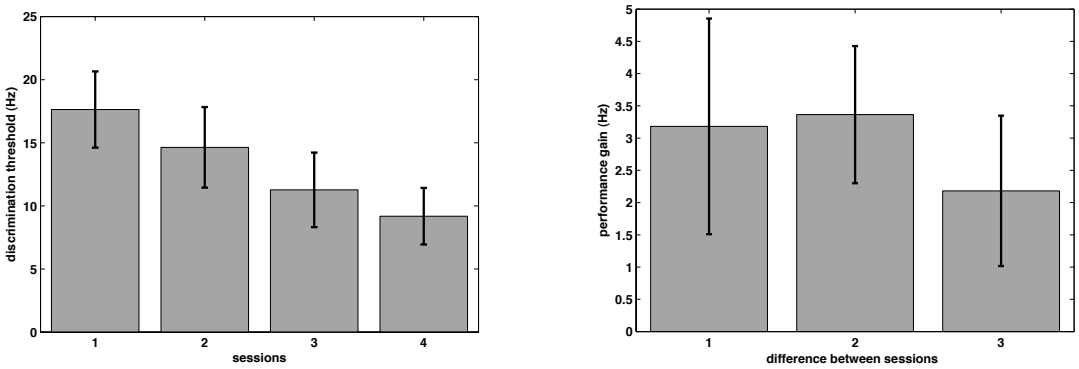

(a) (b)

Figure 6.3: Behavioral data during the experiment. (a) Grand mean and standard error of 11 subjects for threshold detection at the end of each session. (b) Mean performance gain (in Hz) between sessions for 11 subjects ($1^{st} - 2^{nd}, 2^{nd} - 3^{rd}, 3^{rd} - 4^{th}$).

6.2 fMRI Data

Following the procedure described in Section 5.2.2, the first results show the statistical parametric maps for the auditory or visual conditions relative to rest period. Figure 6.4 shows the response of the group of 11 subjects when attending to deviants in the auditory task. There is an important issue if choosing a significance level of 0.05 as in Figure 6.4(a). Because the volume image have a dimension of 64x64x20, we would expect 0.05x81920=4096 voxels to exceed a 5% threshold by chance. This means that a large number of voxels would be declared active when they are, indeed, inactive (*type I* error). This is a result of the multiplicity problem, i.e., many individual voxel hypothesis being tested. One solution that can be adopted is to decrease the significance level, e.g. 0.001 as shown in Figure 6.4(b). However, as we have an anatomically open hypothesis (no effect anywhere in a specific volume), a correction for multiple dependent comparisons is necessary. In this case we should consider other types of error rates which account for the multiplicity problem. The family-wise error rate (FWE) is the probability of at least one false positive on any voxel in the image. This is a very stringent controling method with weak power, as explained in Section 4.3.2 and shown in Figure 6.5(a). Because of that, we used the false discovery rate (FDR) method in which we allow some false positives in the image but relate them to the number of total positive findings (Figure 6.5(b)).

For the auditory attended relative to rest condition, the functional imaging data revealed activation in the temporal, frontal and parietal cortices (Figure 6.5(b)). This frontal component is not seen when the subject is not paying attention to the auditory stimuli, which is the case of the visual attended task (Figure 6.6). In this condition, the right and left temporal cortices are also activated as auditory stimuli is still being delivered, but we can see that the occipital response is stronger than in the auditory attended situation (compare figures 6.5(b) and 6.6). In addition, parietal cortices are activated in both conditions as the subject is constantly pressing a response button. These responses are summarized in Table 6.2. These figures show us preliminary results of the stimulation being performed. Moreover, direct contrast between the auditory attended responses relative to the auditory unattended responses was conducted since one of the aims of this study is the investigation of attention specific to auditory task as general attention is controlled for by the visual task. When we are interested in specific areas of expected activation we can restrict the correction for multiple comparisons to these small volumes of interest as the whole image correction is too conservative. Considerable activity can be seen in left inferior frontal gyrus (-45,24,24; $p<0.05$ SVC corrected), left superior temporal gyrus (-57,-51,6; $p<0.05$ SVC corrected) and right superior temporal gyrus (57,-33,3; $p<0.05$ SVC corrected). In Figure 6.7 the correction was done in a sphere of radius 3 mm centered on each of the voxels located in the coordinates above. The SVC analyses are

based on coordinates given in previous studies of attentional demands: Zhang, Feng, Fox, Gao, and Tan (2004) for the IFG, Kiehl et al. (2001b) for the LSTG and Zatorre et al. (1999) for the RSTG.

Table 6.2: Activated areas during auditory and visual attended tasks.

	Parietal	Temporal	Frontal	Occipital
Auditory vs. rest	X	X	X	
Visual vs. rest	X	X		X

Table 6.3 shows statistical results of the small volume correction in the attentional condition. In the cluster level inference (on the left), given a voxel threshold u, we can compute the likelihood of getting a cluster containing at least n voxels.

Table 6.3: Statistical results of the small volume correction in the attentional condition. Search volume corresponds to 7 voxels of 3x3x3 mm with an FWHM of 11x11x11 mm. Number of resels=0.1 (1 resel=51.56 voxels). Activations are significant at voxel level but not at cluster level.

cluster			voxel				Talairach coordinates x,y,z(mm)
(p_{corr})	(K_e)	(p_{uncorr})	(FWE_{corr})	(FDR_{corr})	(T)	(p_{uncorr})	
0.115	6	0.727	0.092	0.053	2.24	0.023	-45 24 21
0.113	7	0.687	0.005	0.002	4.42	0.001	-57 -51 6
0.113	7	0.687	0.003	0.002	4.59	0.0005	57 -33 3

Since we were interested in assessing learning performance during the experiment, we used each subject specific performance gain over each session in the design matrix. The difference between final and initial thresholds was used, in the first level analysis, as a contrast in each column of the design matrix. For the second level analysis, intersubject performance differences were accounted for using the overall performance gain (simple regression) as weights on the design matrix. The results are shown in Figure 6.8 for $p<0.005$. In sequence, small volume correction was performed for each region of interest (frontal and temporal) with a volume of interest (VOI) of 3x3x3mm. FMRI activity was observed in left frontal (-45,15,36; $p<0.05$; SVC corrected), left temporal (-57,-51,24; $p<0.05$; SVC corrected) and right temporal (60,-39,15; $p<0.05$; SVC corrected). Table 6.4 shows statistical results of the small volume correction in the learning condition.

The above data suggest that attention can be involved and maybe contribute to rapid improvements in specific brain activity during short periods of training. Attentional modulations in sensory modality, in this case auditory, were obtained based on auditory frequency attention trials. Earlier studies of auditory selective attention (Neelon,

Table 6.4: Statistical results of the small volume correction in the learning condition. Search volume corresponds to 7 voxels of 3x3x3 mm with a FWHM of 13x11x12 mm. Number of resels=0.1 (1 resel=66.17 voxels). Activations are significant at voxel and cluster levels.

cluster			voxel				Talairach coordinates x,y,z(mm)
(p_{corr})	(K_e)	(p_{uncorr})	(FWE_{corr})	(FDR_{corr})	(T)	(p_{uncorr})	
0.021	1	0.730	0.004	0.004	3.47	0.004	-45 15 39
0.012	5	0.398	0.0002	0.002	7.65	0.0002	-57 -51 24
0.013	4	0.452	0.0002	0.0002	6.70	0.0004	60 -39 15

Williams, and Garell, 2006; Kiehl, Laurens, Duty, Foster, and Liddle, 2001a) have shown attention-related enhancements of several auditory evoked electromagnetic signals with early modulation at 20-50ms after stimulus onset. The neural source of this early modulated component has been localized in the posterior part of the superior temporal gyrus. The finding of increased responses to attended auditory stimuli suggests the existence of rapid cortical plasticity. Research has shown that minutes of classical conditioning are sufficient to induce changes of neural responses and receptive field properties in auditory cortices (Alain, Snyder, He, and Reinke, 2007). Moreover, in an experiment of deafferentation of the adult auditory cortex, Pantev, Wollbrink, Roberts, Engelien, and Ütkenhöner (1999) showed that reorganization of cortical representations can occur within time periods of a few hours.

With approximately 80 minutes of training, an improvement in auditory frequency perception could be observed with the decrease of the subject's threshold. The finding of task related increased activity in frontal and temporal areas is consistent with the hypothesis that the frontal area is involved with prediction and top-down modulation of auditory selective attention that gives rise to auditory perceptual learning. Although some studies report attentional effects in primary and secondary auditory cortical regions (Grady, van Meter, Maisog, Pietrini, Krasuski, and Rauschecker, 1997), Petkov, Kang, Alho, Bertrand, Yund, and Loods (2004) have reported enhanced effects of auditory attention in higher auditory association areas when one modality is attended and the other is ignored. This is consistent with our current results in the superior temporal cortices. Since attentional effects are very dependent on the task, the exact knowledge about in which conditions the left or right temporal cortices are being activated is still contradictory and deserves further investigation. Eichele, Specht, Moosmann, Jongsma, and Quiroga (2005) and Doeller, Opitz, Mecklinger, Krick, Reith, and Schröger (2003) show evidences of this strong asymmetry in responses with a right-hemisphere specialization. In a preattentive auditory deviance processing task, Doeller, Opitz, Mecklinger, Krick, Re-

ith, and Schröger (2003) observed bilateral IFG activation for large compared to medium pitch deviants (50,24,6 [right], -54,26,8 [left]). Although most IFG activities during attentional and perceptive tasks are reported in right hemisphere, left hemisphere activity has also been observed as in van Wassenhove and Nagarajan (2007). Zhang, Feng, Fox, Gao, and Tan (2004) investigated that LIFG also serves as a general mechanism for selective attention (MNI: -44,15,20; -46,13,21; -42,13,20) as observed in a memory task. The left inferior frontal cortex and the superior temporal lobe (Altmann, Henning, Döring, and Kaiser, 2008) were activated when subjects were presented to different relative to common sound patterns (MNI: -47,3,24). The IFG (-60,4,25), among other areas, has also been elicited in an auditory task for the comparison of target versus novel stimuli (Kiehl, Laurens, Duty, Foster, and Liddle, 2001a). These results suggest that the IFG may play an important role for perception. Superior temporal gyrus activity has been reported during attentional and perceptual tasks as well. Pugh, Shaywitz, Shaywitz, Fulbright, Byrd, Skudlarski, Shankweiler, Katz, Constable, Fletcher, Lacadie, Marchione, and Gore (1996) reported a main effect of the attention condition in a binaural versus dichotic experiment. This effect was observed in STG (brodmann 22) bilaterally. Right STG (60,-30,11; 58,-33,11) activity was also observed for high and low frequency attended conditions (Zatorre, Mondor, and Evans, 1999). These areas, although reported for long period training, are consistent with the results for the rapid training applied in this study.

Additionally, in the fMRI analysis, the enhancement of the responses to the presentation of the auditory deviant stimulus was correlated with behavioral improvements used as weights in the contrasts design. With this procedure we could assess the areas involved in learning as the behavioral data was used as regressors in the data estimation. Worth noting is the fact that these regions intersect with the ones found in attention results, suggesting a role of attention in perceptual learning. The observed auditory perceptual learning was accompanied by auditory cortical plasticity manifested as an enhancement of early bilateral auditory peak currents. These findings are consistent with our hypothesis that activity enhancement should occur in learning experiments even in rapid training procedures. An interesting result is that the enhancement of the energy of the responses to the presentation of the deviant stimuli was in accordance with behavioral improvements, providing additional evidence that the observed plasticity is specific to perceptual learning.

It is important to say that the same procedure was adopted to the visual data, however the results are still not conclusive.

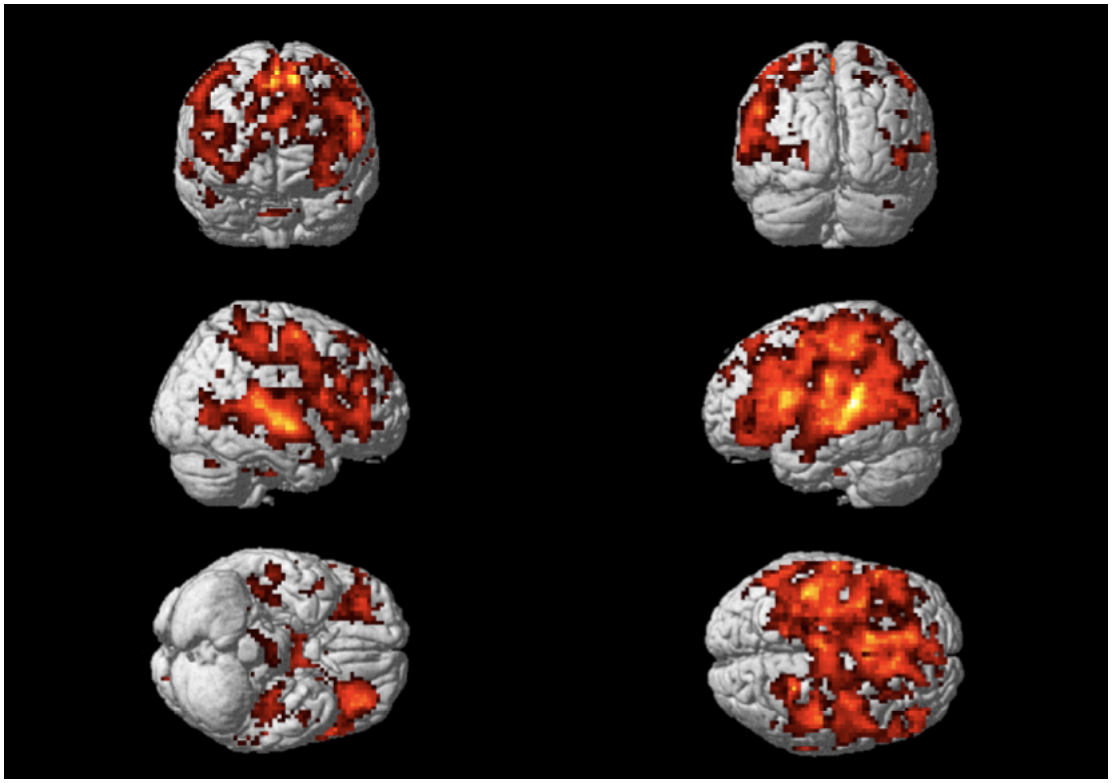

(a) $p<0.05$. Height threshold T=1.81.

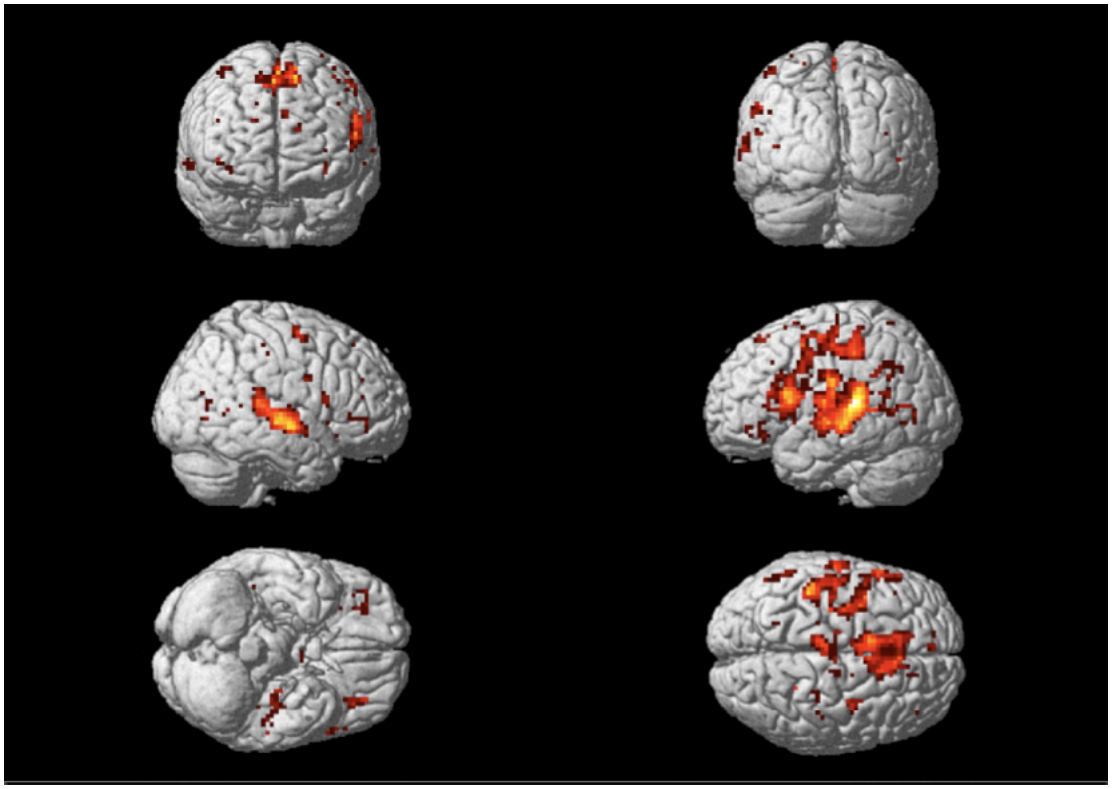

(b) $p<0.001$. Height threshold T=4.14.

Figure 6.4: Auditory responses uncorrected. Single *t*-test performed on each voxel individually. In (a), because of the higher significance level, more voxels are shown active but this also implies in a higher *type I* error.

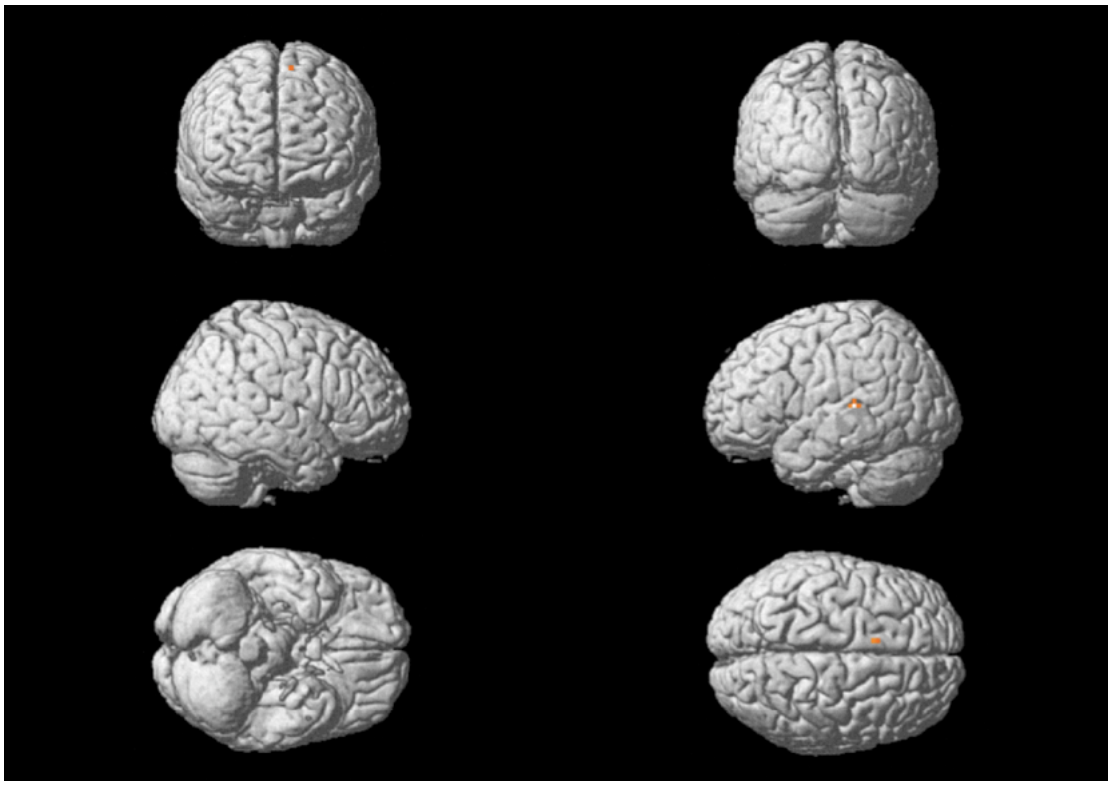

(a) p_{FWE}<0.05. Height threshold T=9.80

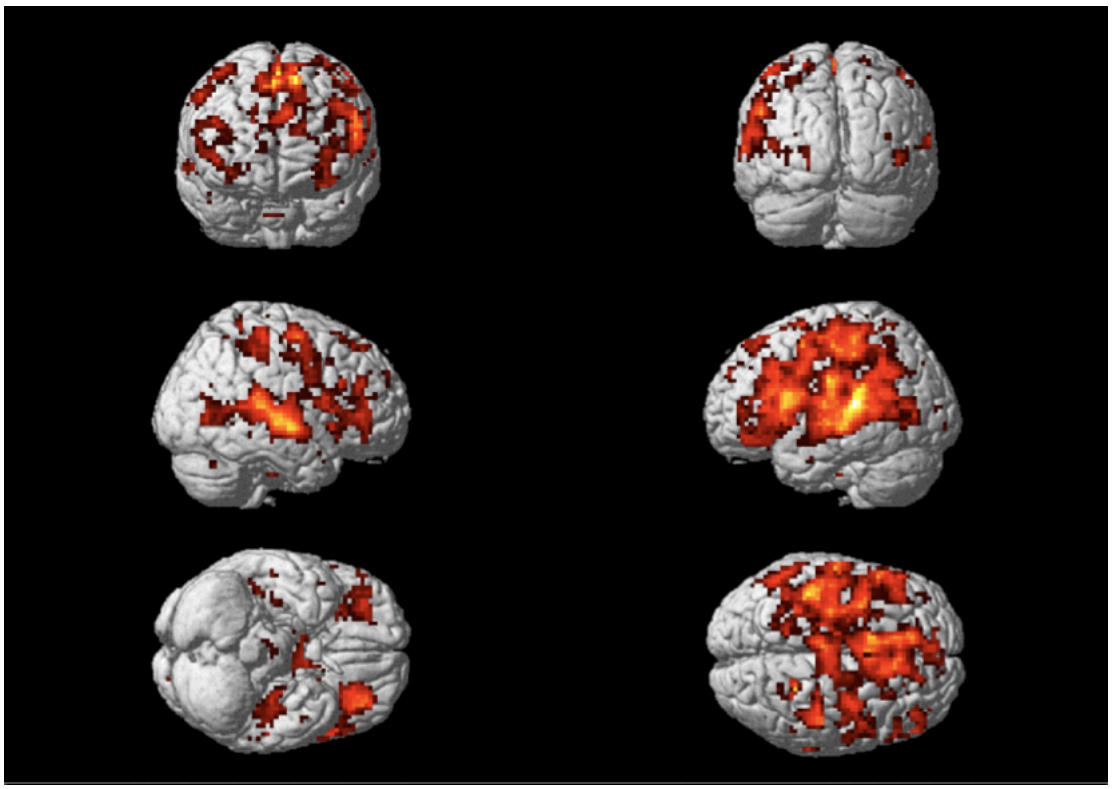

(b) p_{FDR}<0.05. Height threshold T=2.49.

Figure 6.5: Auditory responses corrected for multiple comparisons. FWE and FDR corrections.

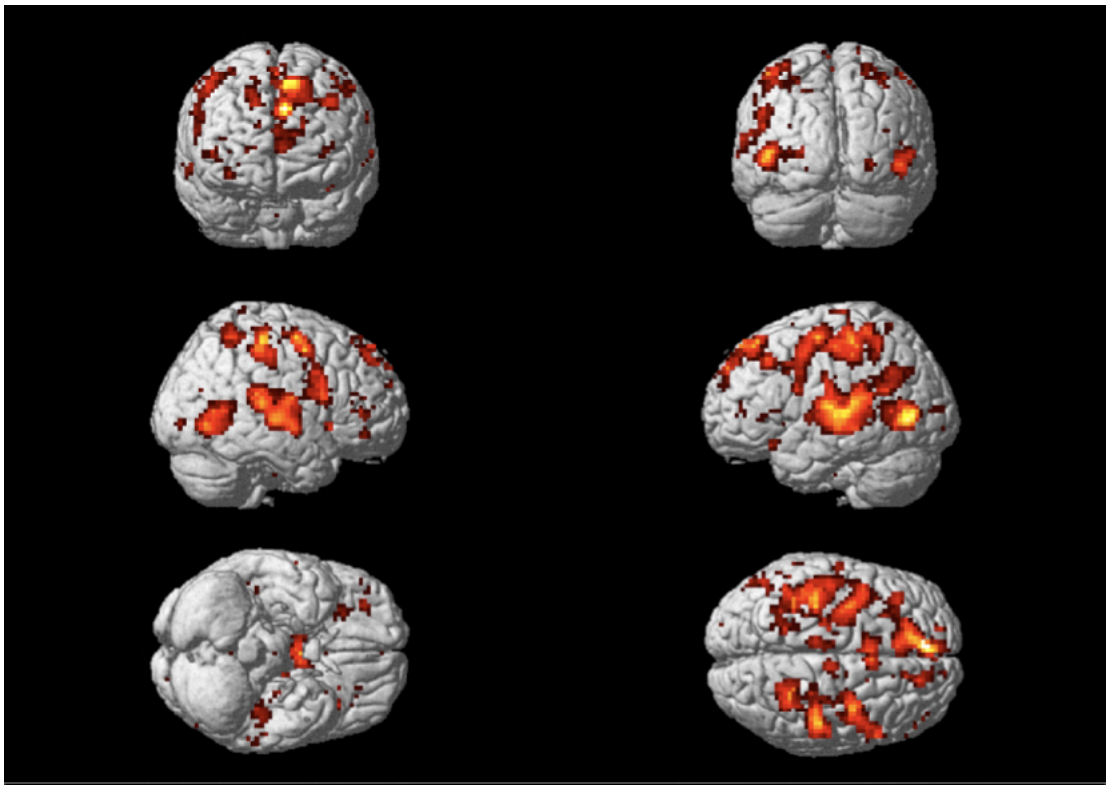

Figure 6.6: Visual attended task responses corrected for multiple comparisons. p_{FDR}<0.05. Height Threshold 2.66.

Figure 6.7: Attentional effect (p<0.05, SVC corrected). Using SVC, the correction is done in a small volume.

Figure 6.8: Learning contrasts weighted by overall gain of each subject. Activations with p<0.005.

6.3 EEG Data

Figure 6.9 shows a segment of the 64 channel data recorded and the stimuli presented to the subject. As explained in Section 5.1.4, EEG data was preprocessed in which trials were visually inspected and removed if the data were highly corrupted by artifacts. The percentage of trials removed is summarized in Table 6.5.

Table 6.5: Percentage of trials removed before analysis of the data.

subject	Percentage of removal (%)
1	5
2	5
3	0.5
4	3
5	10
6	2
7	0.5
8	0
9	3.5
10	2
11	1.5

In the first part of the analysis, ICA was used for the removal of cardiac, ocular and muscular artifacts. We used a histogram to check the correlations between the ECG channel of each subject and 62 independent components. A result is shown in Figure 6.10 for two subjects. Subject 2 does not show any component significantly correlated to the ECG data as we can see from the small correlation values which are very close to each other. Subject 1 suggests two components separate from the others which were further analyzed looking at the components and ECG time courses as in Figure 6.11. Six out of eleven subjects showed at least one component with correlation coefficient with the ECG channel greater than 0.2. We observed that ICs with values greater than 0.2 showed time courses similar to Figure 6.11(a) and 6.11(b) and were considered for rejection. This is in contrast with cases such as the one shown in Figure 6.11(c).

The EOG channel was compared to the ICs as well and nine subjects showed at least one channel with correlation greater than 0.3. Besides the correlation metrics, all the components were inspected in the components map before they were selected for rejection.

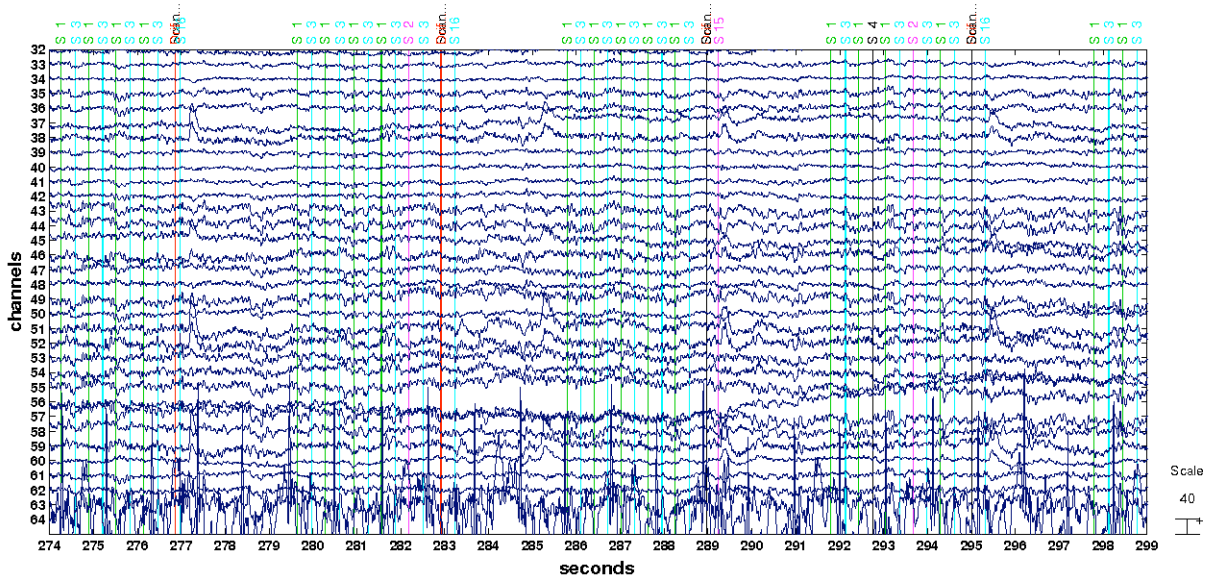

Figure 6.9: View of all 64 recorded channels and the experiment events: stimuli (S1,S2,S3,S4), subjects response (S16 or S15) and the scan start marker. ECG channel is the last channel on the graph (channel 64).

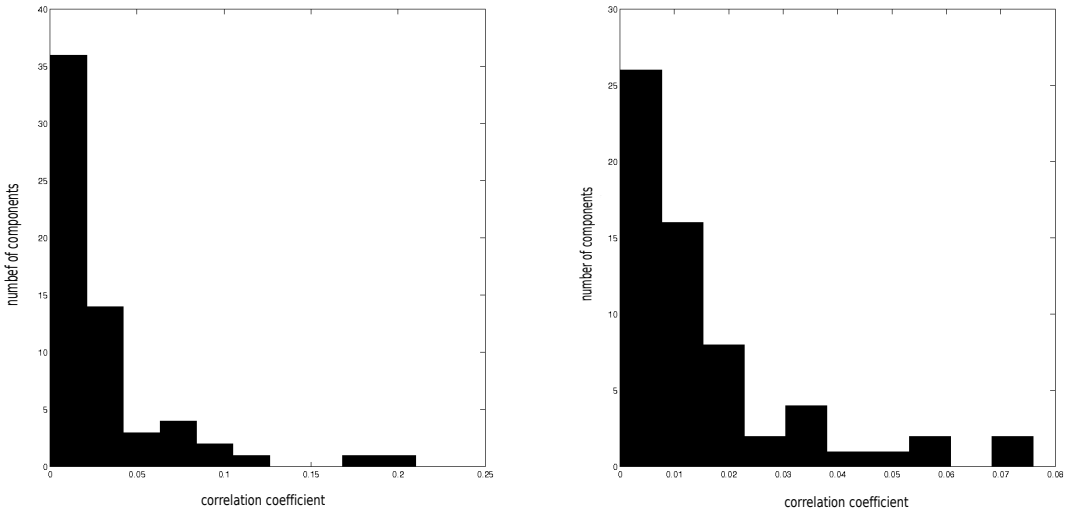

(a) Subject 1

(b) Subject 2

Figure 6.10: Histograms of the correlations between the ECG channel of each subject and the 62 independent components. Subject 2 does not show any component significantly correlated to the ECG data.

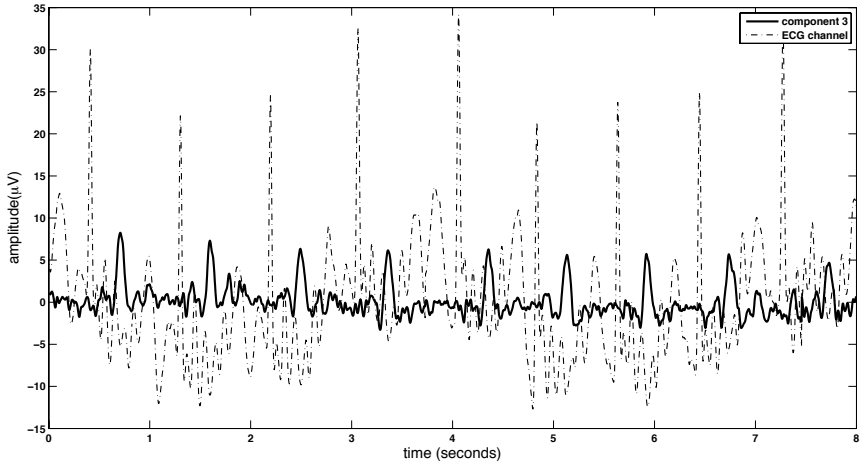

(a)

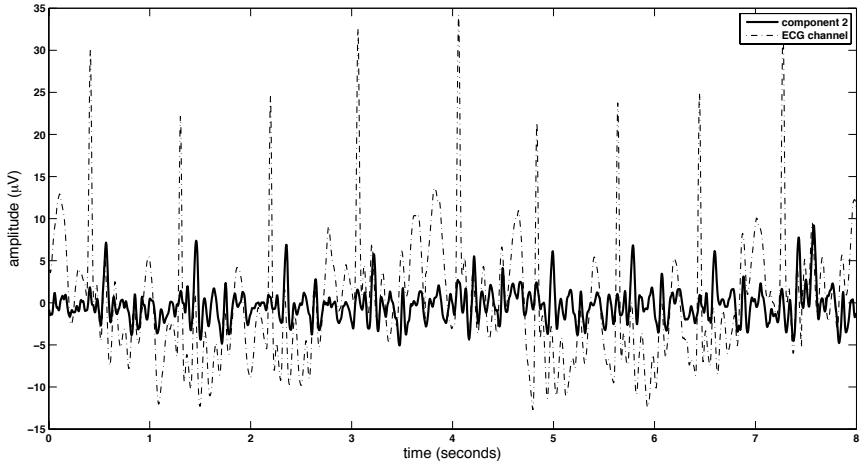

(b)

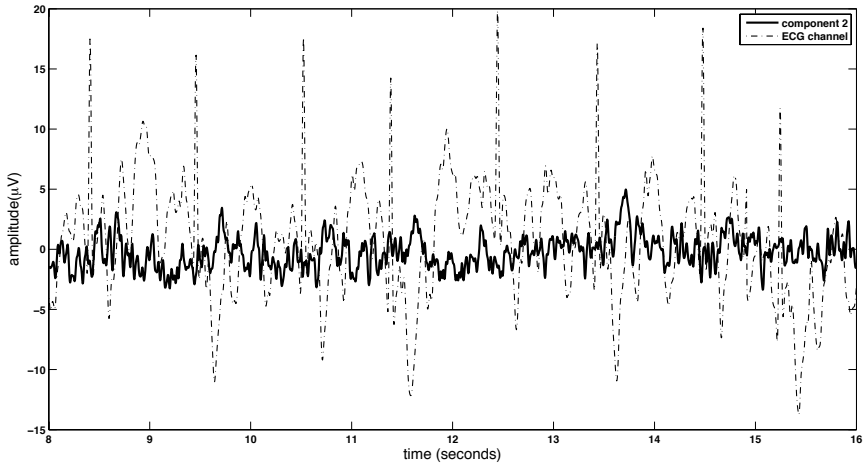

(c)

Figure 6.11: Independent components and cardiac channel. In (a) and (b) there is a peak in the IC following each strong peak in the cardiac data. In (c), no visible relation is seen between the IC and the cardiac channel.

6.4 EEG Data: more on Ballistocardiogram Artifact Removal

Although ICA was adopted for the BCG artifact removal in the first part of this work, we wanted to investigate the template method as well and compare it with the ICA method. The comparison is subjective in the sense that there is no "clean" data to compare since the recorded channel is originally corrupted by the artifact. Noteworthy to say that the ECG channel is also distorted when the subject is inside the MRI scanner as seen in Figure 6.12. However, as shown in Figure 6.13, the BCG artifact is very characteristic, appearing after a QRS peak and is spread across all channels. Figure 6.14 shows the results of both methods applied to the channel F2 of one subject. A reduction of the artifact can be seen when the template method was used. Figure 6.15 shows the same segment of Figure 6.12 but with the removal of the artifact using the template method. The "cleaned" data was further decomposed into independent components (ICA) and compared to the ECG and EOG channels. No component was found to be correlated to the ECG channel. This suggests that artifacts related to this cardiac motion were in fact removed using the template method.

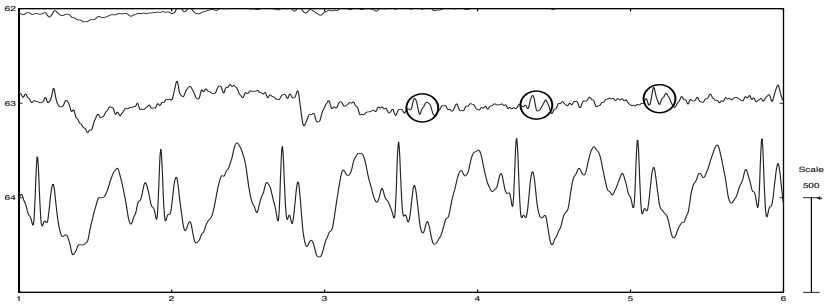

Figure 6.12: Segment of an ECG data recorded inside the MRI scanner. Horizontal axis: time in seconds. Vertical axis: signal amplitude in μV. On the bottom, the ECG channel and above one channel corrupted by the BCG artifact.

One advantage of the template method is that it does not make any assumption about the estacionarity of the data. However, a precise Q detection is necessary in order to select the segments used as reference for the template (Figure 6.16(a)). We observed that, in few cases, the peak was detected erroneously as in Figure 6.16(b), most probably due to the variability between two peaks and the shape variability as well. In the segment shown the variability between subsequente peaks spanned from 702.5 ms to 726.8 ms.

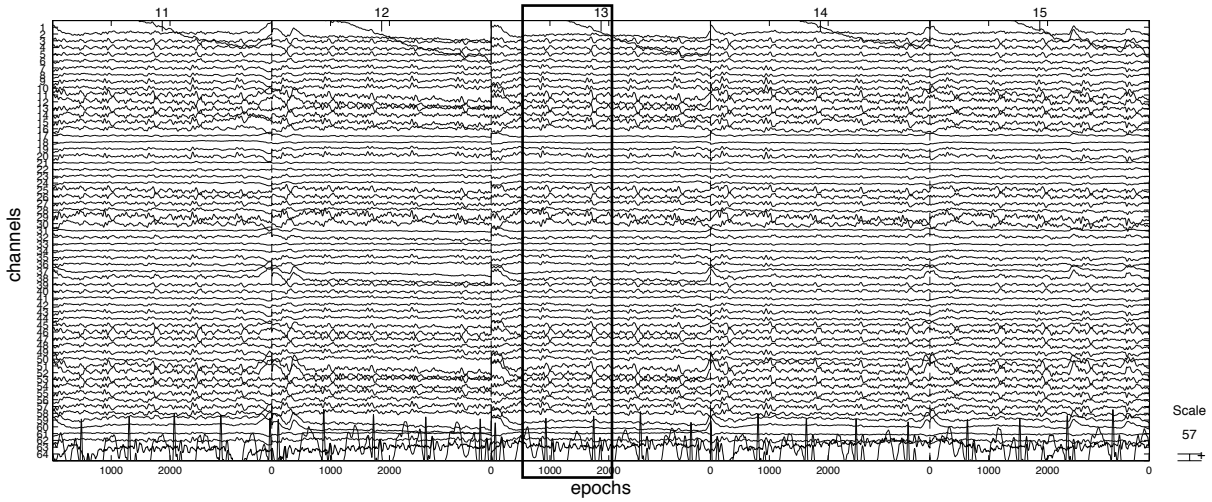

Figure 6.13: View of the 64 recorded channels with the BCG artifact highlighted by a rectangle. ECG channel is the last channel in the graph.

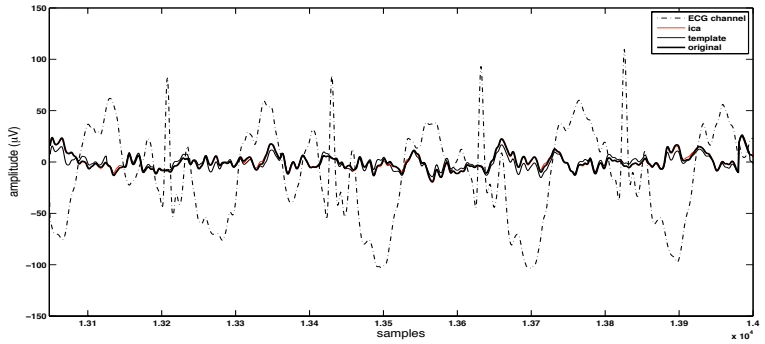

(a) Result of ICA and the template methods applied to channel F2.

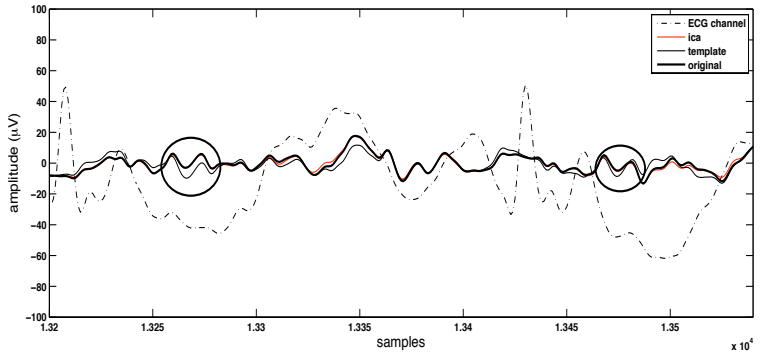

(b) Zoom of the segment.

Figure 6.14: A comparative of ICA artifact removal and the template artifact removal methods. The results of both methods are displayed for one channel as well as the original recorded data and the ECG channel. The elipse highlights the BCG artifact.

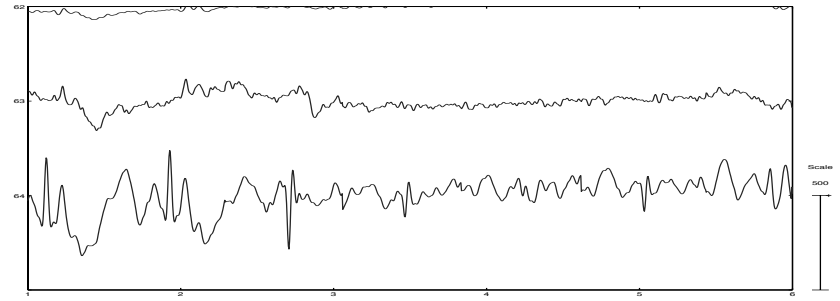

Figure 6.15: BCG artifact removed using the template method, applied to the same data shown in Figure 6.12. Horizontal axis: time in seconds. Vertical axis: signal amplitude in μV.

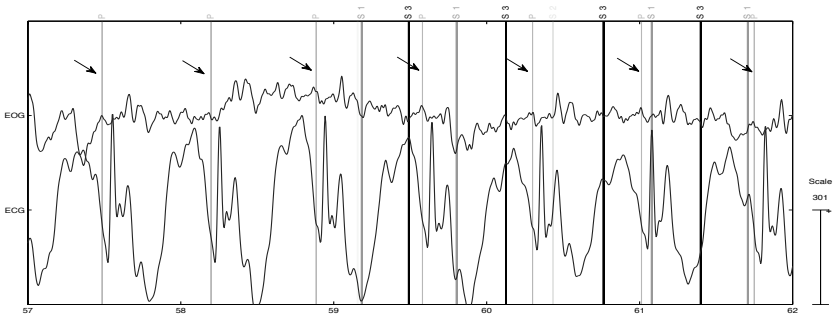

(a) Q wave detection. The beginning of each Q wave is marked with the arrows.

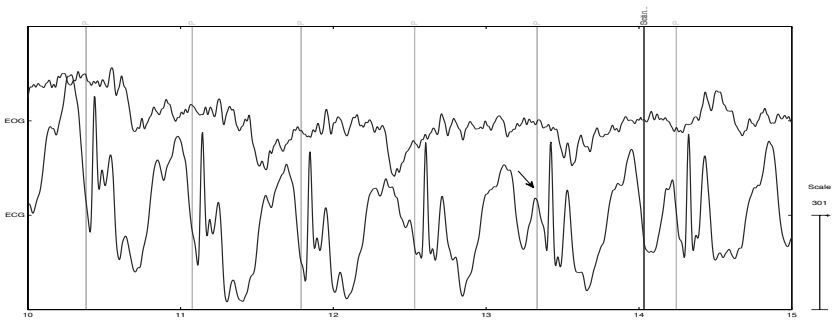

(b) The misplaced detection is pointed with an arrow.

Figure 6.16: Detection of the Q wave at each QRS complex. The detected "events" are pointed with an arrow. The others are the stimuli. In (b), a misplaced detection.

6.5 EEG and fMRI - Variational Bayesian Method Results

The results shown in this section are one of the most important goals of this work: the usage of combined EEG and fMRI in the assessment of auditory attention responses.

Three masks were defined from the statistical parametric map results: left frontal (IFG: -45,15,36), left temporal (LSTG: -57,-51,24) and right temporal (RSTG: 60,-39,15), and peak dipoles were taken within a 3 mm radius from the estimated current peak. The peak dipole with the highest temporal mean was selected for analysis. Subsequently, time frequency analysis was carried out on each of these current dipole in what we call the task related analysis (blocks of auditory deviant relative to blocks of visual deviant) to investigate neuronal oscillation. The amplitudes were averaged regardless of phase. This procedure enhanced stimulus-related EEG changes both phase-locked (i.e. event-related potentials) and non-phase-locked (i.e. event-related synchronization and desynchronization) to stimulus onset. Time-frequency analysis over the peak currents of these three areas reveals different pattern of activation. Figure 6.17 shows the statistical results for regions IFG, LSTG and RSTG, respectively.

The t-statistics of all 11 subjects were performed in three conditions: attention, non-attention and the difference between them. Data were tested against null hypothesis of zero mean. The LSTG shows significant response ($p<0.01$) around 100ms in the attentional condition. This response spans from 25 to 32Hz. Later responses also appear around 300-400ms. We see that, although the attentional effect is not observed at the frontal and right temporal areas for $p<0.01$, a response can be viewed for $p<0.05$. A zoomed view of the attention versus non-attention condition is seen in Figure 6.18 for all 3 regions. It can be seen that the responses in LSTG span a wider range compared to the RSTG response, which is more localized in frequency (10 to 20Hz, the alpha and beta ranges). The IFG response peaks at around 200ms, which is later than the response of the temporal cortices as it has been expected.

In order to account for learning assessment, we checked the correlation coefficient between time-frequency results ($p<0.01$) in each bin of the attentional responses and the threshold values from the behavioral test for each subject.

The results of the group analysis are given in Figure 6.19 ($p<0.01$). The suggestion of correlation shown in this figure was further investigated. Signal was separated in five frequency ranges: delta, theta, alpha, beta and gamma. The energy of each range was computed at each trial: 0.5-3.5Hz, 4-7Hz, 8-13Hz, 14-28Hz, 30-70Hz, respectively. The correlation coefficients (Table 6.6) are sufficient to suggest an evidence of correlation, especially in the gamma and beta bands. It should be noticed that Figure 6.19 shows a clear relation between ERP time-frequency response and results from behavioral tests.

We also showed the hierarchical Bayesian method proposed by Sato, Yoshioka, Kajiwara, Toyama, Goda, Doya, and Kawato (2004) applied to EEG rather than MEG data. Although the efficacy of the method was successfully reported for a visual experiment (Yoshioka, Toyama, Kawato, Yamashita, and Nishina, 2008) and speech perception ex-

Table 6.6: Correlation coefficient between Fourier transformed EEG signal and behavioral detection threshold values for each subject. Energy value for each band was computed and correlation between behavioral data was checked. This table shows only correlation coefficients for $p<0.05$. The others are set to zero.

Subject	LIFG					LSTG					RSTG				
	delta	theta	alpha	beta	gamma	delta	theta	alpha	beta	gamma	delta	theta	alpha	beta	gamma
1	0	0	0	0	-0.29	0	-0.24	0	0	0	0	0	0	-0.25	0
2	0	-0.35	-0.43	0	0.52	0	0	0	0.41	0.22	0	0	0	0.42	0.32
3	0	0.23	0	0.33	0	0	0	0.35	0.39	0	0	-0.22	0	0.35	0
4	0	0	0	0.23	0.30	0	0	0.21	0	0	0	0	-0.23	0	0
5	0	0	0	0.77	0.68	0	0	0.39	0.73	0.77	0	0	0	0.73	0.77
6	0.32	0.35	0.51	0.21	0.28	0.24	0.32	0	0	0	0.32	0.36	0.54	0.26	0.40
7	0	0	0.46	0	0.28	0	0.21	0.2	0	-0.2	0	0.21	-0.43	0	0.47
8	0	0	0	0.44	0.26	0	0	0	0	0	0	0	0	0.43	0.30
9	0	0.22	0	0.29	-0.77	0	-0.49	0	-0.65	-0.76	0	0.22	0	0.29	-0.77
10	0	0	0	0	0.25	0	0	0	0	0.22	0	0	0	0	0.26
11	0	0	-0.41	-0.38	0	0	0	-0.41	-0.38	0	-0.23	-0.30	-0.50	0	0.72

periment (Callan, Callan, Gamez, Sato, and Kawato, 2010) using MEG data, this is the first implementation using EEG data. With this procedure we incorporated the simultaneously recorded fMRI and EEG data to estimate the spatiotemporal patterns of brain activities of an auditory discrimination task. Looking at the attentional effects (auditory versus visual results), the modulation role of attention can also be seen in the later responses of IFG peak currents compared to earlier cortical areas (STG) (Figure 6.18). Although the auditory cortices show earlier and stronger responses (what can be seen as a bottom-up process), the response in frontal area around 200ms in beta range (14-28Hz) during the auditory attention versus non-attention condition is also evidence of an attentional effect ($p<0.05$). In this case, subjects may have learned to pay more attention to the stimuli as part of their learning experience on the trained task.

One of the most interesting findings in our work comes from the source localization analyses showing that plasticity also manifests as an increase in the power of beta (14-28Hz) and gamma (30-70Hz) bands. These results are supported by the attentional load shown in Figure 6.17. Our results also suggest that passive listening is not enough to produce enhanced activity even in auditory cortex as shown in Figure 6.17 for the visual deviant trials in all three ROIs.

Finally, the gamma oscillations found in the correlation between behavioral thresholds and the energy of the current peak values for each trial suggest that plasticity is also manifested as an increase in the power of induced gamma band activity in IFG and RSTG. The results in Figure 6.19 reflect learning effects during the whole experiment and are a very promising finding concerning the role of the recent recognized importance of these neuronal oscillations in cognitive systems.

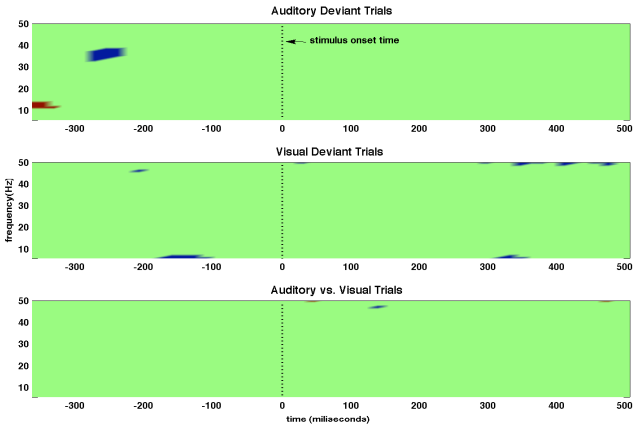

(a) IFG

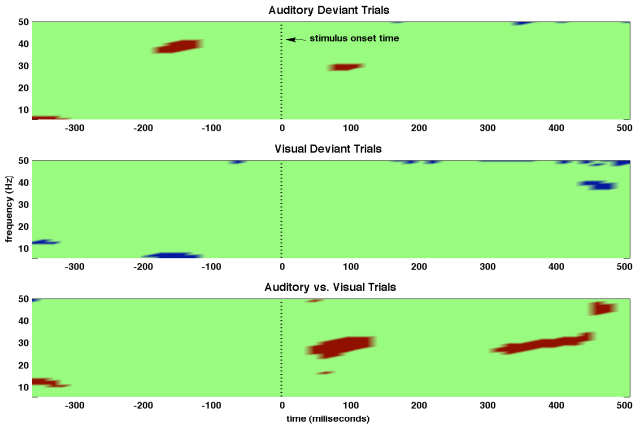

(b) LSTG

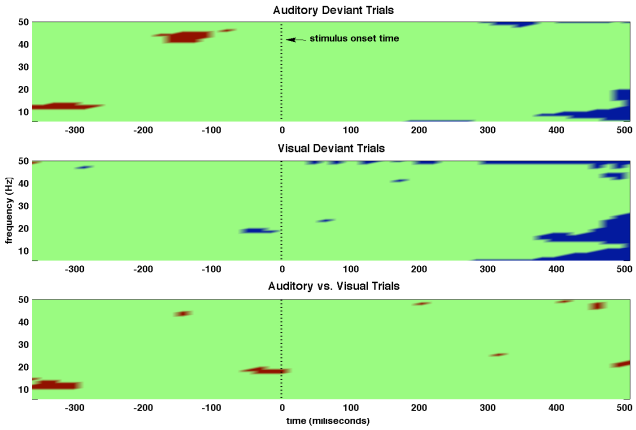

(c) RSTG

Figure 6.17: Statistic tests carried out on the time-frequency representation of peak currents in the 3 ROIs analyzed. t-test (p<0.01) over time-frequency bins (46x200) of 11 subjects (10 degrees of freedom). Time frequency analysis was done over the highest peak current in a) IFG, b) LSTG and c) RSTG. In red: bins whose statistics are greater than the null hypothesis of zero mean. In blue: bins whose statistics are smaller than the null hypothesis of zero mean. Three conditions were tested: Auditory deviant trials (top), Visual deviant trials (middle) and Auditory vs. Visual trials (attended versus non-attended condition) on the bottom.

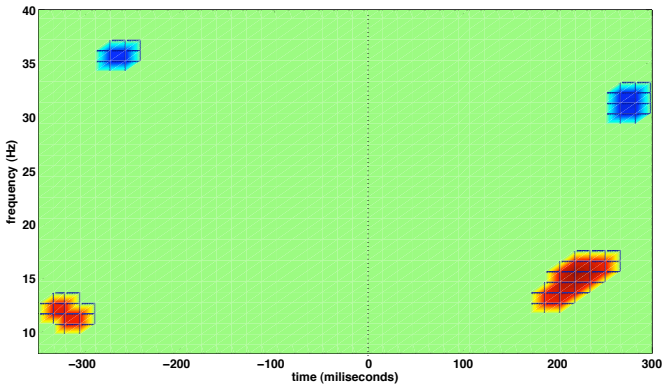

(a) IFG

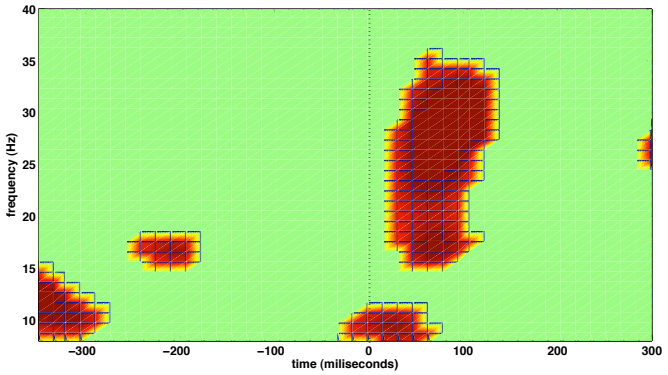

(b) LSTG

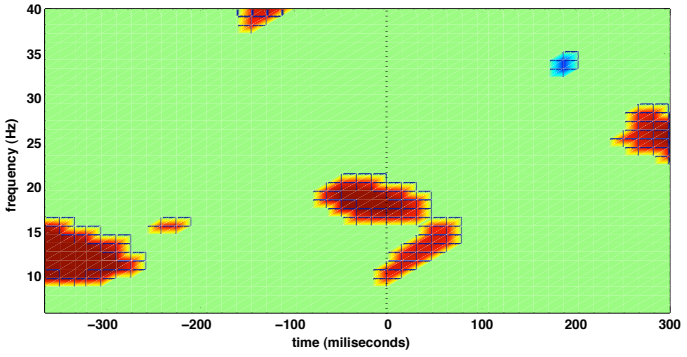

(c) RSTG

Figure 6.18: A zoomed view of the auditory attended versus non-attended condition (p<0.05) during the first 300ms. a) IFG. b) LSTG. c) RSTG.

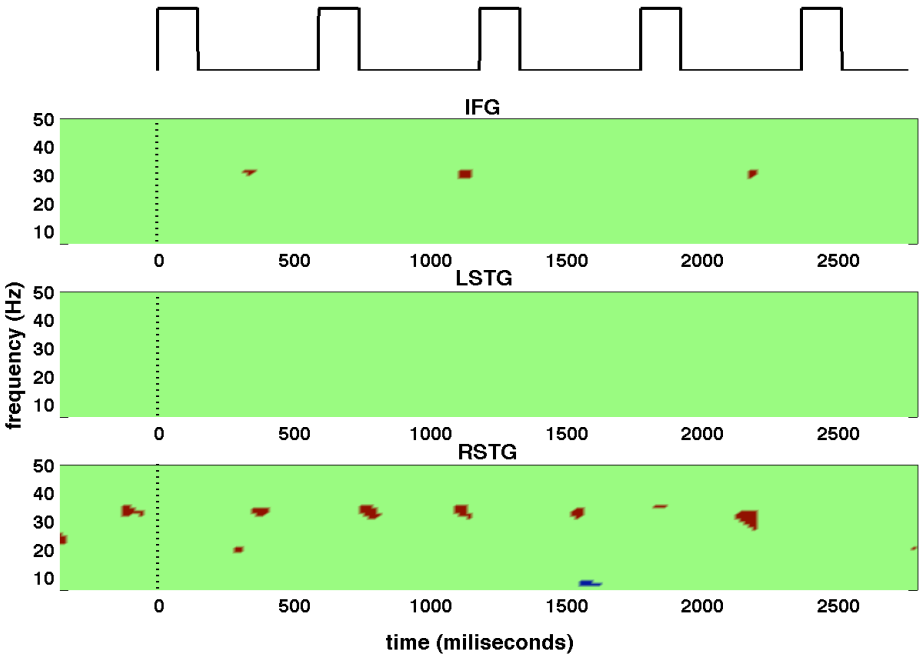

Figure 6.19: Correlation between time-frequency analysis and threshold values from behavioral test. T-statistics of 11 subjects in auditory deviant task. At each time-frequency bin 11 samples were tested against the null hypothesis of zero mean (p<0.01 uncorrected). Results are shown for IFG, LSTG and RSTG. On the top, onset time of the auditory stimuli.

6.6 Summary

In this chapter, the main results obtained from the experiments were presented and analyzed. They are evidences of the importance of attention in rapid training. However more experiments need to be carried out in order to obtain a real comprehension of the mechanisms of perceptual learning.

Stones in the road? I save every single one, one day I'll build a castle.

Fernando Pessoa

7 Conclusion

The study of the brain functioning has gained a lot of attention especially after the employment of functional neuroimaging techniques. Functional magnetic resonance imaging using endogenous blood-oxygenation-level-dependent (BOLD) contrast has been established as a standard technique for mapping human brain function. Its high spatial resolution allows activated brain areas to be localized with milimeter resolution. However, there is much more to cognitive neuroscience than functional neuroanatomy, and event related potentials can be very useful in elucidating cognitive mechanisms and their neural substrates. Because of their high temporal resolution, at milisecond scale, the technique is capable of detecting rapid changes of neurophysiologic processes. Therefore, efforts have been made to integrate information of fMRI with EEG to provide an alternative high-resolution spatiotemporal imaging technique. The combination of both modalities is of particular interest in cognitive studies. Although technically difficult, it allows the comparison of both modalities in the same brain state, which is important when investigating learning. Hence, the simultaneous measurements of fMRI and EEG data carried out in this work formed a more realistic setup to combine high spatial resolution data with high temporal resolution data in cognitive experiments.

The complexity of the design was addressed in this thesis in which the artifacts that happened in both modalities were treated carefully. The impact of the electrophysiological recording system in the MR image was seen especially in the quality of the image when

electrodes were placed inside the scanner. In spite of that, the images were still adequate for the segmentation procedure.

On the other hand, EEG data were also strongly affected by the fMRI image acquisition process. We successfully removed the gradient artifact using a template matching algorithm. In this case, the shape of the artifacts was considered constant over time, which is acceptable, since there is no substantial inter-volume variability. A more difficult source of artifact is the cardiac contamination. This artifact is hard to be eliminated as it varies considerably between channels and subjects. We first adopted ICA for ballistocardiogram artifact removal. The identification of the components representing artifacts is a topic being widely discussed because the correction depends on the removal of a set of components. An identification strategy is necessary and, in this study, visual inspection and correlations with reference signals were adopted. Although not the focus of this study, we are aware that the choice of correct parameters of the ICA algorithm influences the quality of the removal. There is no standard BCG artifact correction procedure and we also employed a method based on average artifact subtraction with optimal basis set for comparison. The artifact subtraction method resulted in better removal of the BCG.

The multimodal neuroimage has a special role in the estimation of the neural sources of the scalp potentials recorded from sensors in the scalp, what is known as the inverse problem. First, the derivation of the scalp potentials from brain current sources, the forward problem, requires the modeling of the head volume conductor. The inverse solution depends on the accuracy of the forward model with the conduction properties and shape of the head. Many studies use the sphere model which consists of spherical compartments representing the layers of the head. In this work, realistic head models were constructed using the T_1 images of the subjects, since they have high contrast and are adequate for the segmentation of the 3 head compartments. This model was incorporated in the boundary element method to solve the forward method. For the inverse problem, the MRI image gave information about the position and orientation of the cortical dipoles, while fMRI was used to provide topographical information about active dipoles. In the variational Bayesian method implemented in this thesis, the variance of the current source at each source location was considered an unknown parameter and was estimated from the observed EEG data. The fMRI information was imposed as prior information on the variance distribution, being a soft constraint on the variance. The estimated current sources were used to investigate the change in brain activity during perceptual learning.

The current study explored the advantage of simultaneous recording to investigate brain activity during rapid perceptual learning. The question under debate is whether or not rapid training can evoke responses in cortical areas and at which extent. The results obtained suggest that listeners can improve quickly at identifying deviant from standard

sound. Rapid improvement in task performance is accompanied by plastic changes in sensory cortex as well as superior areas as evidenced by enhanced activity of sensory responses. Moreover, the correlation between ERP time-frequency response and results from behavioral tests gives support to our hypothesis of learning during short period of training.

In order to make a good usage of the extensive data collected for this study, future work should focus on the analysis and correction of the distortion of ERPs due to overlap from adjacent responses. This problem arises when short interstimulus intervals are employed in the experiment.

Moreover, it would be interesting to investigate the interaction between the visual and auditory modalities. Although we followed the same paradigm used in the auditory modality, some aspects of the visual stimulation were not investigated before the design of the experiment, such as the specificity of the stimulus. It has been shown in the human visual system that perceptual learning is very specific to simple stimulus attributes and paradigms. Because of that an specific study of this modality is necessary in order to obtain conclusive results.

Finally, the results obtained in this thesis cannot be taken as sufficient to affirm the need of attention in all learning processes, as studies have shown the existence of passive learning in which the mere exposure to stimuli can trigger changes in the neural pathway. Nevertheless, especially in short duration training, attention works, at least, as a facilitator in complex learning processes.

A

Variational Bayesian Estimation for the Inverse Problem

Electroencephalography (EEG) measurements can be used to show the sequence of activation of distinct cortical areas during brain functions as well as to estimate the time course of each source within the activation network. However, the spatial resolving power of EEG (and MEG) does not, in general, match that of fMRI. Resolution is limited by the relatively small number of spatial measurements, about a hundred, and by the electromagnetic inverse problem. Resolution similar to that of the fMRI method can be achieved only by placing restrictive models on the sources of EEG signals. In this context, given a set of EEG signals from an array of sensors, the inverse problem consists of estimating the properties of the current sources that produced these signals (Baillet, Mosher, and Leahy, 2001).

Before describing the inverse problem, the forward solution will be briefly addressed. The physics of MEG and EEG generation can be described by the quasi-static approximation of Maxwell's equations. The current flow $\mathbf{J}(\mathbf{r}')$ at location $\mathbf{r}'$ can be related to the magnetic field $\mathbf{B}(\mathbf{r})$ at location $\mathbf{r}$ through the Biot-Savart law

$$\mathbf{B}(\mathbf{r}) = \frac{\mu_0}{4\pi} \int \mathbf{J}(\mathbf{r}') \frac{\mathbf{r} - \mathbf{r}'}{\|\mathbf{r} - \mathbf{r}'\|^3} d\mathbf{v}', \tag{A.1}$$

where μ_0 is the permitivity of free space. The total current density in the head volume

can be separated in a primary current flow $\mathbf{J^P}(\mathbf{r}')$ related to the original neural activity, and a volume (or passive) current flow $\mathbf{J^v}(\mathbf{r}')$ that results from the effect of the electric field in the volume on extracellular charge carriers:

$$\begin{aligned}\mathbf{J}(\mathbf{r}') = \mathbf{J^P}(\mathbf{r}') + \mathbf{J^v}(\mathbf{r}') &= \mathbf{J^P}(\mathbf{r}') + \sigma(\mathbf{r}')\mathbf{E}(\mathbf{r}') \\ &= \mathbf{J^P}(\mathbf{r}') - \sigma(\mathbf{r}')\nabla\mathbf{V}(\mathbf{r}'),\end{aligned} \tag{A.2}$$

$\sigma(\mathbf{r}')$ is the conductivity value of the head tissues and the electric field $\mathbf{E}(\mathbf{r}')$ is the negative gradient of the electric potential $\mathbf{V}(\mathbf{r}')$. Assuming the head a set of regions each with a constant isotropic conductivity $\sigma_\mathbf{i}$, i=1,2,3, representing the brain, skull and scalp, the Biot-Savart law can be rewritten as a sum of contributions from the primary and volume currents:

$$\mathbf{B}(\mathbf{r}) = \mathbf{B_0}(\mathbf{r}) + \frac{\mu_0}{4\pi}\sum_{ij}(\sigma_\mathbf{i} - \sigma_\mathbf{j})\int_{S_{ij}}\mathbf{V}(\mathbf{r}')\frac{\mathbf{r}-\mathbf{r}'}{\|\mathbf{r}-\mathbf{r}'\|^3}dS'_{ij}, \tag{A.3}$$

where B_0 is the magnetic field due to the primary current. The second term is formed by the sum of surface integrals over the brain-skull, skull-scalp and scalp-air boundaries. It represents the volume current contribution to the magnetic field. From Equation A.3, the magnetic field can be calculated if the primary current distribution and the potential $\mathbf{V}(\mathbf{r}')$ on all surfaces are known. It is now possible to calculate the potential

$$(\sigma_i + \sigma_j)\mathbf{V}(\mathbf{r}) = 2\sigma_0\mathbf{V_0}(\mathbf{r}) - \frac{1}{2\pi}\sum_{ij}(\sigma_i - \sigma_j)\int_{S_{ij}}\mathbf{V}(\mathbf{r}')\frac{\mathbf{r}-\mathbf{r}'}{\|\mathbf{r}-\mathbf{r}'\|^3}dS'_{ij}, \tag{A.4}$$

$\mathbf{V_0}$ is the potential at $\mathbf{r}$ due to the primary current distribution. Equations A.3 and A.4 specify the integral solutions for the forward problem. Specifying a primary current distribution $\mathbf{J^P}(\mathbf{r}')$, the primary potential and the primary magnetic field can be calculated:

$$\begin{aligned}\mathbf{V_0}(\mathbf{r}) &= \frac{1}{4\pi\sigma_0}\int\mathbf{J^P}(\mathbf{r}')\frac{\mathbf{r}-\mathbf{r}'}{\|\mathbf{r}-\mathbf{r}'\|^3}d\mathbf{r}', \\ \mathbf{B_0}(\mathbf{r}) &= \frac{\mu_0}{4\pi}\int\mathbf{J^P}(\mathbf{r}')\frac{\mathbf{r}-\mathbf{r}'}{\|\mathbf{r}-\mathbf{r}'\|^3}d\mathbf{r}'.\end{aligned} \tag{A.5}$$

The equations above describe the forward model solutions for heads with conductivity values that can be modeled as a set of concentric homogeneous and isotropic spheres. However, although real heads are anisotropic, inhomogeneous and not spherical, the spherical models can show good results as shown for MEG signals (Kiebel, Daunizeau, Phillips, and

Friston, 2008; Baillet and Garnero, 1997). More accurate solutions can be achieved with high-resolution brain images. Equations A.3 and A.4 can be solved extracting surface boundaries for brain, skull and scalp from these images.

The boundary element method (BEM) can be used to calculate the forward fields (Fuchs, Wagner, and Kastner, 2001), although still assuming isotropy within each region of the head. It also needs the conductivity of head which assumes typical values for the conductivity of the brain, skull and skin. The skull is 40 to 90 times more resistive than the brain and scalp (Baillet, Mosher, and Leahy, 2001; Geddes and Baker, 1967).

A.1 The Inverse Problem

The two approaches used to estimate the EEG and MEG sources are the parametric and imaging methods. Parametric methods assume that the sources can be approximated by a few equivalent current dipoles represented as point sources $\mathbf{J^P}(\mathbf{r}') = q\delta(\mathbf{r}' - \mathbf{r_q})$, where $\delta(\mathbf{r})$ is the Dirac delta function, with moment $\mathbf{q} \equiv \int \mathbf{J^P}(\mathbf{r}')d\mathbf{r}'$. More on parametric methods can be found in Mosher, Lewis, and Leahy (1992); de Munck, van Dijk, and Spekreijse (1988). In the imaging methods, a current dipole is assigned to each of many tens of thousands of tessellation elements on the cortical surface with the dipole orientation normal to the local surface. Given the limited number of sensors available, the problem is ill-posed and requires the use of regularization or Bayesian techniques (Sato, Yoshioka, Kajiwara, Toyama, Goda, Doya, and Kawato, 2004; Wang, Williamson, and Kaufman, 1992).

Imaging approaches to the inverse problem consist of estimating the amplitudes of a dense set of dipoles distributed at fixed locations within the head volume, which resumes to a linear problem of parameter estimation. Moreover, dipoles are distributed over a grid built on the cortical surface that has been extracted from an anatomical MRI volume.

A.1.1 The Hierarchical Bayesian Method

The hierarchical Bayesian method used in this work was proposed by Sato, Yoshioka, Kajiwara, Toyama, Goda, Doya, and Kawato (2004). In their original proposition, MEG data was used. The present work constitutes the first results with EEG data. This method introduces a hierarchical prior that incorporates both structural and functional MRI data. The variance of the source current at each source location is considered an unknown parameter and is estimated from the observed EEG data and prior information by using the variational Bayesian (VB) method (Kiebel, Daunizeau, Phillips, and Friston, 2008). The fMRI information can be imposed as prior information on the variance distribution rather than the variance itself, giving a soft constraint on the variance. There is also a

spatial smoothness constraint in which the neural activity within a few milimeters radius tends to be similar due to neural connections. This constraint can be implemented as a hierarchical prior and, in this case, the estimation is no longer linear. Because of this, the variational bayesian method is used.

A Normal prior for the current is assumed as in

$$P_0(\mathbf{J_{1:T}} \mid \alpha) \propto exp\left[\frac{-1}{2}\sum_{t=1}^{T}\mathbf{J}'(\mathbf{t}).\mathbf{A}.\mathbf{J}(\mathbf{t})\right], \tag{A.6}$$

where $J_{1:T} \equiv \{\mathbf{J}(\mathbf{t}) \mid t = 1 : T\}$ is the primary current source, and $\mathbf{A}$ is the diagonal matrix with diagonal elements $\alpha \equiv \{\alpha_n \mid n = 1 : N\}$. The current inverse variance parameter α is estimated by an hierarchical prior:

$$P_0(\alpha) = \prod_{n=1}^{N}\Gamma(\alpha_n \mid \bar{\alpha}_{0n}, \gamma_{0n\alpha}), \tag{A.7}$$
$$\Gamma(\alpha \mid \bar{\alpha}, \gamma) \equiv \alpha^{-1}(\alpha\gamma/\bar{\alpha})^{\gamma}\Gamma(\gamma)^{-}1e^{-\alpha\gamma/\bar{\alpha}}.$$

where $\Gamma(\alpha \mid \bar{\alpha}, \gamma)$ is the Gamma distribution with mean $\bar{\alpha}$ and γ degrees of freedom. In the case of the Normal prior, the value of the inverse variance parameter α_n is given as prior information. In the hierarchical prior, the inverse variance parameter α_n is considered a random variable. Thus, there is a nonzero probability for any value of the inverse variance parameter α_n, and the prior probability distribution for α_n is given by the Gamma distribution in Equation A.8. The hyperparameters $\gamma_{0n\alpha}$ control the spread of the distribution and represent the confidence of the hierarchical prior. The hyperparameter $\bar{\alpha}_{0n}$ represents the mean value of α_n in the hierarchical prior. For example, if the prior mean α_{0n} is small, the prior probability $P_0(\alpha_n = \alpha_s)$ that α_n takes a small value α_s (large variance), increases. Therefore, the prior information on the current variance is imposed as a soft constraint in the variance estimation. The fMRI information is applied as the prior mean variance $\bar{\alpha}_{0n}^{-1}$ weighted with the confidence parameter $\gamma_{0n\alpha}$.

The smoothness constraint can be imposed in the covariance matrix enforcing high correlations between neighboring current activities:

$$P_0(J_{1:T} \mid \alpha, \lambda) \propto exp\left[\frac{-1}{2}\sum_{t=1}^{T}\mathbf{J}'(\mathbf{t}).\sum_{\alpha}^{-1}.\mathbf{J}(\mathbf{t})\right], \tag{A.8}$$

where the current covariance matriz $\sum_{\alpha}^{-1}$ is given by

$$\sum_{\alpha}^{-1} = \mathbf{A^{-1}} + \mathbf{W}.\Lambda^{-1}.\mathbf{W}'. \tag{A.9}$$

$\mathbf{A}$ and Λ are the diagonal matrices with the diagonal elements $\alpha = \{\alpha_n \mid n = 1 : N\}$ and $\lambda = \{\lambda_n \mid n = 1 : N\}$, respectively. The spatial profile of the correlation function is characterized by the Gaussian smoothing filter $\mathbf{W}$.

The variational Bayesian method is thus used to calculate the posterior distribution according to the observed EEG data as well as the fMRI information. The description of the algorithm and performance of the method for simulated and realistic data can be found in Yoshioka, Toyama, Kawato, Yamashita, and Nishina (2008); Sato, Yoshioka, Kajiwara, Toyama, Goda, Doya, and Kawato (2004).

Bibliography

Aguirre, Geofrrey K. *BOLD-fMRI a Guide to Functional Imaging for Neuroscientists*, chapter Experimental Design and Data Analysis for fMRI. Springer, 2010.

Alain, Claude; Snyder, Joel S.; He, Yu and Reinke, Karen S. Changes in auditory cortex parallel rapid perceptual learning. *Cerebral Cortex*, 17:1074–1084, 2007.

Allen, P. J.; Josephs, O. and Turner, R. A method for removing imaging artifact from continuous EEG recorded during functional MRI. *NeuroImage*, 12(2):230–239, 2000.

Allen, Philip J.; Polizzi, Giovanni; Krakow, Karsten; Fish, David R. and Lemieux, Louis. Identification of EEG events in the MR scanner: The problem of pulse artifact and a method of its subtraction. *NeuroImage*, 8:229–239, 1998.

Altmann, Christian F; Henning, Michaela; Döring, Maria Katharina and Kaiser, Jochen. Effects of feature-selective attention on auditory pattern and location processing. *NeuroImage*, 41:69–79, 2008.

Amabile, Renato Augusto. Remoção de artefatos e análise de parâmetros espectrais em sinais de EEG: Efeitos do fármaco flunitrazepam. Master's thesis, Universidade Federal de Minas Gerais, 2008.

Amaro Jr., Edson and Barker, Gareth J. Study design in fMRI: Basic principles. *Brain and Cognition*, 60:220–232, 2006.

Ashburner, J. and Friston, K.J. Multimodal image coregistration and partitioning - a unified framework. *NeuroImage*, 6:209–217, 1997.

Ashburner, John; Chen, Chun-Chuan; Flandin, Guillaume; Henson, Rik; Kiebel, Stefan; Kilner, James; Litvak, Vladimir; Moran, Rosalyn; Penny, Will; Stephan, Klaas; Hutton, Chloe; Glauche, Volkmar; Mattout, Jéreḿie and Phillips, Christophe. *SPM8 Manual*. Functional Imaging Laboratory, Institute of Neurology, UCL, 2009.

Ashburner, John and Friston, Karl J. *Human Brain Function*, chapter Rigid Body Registration. Academic Press, 2nd edition, 2003.

Atienza, Mercedes; Cantero, Jose L. and Dominguez-Marin, Elena. The time course of neural changes underlying auditory perceptual learning. *Learning and Memory*, 9:138–150, 2002.

Baillet, S. and Garnero, L. A bayesian approach to introducing anatomo-functional priors in the EEG/MEG inverse problem. *IEEE Transactions on Biomedical Engineering*, 1997.

Baillet, Sylvian; Mosher, John C. and Leahy, Richard M. Electromagnetic brain mapping. *IEEE Signal Processing Magazine*, 18(6):14–30, 2001.

Bandettini, Peter A.; Wong, Eric C.; Hinks, R. Scott; Tikofsky, Ronald S. and Hyde, James S. Time course EPI of human brain function during task activation. *Magnetic Resonance in Medicine*, 25:390–3977, 1992.

Basar, Erol. *Memory and Brain Dynamics - Oscillations Integrating Attention, Perception, Learning and Memory.* CRC Press, 2004.

Basar, Erol; Basar-Eroglu, Canan and Schürmann, Martin. Gamma, alpha, delta, and theta oscillations govern cognitive processes. *International Journal of Psychophysiology*, 39:241–248, 2001a.

Basar, Erol and Karakas, Sirel. Neuroscience is awaiting for a breakthrough: An essay bridging the concepts of Descartes, Einstein, Heisenberg, Hebb and Hayek with the explanatory formulations in this special issue. *International Journal of Psychophysiology*, 60:194–201, 2006.

Basar, Erol and Schürmann, Martin. Toward new theories of brain function and brain dynamics. *International Journal of Psychophysiology*, 39(6), 2001.

Basar, Erol; Schürmann, Martin; Demiralp, Tamer; Basar-Eroglu, Canan and Ademoglu, Ahmet. Event-related oscillations are 'real brain responses'- wavelets analysis and new strategies. *International Journal of Psychophysiology*, 39:91–127, 2001b.

Bell, A. J. and Sejnowski, T. J. An information maximisation approach to blind source separation and blind deconvolution. *Neural Computation*, 7(6):1129–1159, 1995.

Bernstein, Matt A.; King, Kevin F. and Zhou, Xiaohong Joe, editors. *Handbook of MRI Pulse Sequences.* Elsevier Academic Press, 2004.

Bonmassar, G.; Purdon, P. L.; Jaaskelainen, I. P.; Chiappa, K.; Solo, V.; Brown, E. N. and Belliveau, J. W. Motion and ballistocardiogram artifact removal for interleaved recording of EEG and EPs during MRI. *NeuroImage*, 16(4):1127–1141, 2002.

Boynton, G. M.; Engel, S. A.; Glover, G. H. and Heeger, D. J. Linear systems analysis of functional magnetic resonance imaging in human v1. *The Journal of Neuroscience*, 16 (13):4207–4221, 1996.

Brandeis, D. and Lehmann, D. Event-related potentials of the brain and cognitive processes: Approaches and applications. *Neuropsychologia*, 24(1):151–168, 1986.

Bressler, Steven L. and Ding, Mingzhou. *Wiley Encyclopedia of Biomedical Engineering*, chapter Event Related Potentials. John Wiley Sons, 2006.

Brett, Matthew; Johnsrude, Ingrid S. and Owen, Adrian M. The problem of functional localization in the human brain. *Nature Reviews Neuroscience*, 3:243–249, 2002.

Brett, Matthew; Penny, Will and Kiebel, Stefan. *Human Brain Function*, chapter An Introduction to Random Field Theory. Academic Press, 2nd edition, 2003.

Bruns, Andreas. Fourier-,hilbert- and wavelet-based signal analysis: are they really different approaches? *Journal of Neuroscience Methods*, 30(2):321–322, 2004.

Buonomano, D. V. and Merzenich, M. M. Cortical plasticity: from synapses to maps. *Annual Review of Neuroscience*, 21:149–186, 1998.

Burkard, Robert; Eggermont, Jos and Don, Manuel, editors. *Auditory Evoked Potentials: Basic Principles and Clinical Application*. Lippincott Williams Wilkins, 2007.

Callan, Daniel; Callan, Akiko; Gamez, Mario; Sato, Masa-aki and Kawato, Mitsuo. Premotor cortex mediates perceptual performance. *NeuroImage*, 52(1):844–858, 2010.

Callan, Daniel E.; Callan, Akiko M.; Kroos, Christian and Vatikiotis-Bateson, Eric. Multimodal contribution to speech perception revealed by independent component analysis: a single-sweep EEG case study. *Cognitive Brain Research*, 10(3):349–353, 2001.

Comon, P. Independent components analysis - a new concept? *Signal Processing*, 36(3): 287–314, 1994.

Cuffin, B. N. A comparison of moving dipole inverse solutions using EEG's and MEG's. *IEEE Transactions on Biomedical Engineering*, 32(11):905–910, 1985.

Dale, A. M.; Liu, A. K.; Fischl, B. R.; Buckner, R. L.; Belliveau, J. M.; Lewine, J. D. and Halgren, E. Dynamic statistical parametric mapping: combining fMRI and MEG for high resolution imaging of cortical activity. *Neuron*, 26:55–67, 2000.

Dale, A.M.; Fischl, B. and Sereno, M.I. Cortical surface-based analysis:i. segmentation and surface reconstruction. *NeuroImage*, 9:179–194, 1999.

Dale, Anders M. Optimal experimental design of event-related fmri. *Human Brain Mapping*, 8:109–114, 1999.

de Munck, J. C.; van Dijk, B. W. and Spekreijse, H. Mathematical dipoles are adequate to describe realistic generators of human brain activity. *IEEE Transactions on Biomedical Engineering*, 35(11):960–966, 1988.

Debener, Stefan; Mullinger, Karen J.; Niazy, Rami K. and Bowtell, Richard W. Properties of the ballistocardiogram artefact as revealed by the EEG recordings at 1.5, 3 and 7t static magnetic field strength. *International Journal of Psychophysiology*, 67:189–199, 2008.

Debener, Stefan; Ullsperger, Markus; Siegel, Markus and Engel, Andreas K. Single-trial EEG-fMRI reveals the dynamics of cognitive function. *Trends in Cognitive Sciences*, 10(12):558–563, 2006.

Deiber, M.; Pascal, M.; Olivier, B.; Gold, G.; Fazio-Costa, L.; Ibanez, V. and Giannakopoulos, P. Distinction between perceptual and attentional processing in working memory tasks: a study of phase-locked and induced oscillatory brain dynamics. *Journal of Cognitive Neuroscience*, 19(1):158–172, 2007.

Delorme, A. and Makeig, S. EEGLAB: an open source toolbox for analysis of single-trial EEG dynamics. *Journal of Neuroscience Methods*, 134:9–21, 2004.

Delorme, Arnauld; Makeig, Scott; Fabre-Thorpe, Michelle and Sejnowski, Terrence. From single-trial EEG to brain area dynamics. *Neurocomputing*, 44:1057–1064, 2002.

Demany, Laurent. Perceptual learning in frequency discrimination. *Journal of Acoustical Society of America*, 78(3):1118–1120, 1985.

Dirlich, G.; Vogl, L.; Plaschke, M. and Strian, F. Cardiac field effects on the EEG. *Electroencephalography and Clinical Neurophysiology*, 102:307–315, 1997.

Doeller, Christian F.; Opitz, Bertram; Mecklinger, Axel; Krick, Christoph; Reith, Wolfgang and Schröger, Erich. Prefrontal cortex involvement in preattentive auditory deviance selection. *NeuroImage*, 20:1270–1282, 2003.

Donaldson, D. L. and Buckner, R. L. *Functional MRI: An Introduction to Methods.* Oxford University, 2001.

Eichele, Tom; Specht, Karsten; Moosmann, Matthias; Jongsma, Maritje L. A. and Quiroga, Rodrigo Quian. Assessing the spatiotemporal evolution of neuronal activation with single-trial event-related potentials and functional MRI. *Proceedings of the National Academy of Science*, 102(49):17798 –17803, 2005.

Etymotic Research,. ER-30 tubephone insert earphones instructions and specifications. Technical report, Etymotic Research, 2002.

Evans, A.C.; Collins, D.L.; Mills, S.R.; Brown, E.D.; Kelly, R.L. and Peters, T.M. 3D statistical neuroanatomical models from 305 mri volumes. pages 1813–1817, 1993.

Fahle, Manfred. Perceptual learning: Specificity versus generalization. *Current Opinion in Neurobiology*, 15:154–164, 2005.

Fahle, Manfred and Poggio, Tomaso. *Perceptual Learning.* Massachusetts Institute of Technology, 2002.

Felblinger, J.; Slotboom, J.; Kreis, R.; Jung, B. and Boesch, C. Restoration of electrophysiological signals distorted by inductive effects of magnetic field gradients during MR sequences. *Magnetic Resonance in Medicine*, 41:715–721, 1999.

Formaggio, Emanuela; Storti, Silvia Francesca; Avesani, Mirko; Cerini, Roberto; Milanese, Franco; Gasparini, Anna; Acler, Michele; Mucelli, Roberto Pozzi; Fiaschi, Antonio and Manganotti, Paolo. EEG and fMRI coregistration to investigate the cortical oscillatory activities during finger movement. *Brain Topography*, 21:100–111, 2008.

Frackowiak, R.S.J.; Friston, K.J.; Frith, C.; Dolan, R.; Price, C.J.; Zeki, S.; Ashburner, J. and Penny, W.D. *Human Brain Function.* Academic Press, 2nd edition, 2003. URL `http://www.fil.ion.ucl.ac.uk/spm/doc/books/hbf2/`.

Friston, K. J.; Zarahn, R.; Josephs, O.; Henson, R. N. A. and Dale, A. M. Stochastic designs in event-related fMRI. *NeuroImage*, 10(5):607–619, 1999.

Friston, Karl J.; Ashburner, John T.; Kiebel, Stefan J. and Nichols, Thomas. *Statistical Parametric Mapping: the Analysis of Functional Brain Images.* Academic Press, 2006.

Friston, K.J; Williams, S; Horward, R; Frackowiak, R.S.J and Turner, R. Movement related effects in fMRI time series. *Magnetic Resonance in Medicine*, 35:346–355, 1996.

Frith, Chris D. and Friston, Karl J. *The Role of the Thalamus in "Top Down" Modulation of Attention to Sound*, volume 4. 1996.

Fritz, Jonathan B.; Elhilali, Mounya; David, Stephen V. and Shamma, Shihab A. Auditory attention - focusing the searchlight on sound. *Current Opinion in Neurobiology*, 17:437–455, 2007.

Fuchs, Manfred; Wagner, Michael and Kastner, Jörn. Boundary element method volume conductor models for EEG source reconstruction. *Clinical Neurophysiology*, 112:1400–1407, 2001.

Garcia-Perez, Miguel A. Forced-choice staircases with fixed step sizes: asymptotic and small-sample properties. *Vision Research*, 38:1861–1881, 1998.

Garreffa, Girolamo; Bianciardi, Marta; Hagberg, Gisela E.; Macaluso, Emiliano; Marciani, Maria Grazia; Maraviglia, Bruno; Abbafati, Manuel; Carni, Marco; Bruni, Ivo and Bianchi, Luigi. Simultaneous EEG-fMRI acquisition: How far is it from being a standardized technique. *Magnetic Resonance Imaging*, 22:1445–1455, 2004.

Geddes, L. A. and Baker, L. E. The specific resistance of biological material - a compendium of data for the biomedical engineer and physiologist. *Medical and Biological Engineering*, 5:271–293, 1967.

Genovese, Christopher R.; Lazar, Nicole A. and Nichols, Thomas. Thresholding of statistical maps in functional neuroimaging using the false discovery rate. *Neuroimage*, 15: 870–878, 2002.

Gilbert, C. D. Early perceptual learning. *Proceedings of the National Academy of Sciences*, 91:1195–1197, 1994.

Grady, Cheryl L.; van Meter, John W.; Maisog, Jose Ma.; Pietrini, Pietro; Krasuski, Jack and Rauschecker, Josef P. Attention-related modulation of activity in primary and secondary auditory cortex. *Cognitive Neuroscience and Neuropsychology*, 8:2511–2516, 1997.

Gray, Charles M. The temporal correlation hypothesis of visual feature integration: Still alive and well. *Neuron*, 24:31–47, 1999.

Green, D. M. Detection of auditory sinusoids of uncertain frequency. *Journal of the Acoustical Society of America*, 67:1304–1311, 1961.

Grimmes, Sverre and Grottem, Orjan. *Bioimpedance and Bioelectricity Basics*. Academic Press, 2000.

Haas, Shane M.; Frei, Mark G.; Osorio, Ivan and Pasik-Duncan, Bozenna. EEG ocular artifact removal through armax model system identification using extended least squares. *Communications in Information and Systems*, 3(1):19–40, 2003.

Hamalainen, M.S. and Ilmoniemi, R. J. Interpreting magnetic fields of the brain: Minimum norm estimates. *Medical and Biological Engineering and Computing*, 32(1):35–42, 1994.

Hawkey, David; Amitay, Sygal and Moore, David R. Early and rapid perceptual learning. *Nature Neuroscience*, 7:1055–1056, 2004.

He, Ping; Wilson, Glenn; Russell, Christopher and Gerschutz, Maria. Removal of ocular artifacts from EEG: A comparison of adaptive filtering method and regression method using simulated data. *Medical and Biological Engineering and Computing*, 45:495–503, 2005.

Heinze, H. J.; Mangun, G. R.; Burchert, W.; Hinrichs, H.; Scholz, M.; Munte, T. F.; Gos, A.; Scherg, M.; Johannes, S. and Hundeshagen, H. Combined spatial and temporal imaging of brain activity during visual selective attention in humans. *Nature*, 372(6506): 543–546, 1994.

Henson, R.; Büchel, C.; Josephs, O. and Friston, K. The slice-timing problem in event-related fMRI. *NeuroImage*, 9:S125, 1999.

Herrmann, Christoph S. and Debener, Stephan. Simultaneous recording of EEG and BOLD responses: A historical perspective. *International Journal of Psychophysiology*, 67:161–168, 2008.

Heuralt, J. and Jutten, J. Space or time adaptive signal processing by neural network models. In *Neural Networks for Computing: AIP Conference Proceedings*, volume 151. American Institure for Physics, 1986.

Hubel, D. H.; Henson, C. O.; Rupert, A. and Galambos, R. Attention units in the auditory cortex. *Science*, 129:1279–1280, 1959.

Ives, R. J.; Warach, S.; Schmitt, F.; Edelmann, R. R. and Schmoer, D. L. Monitoring the patient's EEG during echo planar MRI. *Electroencephalography and Clinical Neurophysiology*, pages 417–420, 1993.

Jung, Tzyy-Ping; Makeig, Scott; Humphries, Colin; Lee, Te-Won and Mckeown, Martin J. Removing electroencephalography artifacts by blind source separation. *Psychophysiology*, 37(2):163–178, 2000.

Jung, Tzyy-Ping; Makeig, Scott and Westerfield, Marissa. Analysis and visualization of single-trial event-related potentials. *Human Brain Mapping*, 14(3):166–185, 2002.

Kaiser, Jochen; Lennert, Therese and Lutzenberger, Werner. Dynamics of oscillatory activity during auditory decision making. *Cerebral Cortex*, 17:2258–2267, 2007.

Kandel, Erik R.; Schwartz, James H. and Jessell, Thomas M. *Principles of Neural Sciences*. McGraw-Hill, 2000.

Karmarkar, Uma R. and Buonomano, Dean V. Temporal specificity of perceptual learning in an auditory discrimination task. *Learning and Memory*, 10:141–147, 2003.

Kiebel, Stefan J.; Daunizeau, Jean; Phillips, Christophe and Friston, Karl J. Variational bayesian inversion of the equivalent current dipole model in EEG/MEG. *NeuroImage*, 39(2):728–741, 2008.

Kiebel, Stefan J. and Friston, Karl J. Statistical parametric mapping for event-related potentials: I. generic considerations. *NeuroImage*, 16:492–502, 2004.

Kiehl, Kent A.; Laurens, Kristin R.; Duty, Timothy L.; Foster, Bruce B. and Liddle, Peter F. An event-related fMRI study of visual and auditory oddball tasks. *Journal of Psychophysiology*, 15:221–240, 2001a.

Kiehl, Kent A.; Laurens, Kristin R.; Duty, Timothy L.; Foster, Bruce B. and Liddle, Peter F. Neural sources involved in auditory target detection and novelty processing: An event-related fMRI study. *Psychophysiology*, 38:133–142, 2001b.

Kierkels, Joep J. M.; Riani, Jamal; Bergmans, Jan W. M. and van Boxtel, Geert J. M. Using eye tracker for accurate eye movement artifact correction. *IEEE Transactions on Biomedical Engineering*, 54(7):1256–1267, 2007.

Kim, Jeejoong; Matthews, Natasha L. and Park, Sohee. An event-related fMRI study of phonological verbal working memory in schizophrenia. *PLoS ONE*, 5(8):1–9, 2010.

King, Andrew J and Nelken, Israel. Unraveling the principles of auditory cortical processing: Can we learn from the visual system? *Nature Neuroscience*, 12(6):698–701, 2009.

Klem, G. H.; Lüders, H. O.; Jasper, H. H. and Elger, C. The ten-twenty electrode system of the international federation. the international federation of clinical neurophysiology. *Electroencephalography and clinical neurophysiology. Supplement*, 52:3–6, 1999.

Klimesch, W. EEG alpha and theta oscillations reflect cognitive and memory performance: a review and analysis. *Brain Research*, 29:169–195, 1999.

Kollmeier, Birger; Gilkey, Robert H. and Sieben, Ulrich K. Adaptive staircase techniques in psychoacoustics: A comparison of human data and a mathematical model. *Journal of the Acoustical Society of America*, 83(5):1852–1862, 1988.

Krüger, Gunnar; Kastrup, Andreas and Glover, Gary H. Neuroimaging at 1.5T and 3.0T: Comparison of oxygenation-sensitive magnetic resonance imaging. *Magnetic Resonance in Medicine*, 45:595–604, 2001.

Laudon, M. K.; Webster, J. G.; Frayne, R. and Grist, T. M. Minimizing interference from magnetic resonance imagers during electrocardiography. *IEEE Transactions on Biomedical Engineering*, 45:160–163, 1998.

Lee, T-W; Girolami, M.; Bell, A.J. and Sejnowski, T.J. A unifying information-theoretic framework for independent component analysis. *International Journal on Mathematical and Computer Modeling*, 39:1–21, 2000.

Leek, M. R. and Watson, C. S. Learning to detect auditory components. *Journal of the Acoustical Society of America*, 76:1037–1044, 1984.

Levitt, H. Transformed up-down methods in psychoacoustics. *The Journal of the Acoustical Society of America*, 49:467–477, 1971.

Li, Wu; Piëch, Valentin and Gilbert, Charles D. Perceptual learning and top-down influences in primary visual cortex. *Nature Neuroscience*, 7(6):651–657, 2004.

Liang, Zhi-Pei and Lauterbur, Paul C., editors. *Principles of Magnetic Resonance Imaging: a Signal Processing Perspective*. IEEE Engineering in Medicine and Biology Society, 2000.

Liebenthal, Einat; Ellingson, Michael L.; Spanaki, Marianna V.; Prieto, Thomas E.; Ropella, Kristina M. and Binder, Jeffrey R. Simultaneous ERP and fMRI of the auditory cortex in a passive oddball paradigm. *NeuroImage*, 19:1395–1404, 2003.

Liu, Zhongming; Ding, Lei and He, Bin. Integration of EEG/MEG with MRI and fMRI. *IEEE Engineering in Medicine and Biology*, 25(4):46–53, 2006.

Llinas, R. R. The intrinsic electrophysiological properties of mammalian neurons: Insights into central nervous system function. *Science*, 23:1654–1664, 1988.

Logothetis, Nikos K.; Pauls, Jon; Augath, Mark; Trinath, Torsten and Oeltermann, Axel. Neurophysiological investigation of the basis of the fMRI signal. *Nature*, pages 150–157, 2001.

Logothetis, Nikos K. and Wandel, Brian A. Interpreting the BOLD signal. *Annual Review of Physiology*, 66:735–769, 2004.

Luck, Steven J., editor. *An Introduction to the event-related potential technique*. MIT Press, 2005.

Luck, Steven J.; Fan, Silu and Hillyard, Steven A. Attention-related modulation of sensory-evoked brain activity in a visual search task. *Journal of Cognitive Neuroscience*, 5(2):188–195, 1993.

Luck, Steven. J.; Woodman, Geoffrey F. and Vogel, Edward K. Event-related potential studies of attention. *Trends in Cognitive Neuroscience*, 4(11):432–440, 2000.

Maintz, J. B. Antoine and Viergever, Max A. A survey of medical image registration. *Medical Image Analysis*, 2(1):1–36, 1998.

Makeig, S.; Bell, A. J.; J., T-P Jung T. and Sejnowski,. *Independent Component Analysis of Electroencephalographic Data*, volume 8. 1996.

Makeig, Scott. Auditory event-related dynamics of the EEG spectrum and effects of exposure to tones. *Electroencephalography and Clinical Neurophysiology*, 86:283–293, 1993.

Malmivuo, Jaakko and Plonsey, Robert. *Bioelectromagnetism: Principles and Applications of Bioelectric and Biomagnetic Fields*. Oxford University Press, 1995.

Mancini, D.; Perrucci, M. G.; Cugini, S.; Ferretti, A.; Romani, G. L. and Gratta, C. Del. Complete artifact removal for EEG recorded during continuous fMRI using independent component analysis. *NeuroImage*, 34:598–607, 2006.

Mansfield, P.; Haywood, B. and Coxon, R. Active acoustic control in gradient coils for MRI. *Magnetic Resonance in Medicine*, 46:807–818, 2001.

Mansfield, Peter. Imaging by nuclear magnetic resonance. *Journal of Physics E: Scientific Instruments*, 21:18–30, 1988.

Mantini, D.; Perrucci, M. G.; Cugini, S.; Ferretti, A.; Romani, G. L. and Gratta, C. Del. Complete artifact removal for EEG recorded during continuous fMRI using independent component analysis. *NeuroImage*, 34(2):598–607, 2007.

Mayhew, Stephen D.; Dirckx, Sharon G.; Niazy, Rami K.; Iannetti, Gian D. and Wise, Richard G. EEG signatures of auditory activity correlate with simultaneously recorded fMRI responses in humans. *NeuroImage*, 49:849–864, 2010.

Mayo, 1986-1995. ANALYZE Header File Format. Mayo Foundation, 1986-1995.

McCarthy, G.; Luby, M.; Gore, J. and Goldman-Rakic, P. Infrequent events transiently activate human prefrontal and parietal cortex as measured by functional MRI. *Journal of Neurophysiology*, 77:1630–1634, 1997.

McJury, Mark and Shellock, Frank G. Auditory noise associated with MR procedures: A review. *Journal of Magnetic Resonance Imaging*, 12:37–45, 2000.

Michel, Christoph M.; Murray, Micah M.; Lantz, Göran; Gonzalez, Sara; Spinelli, Laurent and Peralta, Rolando Grave de. EEG source imaging. *Clinical Neurophysiology*, 115 (10):2195–2222, 2004.

Miranda de Sá, Antônio Mauricio F. L. and Felix, Leonardo Bonato. Improving the detection of evoked responses to periodic stimulation by using multiple coherence - application to EEG during photic stimulation. *Medical Engineering in Physics*, 24(4): 245–252, 2002.

Molholm, Sophie; Martinez, Antigona; Ritter, Walter; Javitt, Daniel C. and Foxe, John J. The neural circuitry of pre-attentive auditory change-detection: An fMRI study of pitch and duration mismatch negativity generators. *Cerebral Cortex*, 15:545–551, 2005.

Moore, David R.; Amitay, Sygal and Hawkey, David. Auditory perceptual learning. *Learning and Memory*, 10:83–85, 2003.

Mosher, J.C.; Lewis, P.S. and Leahy, R.M. Multiple dipole modelling and localization from spatio-temporal MEG data. *IEEE Transactions on Biomedical Engineering*, 39: 541–557, 1992.

Mosher, John C.; Leahy, Richard M. and Lewis, Paul S. EEG and MEG: Forward solutions for inverse methods. *IEEE Transactions on Biomedical Engineering*, 46(3):245–258, 1999.

Mueller, Viktor; Brehmer, Yvone; Oertzen, Timo von; Li, Shu-Chen and Lindenberger, Ulman. Electrophysiological correlates of selective attention: a lifespan comparison. *BMC Neuroscience*, 9(18):1–21, 2008.

Mukai, Ikuko; Kim, David; Fukunaga, Masaki; Japee, Shruti; Marrett, Sean and Ungerleider, Leslie G. Activations in visual and attention-related areas predict and correlate

with the degree of perceptual learning. *The Journal of Neuroscience*, 27(42):11401–11411, 2007.

Mulert, Christoph. *EEG-fMRI: Physiological Basis, Technique and Applications*, chapter What Can fMRI Add to the ERP Story? Springer, 2010.

Mullinger, Karen; Debener, Stefan; Coxon, Ronald and Bowtell, Richard. Effects of simultaneous EEG recording on MRI data quality at 1.5, 3 and 7 tesla. *International Journal of Psychophysiology*, 67(3):178–188, 2007.

Muthuswamy, Jitendran and Thakor, Nitish V. Spectral analysis methods for neurological signals. *Journal of Neuroscience Methods*, 83(1):1–14, 1998.

Näätänen, Risto and Alho, Kimmo. Mismatch negativity - a unique measure of sensory processing in audition. *International Journal of Neuroscience*, 80:317–337, 1995.

Narayan, Veena M.; Kimberg, Daniel Y.; Tang, Kathy Z. and Detre, John A. Experimental design for functional MRI of scene memory encoding. *Epilepsy and Behavior*, 6(2):242–249, 2005.

Neelon, Michael F.; Williams, Justin and Garell, P. Charles. The effects of attentional load on auditory ERPs recorded from human cortex. *Brain Research*, 1118:94–105, 2006.

Niazy, R K.; Beckmann, C. F.; Iannetti, G. D.; Brady, J. M. and Smith, S. M. Removal of FMRI environment artifacts from EEG data using optimal basis sets. *NeuroImage*, 28:720–737, 2005.

Nunez, P. L. and Silberstein, R. B. On the relationship of synaptic activity to macroscopic measurements: Does co-registration of EEG with fMRI make sense? *Brain Topography*, 13:79–96, 2000.

Nunez, Paul L. and Srinivasa, Ramesh. *Electric Fields of the Brain: The Neurophysics of EEG*. Oxford University Press, 1981.

Ogawa, S.; Lee, T.; Nayak, A. and Glynn, P. Oxygenation-sensitive contrast in magnetic resonance image of rodent brain at high magnetic fields. *Journal of Magnetic Resonance in Medicine*, 14:68–78, 1990.

Ogawa, S.; Tank, D.W.; Menon, R.; Ellermann, J.M.; Kim, S-G and Merkle, H. Intrinsic signal changes accompanying sensory stimulation: Functional brain mapping with magnetic resonance imaging. *Proceedings of National Academic Science*, 89:5951–5955, 1992.

Olejniczak, Piotr. Neurophysiologic basis of EEG. *Journal of Clinical Neurophysiology*, 23(3):186–189, 2006.

Ozus, Bahadir; Liu, Ho-Ling; Chen, Lin; Iyer, Meenakshi B.; Fox, Peter T. and Gao, Jia-Hong. Rate dependence of human visual cortical response due to brief stimulation: an event-related fMRI study. *Magnetic Resonance Imaging*, 19(1):21–25, 2000.

Paffen, Chris L. E.; Verstraten, Frans A. J. and Vidnyánszky, Zoltán. Attention-based perceptual learning increases binocular rivalry suppression of irrelevant visual features. *Journal of Vision*, 8(4):1–11, 2008. ISSN 1534-7362.

Pakarinen, Satu; Lovio, Riika; Huotilainen, Minna; Alku, Paavo; Näätänen, Risto and Kujala, Teija. Fast multi-feature paradigm for recovering several mismatch negativities (MMNs) to phonetic and acoustic changes in speech sounds. *Biological Psychology*, 82: 219–226, 2009.

Pantev, Christo; Wollbrink, Andreas; Roberts, Larry E.; Engelien, Almut and Ütken-höner, Bernd. Short-term plasticity of the human auditory cortex. *Brain Research*, 842:192–199, 1999.

Pascual-Marqui, Roberto Domingo. Reviews of methods for solving the EEG inverse problem. *International Journal of Biolectromagnetism*, 1(1):75–86, 1999.

Penny, W. D. and Holmes, A. J. Random effects analysis, 2004.

Petkov, Christopher; Kang, Xiaojian; Alho, Kimmo; Bertrand, Olivier; Yund, E William and Loods, David. Attentional modulation of human auditory cortex. *Nature Neuroscience*, 7(6):658–663, 2004.

Pfurtscheller, G. Graphical display and statistical evaluation of event-related desynchronization (ERD). *Electroencephalography and Clinical Neurophysiology*, 43:757–750, 1977.

Pfurtscheller, G. and Lopes da Silva, F.H. Event-related EEG/MEG synchronization and desynchronization: Basic principles. *Clinical Neurophysiology*, 110(11):1842–1857, 1999.

Phillips, W. and Singer, W. In search of common foundations for cortical computation. *Behavioral and Brain Sciences*, 20:657–722, 1997.

Picton, Terence W. The P300 wave of the human event-related potential. *Journal of Neurophysiology*, 9(4):456–479, 1992.

Pleger, Burkhard; Foerster, Ann-Freya; Ragert, Patrick; Dinse, Hubert R.; Schwenkreis, Peter; Malin, Jean-Pierre; Nicolas, Volkmar and Tegenthoff, Martin. Functional imaging of perceptual learning in human primary and secondary somatosensory cortex. *Neuron*, 40:643–653, 2003.

Polich, John and Kok, Albert. Cognitive and biological determinants of P300: an integrative review. *Biological Psychology*, 41(2):103–146, 1995.

Polley, Daniel B.; Steinberg, Elizabeth E. and Merzenich, Michael M. Perceptual learning: specificity versus generalization. *Current Opinion in Neurobiology*, 15:154–160, 2005.

Polley, Daniel B.; Steinberg, Elizabeth E. and Merzenich, Michael M. Perceptual learning directs auditory cortical map reorganization through top-down influences. *The Journal of Neuroscience*, 26:4970–4982, 2006.

Pugh, Kenneth R.; Shaywitz, Bennett A.; Shaywitz, Sally E.; Fulbright, Robert K.; Byrd, Dani; Skudlarski, Pawel; Shankweiler, Donald P.; Katz, Leonard; Constable, R. Todd; Fletcher, Jack; Lacadie, Cheryl; Marchione, Karen and Gore, John C. Auditory selective attention: an fMRI investigation. *NeuroImage*, 4:159–173, 1996.

Raichle, Marcus E. Cognitive neuroscience: Bold insights. *Nature*, pages 128–130, 2001.

Recanzone, G. H.; Merzenich, M. M.; Jenkins, W. M.; Grajski, K. and Dinse, H. R. Topographic reorganization of the hand representation in cortical area 3b of owl monkeys trained in a frequency discrimination task. *Journal of Neurophysiology*, 67:1031–1056, 1992.

Ritter, Petra; Becker, Robert; Graefe, Christine and Villringer, Arno. Evaluating gradient artifact correction of eeg data acquired simultaneously with fmri. *Magnetic Resonance Imaging*, 25(6):923–932, 2006.

Rosen, B. R. and Dale, R. L. Buckner Anders M. Event-related functional MRI: Past, present and future. *Proceedings of the National Academy of Sciences of the United States of America*, 95:773–780, 1998.

Roth, Corinne; Achermann, Peter and Borbély, Alexander A. Alpha activity in the human REM sleep EEG: Topography and effect of REM sleep deprivation. *Clinical Neurophysiology*, 110(4):632–635, 1999.

Sato, Masa-aki; Yoshioka, Taku; Kajiwara, Shigeki; Toyama, Keisuke; Goda, Naokazu; Doya, Kenji and Kawato, Mitsuo. Hierarchical bayesian estimation for MEG inverse problem. *NeuroImage*, 23:806–826, 2004.

Scherg, M. and von Cramon, D. Evoked dipole source potentials of the human auditory cortex. *Electroencephalography and Clinical Neurology*, 65(5):344–360, 1986.

Scherg, Michael; Bast, Thomas and Berg, Patrick. Multiple source analysis of interictal spikes: Goals, requirements and clinical value. *Journal of Clinical Neurophysiology*, 16 (3):214–224, 1999.

Schicker, Tobias; Muckli, Lars; Beer, Anton L.; Wibral, Michael; Singer, Wolf; Goebel, Rainer and Röder, Brigitte. Tight covariance of BOLD signal changes and slow ERPs in the parietal cortex in a parametric spatial imagery task with haptic acquisition. *European Journal of Neuroscience*, 23(7):1910–1918, 2005.

Schmidt, Conny F.; Zaehle, Tino; Meyer, Martin; Geiser, Eveline; Boesiger, Peter and Jancke, Lutz. Silent and continuous fmri scanning differentially modulate activation in an auditory language comprehension task. *Human Brain Mapping*, 29:46–56, 2008.

Schoups, Aniek A.; Vogels, Rufin and Orban, Guy A. Human perceptual learning in identifying the oblique orientation: Retinotopy, orientation specificy and monocularity. *Journal of Physiology*, 483(3):797–810, 1995.

Schreckenberger, Mathias; Lange-Asschenfeld, Christian; Lochmann, Matthias; Mann, Klaus; Siessmeier, Thomas; Buchholz, Hans-Georg; Bartenstein, Peter and Gründer, Gerhard. The thalamus as the generator and modulator of EEG alpha rhythm: a combined PET/EEG study with lorazepam challenge in humans. *NeuroImage*, 22(2): 637–644, 2004.

Seitz, Aaron R. and Dinse, Hubert R. A common framework for perceptual learning. *Current Opinion in Neurobiology*, 17:148–153, 2007.

Seitz, Aaron R. and Watanabe, Takeo. Is subliminal learning really passive? *Nature*, 422: 36, 2003.

Seitz, Aaron R. and Watanabe, Takeo. A unified model for perceptual learning. *Trends in Cognitive Neuroscience*, 9(7):329–334, 2005.

Sharbrough, F.; Chatrian, G-E; Lesser, R.P.; Lüders, H. and Picton, T.W. American electroencephalographic society guidelines for standard electrode position nomenclature. *Journal of Clinical Neurophysiology*, 8:200–202, 1991.

Shiu, Ling-Po and Pashler, Harold. Improvement in line orientation discrimination is retinally local but dependent on cognitive set. *Perception and Psychophysics*, 52(5): 582–588, 1992.

Shyu, Hsuen-Chyun and Sun, Yuh-Sien. Construction of a morlet wavelet power spectrum. *Multidimensional Systems and Signal Processing*, 13:101–111, 2002.

Sijbers, J.; Michiels, I.; Verhoye, M.; Auderkerke, J.; van der Linden, A. and van Dyck, D. Restoration of MR-induced artifacts in simultaneously recorded MR/EEG data. *Magnetic Resonance in Medicine*, 17:1383–1391, 1999.

Smith, Stephen M. *Functional MRI: An Introduction to Methods*, chapter Overview of fMRI analysis. Oxford University, 2001.

Spinelli, Laurent; Andino, Sara Gonzalez; Lantz, Goran; Seeck, Margitta and Michel, Christoph M. Electromagnetic inverse solutions in anatomically constrained spherical head models. *Brain Topography*, 13(2):115–125, 2000.

Srivastava, G.; Crottaz-Herbette, S.; Lau, K. M.; Glover, G. H. and Menon, V. ICA-based procedures for removing ballistocardiogram artifacts from EEG data acquired in the MRI scanner. *NeuroImage*, 24(1):50–60, 2005.

Stehling, Michael K.; Turner, Robert and Mansfield, Peter. Echo-planar imaging: Magnetic resonance imaging in a fraction of a second. *Science*, 254(5028):43–50, 1991.

Stroganova, Tatiana A.; Orekhova, Elena V. and Posikera, Irina N. EEG alpha rythm in infants. *Clinical Neurophysiology*, 10(6):997–1012, 1999.

Talairach, P and Tournoux, J. *A Stereotactic Coplanar Atlas of the Human Brain.* Stuttgart Thieme, 1988.

Teixeira, Bruno N. Registro de imagens tridimensionais das vias aéreas superiores para geração de modelos para pacientes. Master's thesis, Universidade Federal de Minas Gerais, 2009.

Thornton, C. and Sharpe, M. Evoked responses in anaesthesia. *British Journal of Anaesthesia*, 81:771–781, 1998.

Tiitinen, H.; Sinkkonen, J.; Reinikainen, K.; Alho, K.; Lavikainen, J. and Näätänen, R. Selective attention enhances the auditory 40 Hz transient response in humans. *Nature*, 364:59–60, 1993.

Ullsperger, M. and Cramon, D.Y. von. Subprocesses of performance monitoring: a dissociation of error processing and response competition revealed by event-related fMRI and ERPs. *NeuroImage*, 14:1387–1401, 2001.

van Wassenhove, Virginie and Nagarajan, Srikantan S. Auditory cortical plasticity in learning to discriminate modulation rate. *The Jornal of Neuroscience*, 7:2663–2672, 2007.

van Winsum, W.; Sergeant, J. and Gueze, R. The functional significance of event-related desynchronization of alpha rhythms in attentional and activating tasks. *Electroencephalography and Clinical Neurophysiology*, 58:519–524, 1984.

Vanderperren, Katrien; Ramautar, Jennifer; Novitski, Nikolai; Vos, Maarten De; Mennes, Maarten; Vanrumste, Bart; Stiers, Peter; van den Bergh, Bea; Wagemans, Johan; Lagae, Lieven; Sunaert, Stefan and van Huffel, Sabine. Ballistocardiogram artifacts in simultaneous EEG-fMRI acquisitions. *International Journal of Bioelectromagnetism*, 9(3):146–150, 2007.

Varela, Francisco; Lachaux, Jean-Philippe; Rodrigues, Eugenio and Martinerie, Jacques. The brainweb: Phase synchronization and large-scale integration. *Nature Reviews Neuroscience*, 2:229–239, 2001.

Vullemoz, S.; Rodionov, R.; Carmichael, D. W.; Thornton, R.; Guye, M.; Lhatoo, S. D.; Michel, C. M.; Duncan, J. S. and Lemieux, L. Continuous EEG source imaging enhances analysis of EEG-fMRI in focal epilepsy. *NeuroImage*, 49(4):3219–3229, 2010.

Wang, J. Z.; Williamson, S. J. and Kaufman, L. Multiple dipole modelling and localization from spatio-temporal MEG data. *IEEE Transactions on Biomedical Engineering*, 39 (7):665–675, 1992.

Ward, Lawrence M. Synchronous neural oscillations and cognitive processes. *Trends in Cognitive Sciences*, 7:553–559, 2003.

Watanabe, Takeo; Nanez, Jose E. and Sasaki, Yuka. Perceptual learning without perception. *Nature*, 413:844–848, 2001.

Watson, C.S. Time course of auditory perceptual learning. *Ann Otol Rhinol Laryngol Suppl*, 89:96–102, 1980.

Wickens, J. R. and Miller, R. A formalisation of the neural assembly concept: Constraints on neural assembly size. *Biological Cybernetics*, 77(5):351–358, 1997.

Widrow, B.; Glover, J. R.; McCool, J. M.; Kaunitz, J.; Williams, C. S.; Hearn, R. H.; Zeidler, J. R.; Dong, Jr. Eugene and Goodlin, R. C. Adaptive noise cancelling: Principles and applications. *Proceedings of the IEEE*, 63(12):1692–1716, 1975.

Winkler, I.; Czigler, I.; Sussman, E.; Horvath, J. and Balazs, L. Preattentive binding of auditory and visual stimulus features. *Journal of Cognition Neuroscience*, 17:320–339, 2005.

Worsley, K. J.; Evans, A. C.; Marrett, S. and Neelin, P. A three dimensional statistical analysis for CBF activation studies in the human brain. *Journal of Cerebral Blood Flow and Metabolism*, 12:900–918, 1993.

Worsley, Keith J. *Functional MRI: An Introduction to Methods*, chapter Statistical Analysis of Activation Images, pages 251–271. Oxford University, 2001.

Yan, Winston X.; Mullinger, Karen J.; Brookes, Matt J. and Bowtell, Richard. Understanding gradient artefacts in simultaneous EEG/fMRI. *NeuroImage*, 46:459–471, 2009.

Yoshioka, Taku; Toyama, Keisuke; Kawato, Mitsuo; Yamashita, Okito and Nishina, Shigeaki. Evaluation of hierarchical bayesian method through retinotopic brain activities reconstruction from fMRI and MEG signals. *NeuroImage*, 42:1397–1413, 2008.

Yotsumoto, Yuko and Watanabe, Takeo. Defining a link between perceptual learning and attention. *PLOS Biology*, 6(8):1623–1625, 2008.

Zatorre, Robert J.; Mondor, Todd A. and Evans, Alan C. Auditory attention to space and frequency activates similar cerebral systems. *NeuroImage*, 10:544–554, 1999.

Zhang, John X.; Feng, Ching-Mei; Fox, Peter T.; Gao, Jia-Hong and Tan, Li Hai. Is left inferior frontal gyrus a general mechanism for selection? *NeuroImage*, 23:596–603, 2004.